BUMPER AND GRILLE AIRBAGS CONCEPT FOR IMPROVED VEHICLE COMPATIBILITY IN SIDE IMPACT: PHASE I

Saeed Barbat

Xiaowei Li

Ford Motor Company
United States of America

Priya Prasad

Prasad Engineering, LLC
United States of America

Paper Number 13-0140

ABSTRACT

Fundamental physics and numerous field studies have clearly shown a higher injury and fatality risk for occupants in smaller and lighter vehicles when colliding with a heavier, taller and a higher one. The consensus is that the significant parameters influencing compatibility in front-to-side crashes are geometric interaction, vehicle stiffness, and vehicle mass. The objective of this research is developing a concept of deployable bumper and grille airbags for improved vehicle compatibility in side impact. The external airbags, activated by signals from pre-crash sensors, may help mitigate the effect of weight, geometry and stiffness differences and reduce side intrusions. However, a highly reliable pre-crash sensing system is required to enable the reliable deployment, which is currently not technologically feasible.

Analytical and numerical methods and hardware tests were used to help develop the deployable external airbags concept. A simplified spring-mass model was initially developed to set the target for bumper and grille airbags parameters. Finite Element (FE) models of the inflatable structure (bumper airbag) were developed and exercised. Several iterations were executed to help develop the airbags and guide efficient test plans. The concept development was executed and validated in two phases. This paper covers "Phase I" only, which consists of extensive analytical, simulation and test iterations to achieve the inflatable structural system design for integrity and performance on component, subsystem and VIA sled testing levels. Examples of Phase I tasks were: Fabric Material testing and evaluation for ultimate strength and module of elasticity properties; Sewn versus bonded airbag construction technique; Airbag vent types; Overall bumper and grille inflatables and canister design and fabrication; and VIA sled testing to evaluate inflatable design, integrity and performance.

For the initial assessment of the inflatable system, a 48 kph perpendicular side impact of an SUV-type impactor against a stationary passenger car equipped with a US-SID-H3 crash dummy mounted on the sled was executed. Test results in terms of the airbags initial parameters, Head Injury Criteria (HIC), Thoracic Trauma Index (TTI), and Pelvic acceleration for the SID-H3 dummy, with bumper and grille airbags, were compared to those of baseline test results with no external airbags. This Phase 1 of the study was deemed successful in achieving the initial design parameters of the airbags, their integrity and their deployment and successfully staged the research for Phase II. The Phase II research investigated the concept of the inflatables and pre-crash sensing development, and was beyond the scope of this paper.

INTRODUCTION

Vehicle compatibility has been investigated in many studies using different approaches such as real-world crash statistics, crash testing and computer modeling [1-6]. Field data analysis shows that side impacts can be severe, harm-producing crashes, even though they occur less frequently than frontal impacts [7]. In vehicle designs, in general, front-end and side stiffness of vehicles are often inherently incompatible. Therefore, occupants in vehicles, particularly passenger cars, are at more risk when their vehicle (the "Target" vehicle) is struck from the side by another vehicle (the "Bullet" vehicle). The increased risk for the occupant of the Target vehicle results from at least two factors: there is less "crush" space in a side impact, and the "side-impact" stiffness of the Target vehicle, particularly when struck by a high-mounted bumper, is relatively low. This difference is particularly acute when the Target vehicle is a

passenger car and the Bullet vehicle is a truck or SUV, since the latter types of vehicle are generally stiffer in the frontal direction, are higher mass, and have high bumpers.

Barbat et. al. [6] investigated the effect of mass, geometry and stiffness on occupant responses in front-to-side impacts using computer simulations. A FE model-based DOE methodology focused on discerning the effects of a few design variables on dummy responses in front-to-side vehicle crash was developed in their study. The striking vehicle was selected to be an SUV while the struck vehicle was a mid-sized passenger car. It was concluded that the geometrical compatibility and interaction were the dominating factors in increasing dummy responses and side intrusions. Dummy responses in side impact are related to the side and B-pillar intrusions and door's inner velocities at the instant when contact with the side impact dummy occurs. The structural stiffness and the energy absorbing capacity at the vertical mid point of the door and above, in which the front-end of the striking SUV interact, are significantly less compared to the stiffness and energy absorbing capacity of the side structure below the vertical mid point of the door and close to the rocker.

In this research, the authors investigated the concept of external airbags on SUVs to mitigate the effect of mass, stiffness and geometrical interaction differences in SUV-to-passenger car side impacts. Some authors of this paper conducted the bumper airbag research in late 1999 and are co-inventors on US granted patents associated with this concept [8-11]. An early investigation of bumper airbag concept for improved compatibility in front and side impacts was conducted by Clark, C. and Young, W. [12-14]. Their work involved two commercial airbags, low pressure and high pressure airbags, built for other purposes. The low pressure airbag was a modified 'pillow bag" bladder bag, made of coated nylon and used commercially for storage of liquids or gases at less than 69 kpa pressure. The high pressure airbag was a Maxiforce KPI 35L Air Lifting bag made of coated Kevlar. Clark and Young [14] carried out two crashes with a 1989 Cutlass Ciera four door sedan equipped with bumper airbags. The first test was a frontal crash into a rigid barrier at 48.5 kph with high pressure (221 kpa, 2.21 bars outboard) and low pressure (20 kpa, 0.35 bars inboard) airbags totaling 84 cm thickness. The airbags were roped together, in a Kevlar sheet attached below the bumper and above the luggage rack on the roof. The low pressure airbag ruptured as expected in the frontal impact and the external airbags system absorbed approximately 19% of the crash energy. The second test was a side impact crash in which a 48.5 kph moving rigid barrier impacted just the 20 cm thick high pressure airbag (76 kpa, 0.6 bars) mounted on the side of the passenger door above the sill, overlapping the side door and centered on the B-pillar. The result of this test was unsatisfactory due to excessive penetration of the airbag into the yielding side structure of the struck vehicle.

The study is focused on concept development of the external bumper and grille airbags for improved vehicle compatibility in side impact, and it consists of two Phases. This paper covers Phase I ONLY, associated with the feasibility study of the external airbags concept. In this Phase, extensive component, subsystem and VIA sled testing were used to help establish the initial airbag design parameters (volume, initial pressure, burst pressure, venting mechanism, chambering, tethering), fabric selection, and construction method. The initial airbag design parameters were optimized through extensive FE simulations and helped develop test methods for preliminary performance evaluation of the concept. A simplified 1-D spring-mass model was developed and used to set up the initial airbag parameters. Results associated with structural intrusion, dummy responses and external airbag parameters, obtained from the VIA sled tests and simulations, are presented and discussed in this paper.

This futuristic external airbags concept requires highly reliable pre-crash sensors for target vehicle recognition and timely deployment of the airbags to minimized false positive triggering. The development of the required sensors has not been addressed in this paper and was beyond the scope of this research. Recently introduced safety features such as curtain airbags in passenger cars offer additional opportunities for improved front-to-side compatibility and traffic safety, but the concept of external airbags may also have potential in mitigating pedestrian injuries.

VEHICLE-TO-VEHICLE SIDE IMPACT PHYSICAL EVENT AND MODEL

Physical event

Stiffness incompatibility between the front-end and the side structures of a vehicle is an outcome of the nature of vehicle designs. Stiffness is only one parameter, in addition to mass and geometry,

influencing vehicle compatibility in front-to-side crashes. Generally, higher Bullet vehicle front-end stiffness may cause higher side intrusions in the side of the struck Target vehicle, in a vehicle-to-vehicle side impact. The side structural intrusions in the Target vehicle can be higher when the Bullet vehicle is an SUV/LTV, due to higher front-end stiffness of these types of vehicles as compared to passenger cars. In side impact crash tests, higher dummy responses' are related to higher door and B-pillar intrusions and velocities, and in some cases with direct contact of the Target vehicle dummy's head with the intruding structures of the Bullet vehicle. In an SUV/LTV-to-car side impact, the intruding structure of the Bullet vehicle may potentially cause higher dummy responses in the head and thorax area, due to geometrical and mass incompatibility in addition to the stiffness incompatibility.

Therefore, the concept of providing adaptively to the front-end structure of the Bullet vehicle, enabled by reliable pre-crash sensing, has the potential to help mitigate the effect of stiffness, mass and geometrical incompatibility between SUV/LTV and passenger cars in side impacts. Introducing the futuristic bumper and grille external airbags concept on an SUV/LTV may have the potential to help in two ways: first, the bumper airbag may absorb part of the crash energy before the vehicle structures come in contact during a crash tests and second, the grille airbag may have the potential to prevent dummy head contact with the leading edge of the intruding hood of the bullet vehicle.

Spring-mass model

To develop a simplified spring-mass model for setting the initial parameters of the bumper airbag, information about the average stiffness of the vehicle cab in standard front and side impact crash tests is needed. Average longitudinal and lateral vehicle crash pulses with their corresponding step function approximations studied by Barbat et.al., were used [18]. Figure 1 show an average passenger car's lateral acceleration crash pulse measured at the vehicle center of gravity (C.G) obtained from standard tests such as IIHS and FMVSS214 MDB crash tests. The average acceleration of this crash pulse is approximated by an idealized one-step function shown on the same figure [18]. The impact force can be estimated by multiplying the average acceleration by the mass of the vehicle. Similarly, Figure 2 shows a typical average longitudinal crash pulse obtained from the standard frontal impact NCAP crash tests at 56 kph against a rigid barrier. On the same figure, its corresponding idealized two-step function approximation is also shown [18]. The accelerometers location for this average crash pulse was either at the B-pillar at Rocker or at the vehicle C.G. location. The approximated impact force in frontal impact can be calculated by multiplying the average longitudinal acceleration by the vehicle mass.

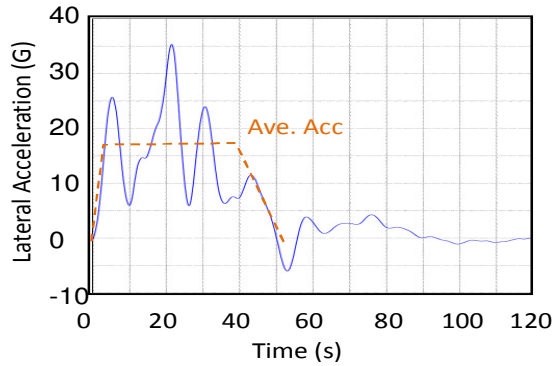

Figure 1. An average lateral acceleration crash pulse of a mid-size passenger car.

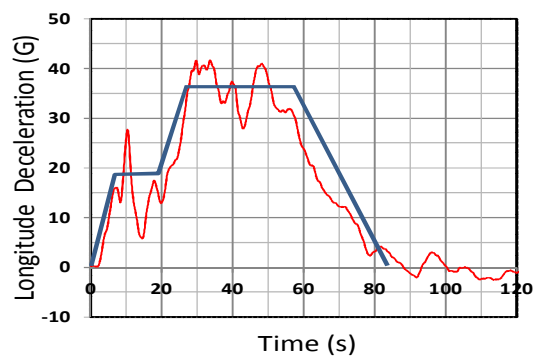

Figure 2. An average of a longitudinal deceleration crash pulse from NCAP test.

For this study, the front-end stiffness of the Bullet vehicle and the side structure stiffness of the Target vehicle were represented by the initial slopes of their idealized pulses. Stiffness differences in vehicle-to-vehicle side impact are shown in Figure 3, in which the stiffness of the striking vehicle is higher than that of the struck vehicle.

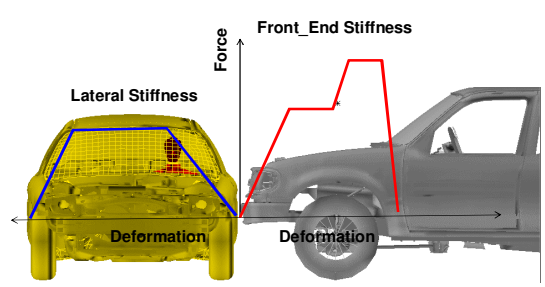

Figure 3. Stiffness incompatibility between the front and side structures.

The initial front-end stiffness of the striking Bullet vehicle can be conceptually adapted by adding an inflatable structure such as external bumper airbag, see Figure 4. The external bumper airbag stiffness can be adjusted through internal pressure and venting to adapt to the level of impact force. The external bumper airbag can decelerate the Bullet vehicle while managing a portion of the impact energy during impact. This will soften the initial structural front-end stiffness resulting in a reduced impact velocity when the structures of both struck and striking vehicles get in contact. In addition, the bumper airbag can help distribute the impact force across a larger contact area of the struck side of the Target vehicle. This can result in reduced local intrusion and reduced potential contact of the dummy with hard points of the intruded metal and trim.

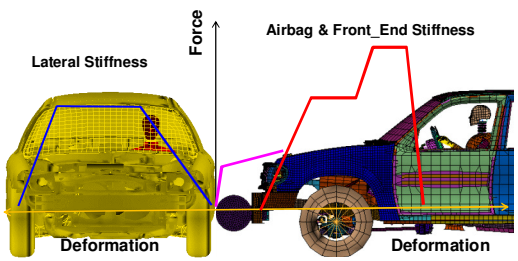

Figure 4. Added bumper airbag stiffness.

Figure 5 provides an illustration of a simplified 1-D vehicle-to-vehicle side impact spring-mass model, in which the striking vehicle is equipped with an external airbag. K1, represents the lateral stiffness of the struck vehicle; K2 represents the longitudinal front-end stiffness of the striking vehicle, and Ka1 and Ka2 represent the stiffness function of the bumper airbag. The C represents the damping coefficient of bumper the airbag.

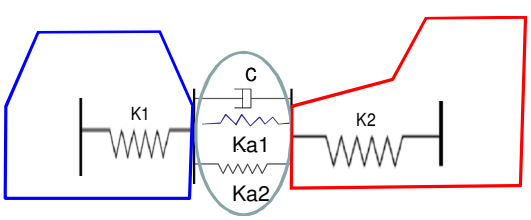

Figure 5. Simplified spring – mass model with bumper airbag.

<u>Spring's coefficient of the bumper airbag</u>
The contact force generated by the bumper airbag (F) is defined by airbag pressure (P) multiplied by the effective contact area (A).

$$F = P \cdot A \qquad (1).$$

Where, P, is the internal pressure in the airbag, which can be controlled by vent opening; and, A, is the effective contact area in Y_Z plane of the airbag, which varies with airbag deformation. In Eq. 2, the total stiffness of the airbag (K_x) is determined by differentiating the force, F, with respect to x, (dF/dx). Both the pressure, P, and the contact area, A, varies with compression or deformation during impact. Therefore, Eq. 2 can be expressed as:

$$K_x = \frac{dF}{dx} = \frac{d(P.A)}{dx} = A\frac{dP}{dx} + P\frac{dA}{dx} \qquad (2).$$

The spring coefficient can be represented in time domain by introducing dx =V dt into Eq. (2).

$$K_x = \frac{A}{V}\frac{dP}{dt} + \frac{P}{V}\frac{dA}{dt} = K_{a1} + K_{a2} \qquad (3).$$

Where, V= dx/dt is the impact velocity. The first term in Eq. 3 represents the pressure change with time, while the second term represents the bag contact area change with time.

Determine bumper airbag characteristics

<u>Side structure contact force</u> The initial pressure of the bumper airbag can be calculated from Eq. 1, if the bumper airbag size and the estimated contact force, sustained by the side structure of a passenger vehicle in an FMVSS 214 MDB crash test are given. In the FMVSS214 MDB crash test, the barrier may engage a few major structural components such as the rocker, lower B-pillar, front door and rear door. Jayasuriya and Saha [17] used computer simulations to evaluate the force distributions on the contact area in an FMVSS214 MDB side impact, see Figure 6. The total contact force ranged between 155 ~ 200 KN. This force magnitude was used for the calculations of the bumper airbag pressure.

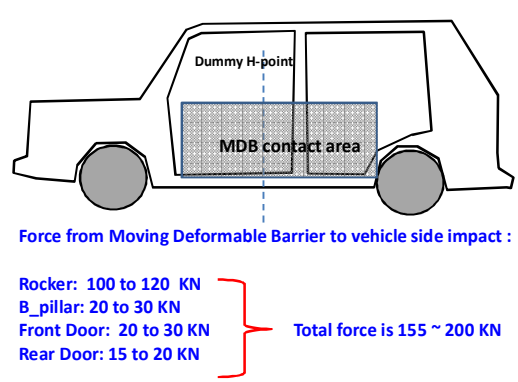

Figure 6. Contact force distribution on the side structure in an FMVSS214 with MDB.

Bumper airbag's initial pressure As shown in Figure 7, during the initial contact of the airbag to the side structure, the airbag only makes contact with the doors and B_pillar, no contact with rocker. The estimated contact force for the doors and B_pillar is between 55 KN and 80 KN, see Figure 6. The doors and B_pillar will only start to deform when the initial force exceeds 55 KN. If the diameter and length of the circular cylindrical airbag are 0.37 m and 1.22 m, respectively, then the airbag's effective contact area is 0.50 m^2. The initial pressure, P, of the bumper airbag is calculated by Eq 1 to be 110 KPa.

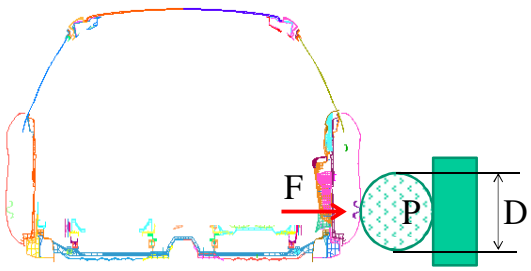

Figure 7. Initial contact of the bumper airbag to the side structure.

Maximum airbag pressure The bumper airbag contact area increases, and may engage the rocker, as the deformation of the airbag increases. As the contact area increase the load distribution will be more uniform and the contact force increases by engaging the rocker, which can sustain a higher impact load compared to other side structural components. The total side impact force, calculated from the major contact structures was ranging between 155 KN to 200 KN (see Figure 6). These calculations were made based on the contact area of the FMVSS214 MDB face. Since the contact area of the bumper airbag, suggested for this study, is smaller than that of the deformable barrier face, a contact force ranging between 80 KN and 100 KN, was chosen in this study.

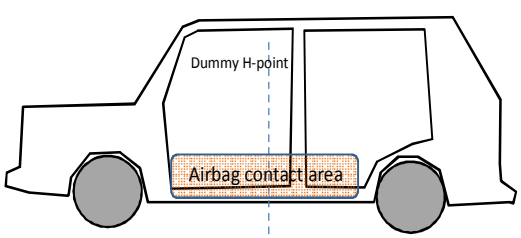

Design force from Airbag to vehicle side impact :
Total force acted in this contact area need less than
80 ~ 100 KN, before more intrusion happen

Figure 8. Bumper airbag design force and pressure.

It is assumed that the cross section of the airbag across the length does not change and the vent pressure can be controlled between 160 KPa and 200 KPa.

Stiffness change with airbag deformation

Eq. 2 states that the total airbag stiffness (Kx) changes as the cross sectional area of the airbag changes with deformation (dA/dx). A simple model was constructed to calculate the section change as a function of deformation x (see Figure 9). It was assumed that the circular cross sectional airbag will progressively deform into elliptical cross sectional airbag.

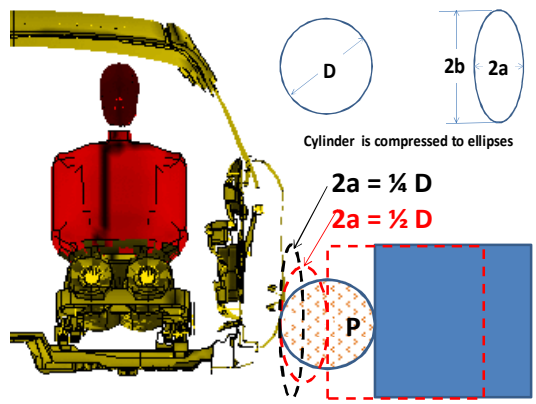

Figure 9. Circular section airbag deformed into elliptical section airbag.

In Figure 9, "D" represents the initial diameter of the circular cross section of the airbag. If the stretch of the fabric is ignored during bags pressurization, then the original perimeter of the airbag cross section (π D) remains constant during the progressive deformation and compression of the airbag.

The circle perimeter is (πD) ;

The elliptical perimeter is $2\pi\sqrt{\frac{a^2+b^2}{2}}$;

where, "a" and "b" represent the minor and major radii of the ellipse, respectively.

$$\pi D = 2\pi\sqrt{\frac{a^2+b^2}{2}} \qquad (4).$$

If the minor radius of the elliptical section "a" is expressed as a function of "D" then the major radius "b" of the elliptical section can be solved as a function of "D", using Eq. 4. The progressive contact area (2 b * L) and the total contact force can be calculated, see the

relationship of the bag deformation with the force in Figure 10. Example, if the airbag is compressed to ½ D (2a = ½ D) the major diameter of the ellipse 2b=1.33 D. If the pressure and L (length of the airbag across the width of the vehicle front end) are kept constant, the contact force becomes 1.33 times the initial contact force.

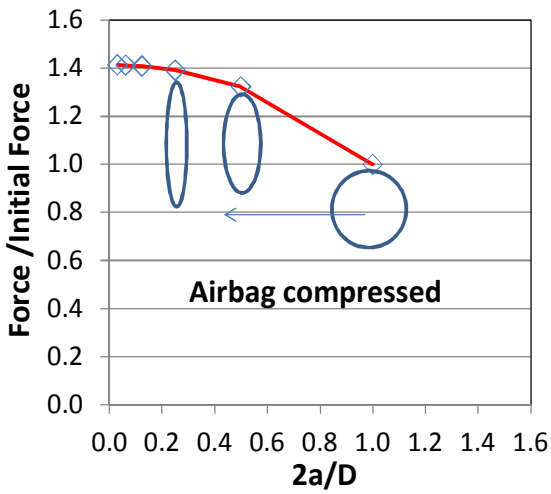

Figure 11. Variation of total contact force with airbag deformation.

EXTERNAL AIRBAG DESIGN

Analytical models, finite element models, and hardware testing were used during all stages of the external airbag development. Significant number of iterations was executed, starting with fabric material selection and ending with the concept readiness demonstration. Examples of Phase I hardware testing conducted to guide the structural integrity of the bags and the pyrotechnic inflation system to meet the targeted collision severity reduction and deployment requirements are listed below:

- Fabric material testing and evaluation (ultimate strength, modulus of elasticity, ability to package)
- Construction technique (sewn versus bonded bags)
- Seam Type evaluation (a solid baseline of double needle chain stitch with spectra 138 thread)
- Overall inflatable structure and canister design and fabrication
- Energy management features (burst type vent ports)
- Component Testing (fabric, fabric with seams, burst type vent, performance under approximate loading and boundary conditions with parallel rigid plates)
- Sled testing (evaluate inflatable design with a moving impactor approximation)
- VIA sled testing (evaluate inflatable design, integrity and performance on pre-inflated bags mounted on an SUV-type sled impacting a stationary passenger car in perpendicular side impact at approximately 48kph)

SLED TEST TO EVALUATE INFLATABLE SYSTEM PERFORMANCE

In an attempt to evaluate fabric integrity, vent performance, and prove out the inflatable system, sled tests were designed and executed. The sled test setup, shown in Figure 12, consisted of a moving Bullet sled of 1994 Kg with two aluminum honeycomb blocks, mounted on its front face, and a stationary Target sled that has a sliding carriage to simulate door crush with honeycomb. On the Bullet sled, the honeycomb block at the top is to interact with the grille airbag while the bottom one is to interact with bumper airbag. Both folded airbags are mounted on the stationary target sled. The Bullet sled impacted the stationary one at an impact speed of 48 kph.

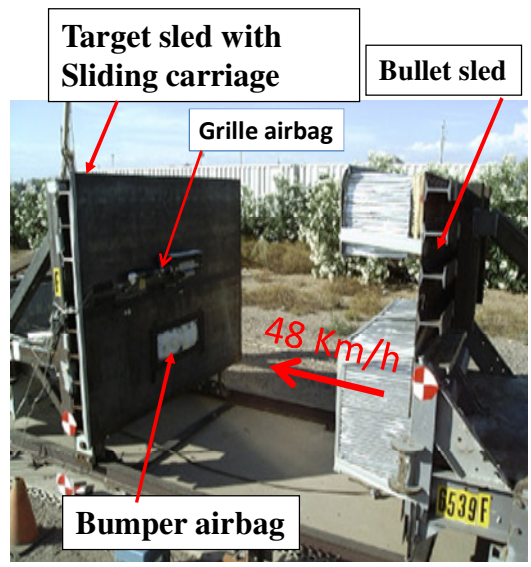

Figure 12. The sled setup.

The lower honeycomb block has a crush strength of 321 KPa and is the same as that of the standard NHTSA FMVSS-214 side impact MDB, without bumper structure. The dimensions of the lower honeycomb block were 127 cm width, 56 cm height and 38 cm depth. The upper honeycomb block had a crush strength of 178 KPa and dimensions of 127 cm width, 30 cm height and 38 cm depth.

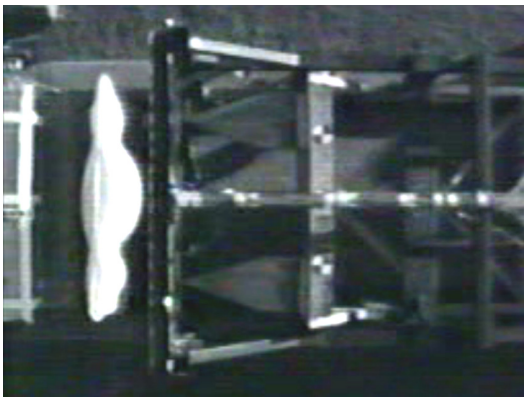

Figure 13. Top view of the real time grille airbag deployment.

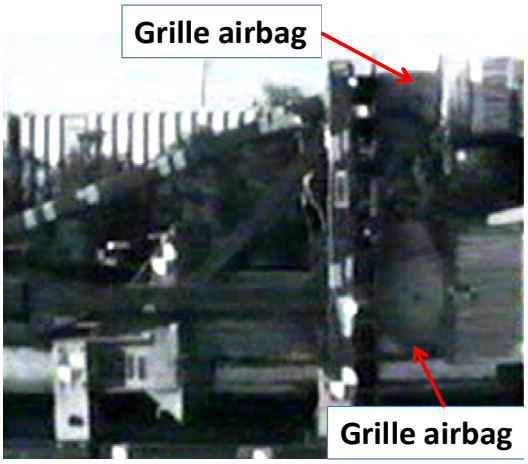

Figure 14. Side view of the real time airbag deployment.

Three tests were conducted, one baseline test with no airbags and two tests with airbags of different venting mechanisms, a discrete open vent design and a rupture disk vent design (disk ruptures at a pre-set pressure range).

Sled test results

<u>Baseline test</u> This test did not have any airbags mounted on the sliding carriage of the Target sled. Although this test did not have any inflators, the Trip-Stick mechanism was included to check for accuracy of ability to fire inflators at a certain time (flash bulbs were utilized to measure this data). The Trip-Stick was located such that the distance between the front face of the honeycomb blocks and the flat surface of the sliding carriage was 175 cm.

<u>Inflatables test with bumper and grille airbags</u> The circular cylindrical bumper airbag and the grille airbag canister assemblies were mounted on the sliding carriage. The discrete open vent and rupture disk vent airbags were used in the tests. The same grille airbag was used in both tests. The circular cylinder bumper airbag was compressed 100%. The peak pressure in the discrete open vent reached 350 KPa and the peak pressure in the rupture disk vent case was 286 KPa. The airbag integrity was maintained. The sliding carriage relative velocity curves of the test with an airbag with discrete open vent and the baseline test are shown in the Figure 15. The sliding carriage relative velocity curves of the test with an airbag with rupture open vent and the baseline test are shown in the Figure 16. Comparing the relative velocity of the three tests, the bumper airbag with rupture disk vent yielded the lowest relative speed for the sliding carriage. The test with rupture disc vented airbag absorbed more energy during the impact. Figures 17 and 18 show the variation of the airbag pressure versus the airbag compressing time for both venting mechanisms.

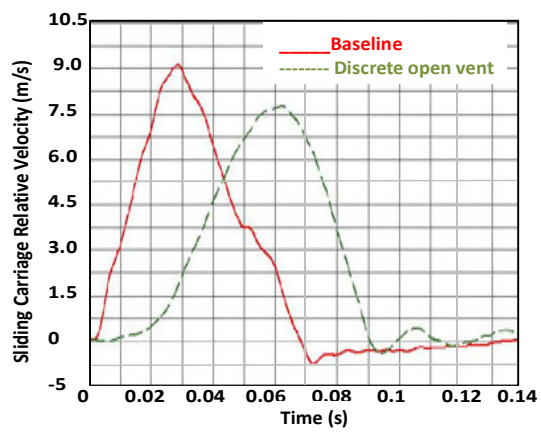

Figure 15. Sliding carriage relative velocity of baseline vs. discrete vent airbag.

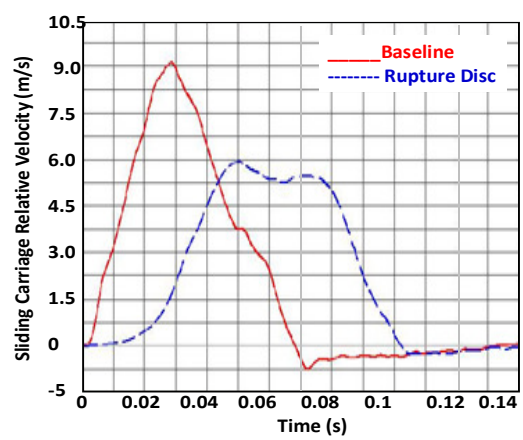

Figure 16. Sliding carriage relative velocity of the baseline vs. rupture disc airbag.

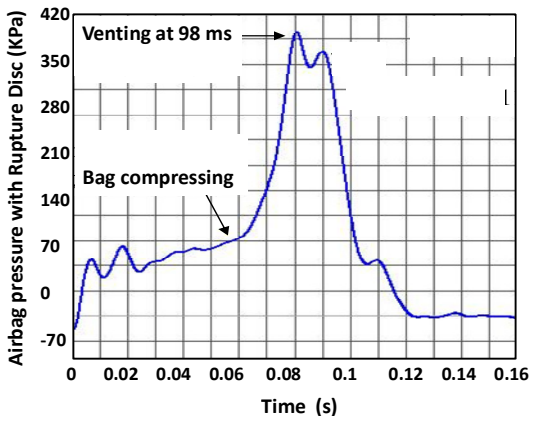

Figure 17. Pressure curve of the rupture disk vent airbag test.

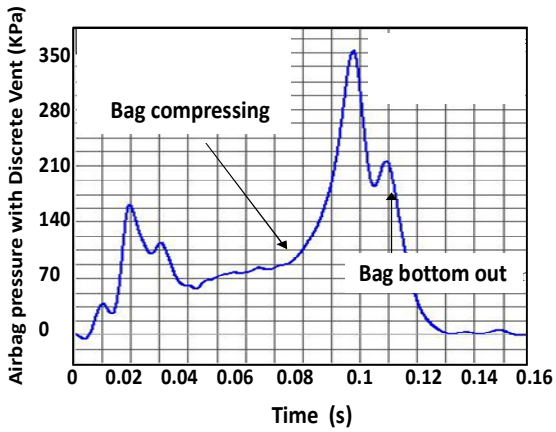

Figure 18. Pressure curve of the discrete disk open vent airbag test.

SIDE IMPACT VIA SLED TEST AND CAE MODEL DEVELOPMENT

In order to develop a successful and efficient test plan, FE models of the inflatable structure (bumper airbag) mounted on a test buck impactor were used. The models were validated with tests and used to set up the initial parameters of the inflatable system and to help optimize airbag and inflator parameters to achieve the intended targets. The airbag shape and design parameters were determined in Phase I and carried over to Phase II (subject of another paper) for further refinements. As a result, the initial bumper airbag system's specification developed in Phase I and to be used in Phase II for further refinement are as follows: 122 cm long untethered circular cylinder shape bumper airbag with initial pressure of 105 KPa, peak pressure of 186 KPa, and vent pressure of 106 KPa; bumper face in which the airbag canister was mounted at its center was a 40 cm high and acted as a reaction surface to prevent the airbag rolling back.

SUV-Type impact buck

Figures 19 shows the developed SUV-type impactor mounted on the VIA sled with the bumper and the airbag module. The bumper face was extended to provide a reaction surface for the deployed airbag. The Bullet vehicle had a mass of 1825 kg and was a rigid construction so it could be used for multiple tests but with the capability to replace the hood for each test. Figure 20 shows the bumper and grille airbag module housed in the extended bumper. A finite element model for this impactor, including the airbags and module, was also generated for the FE analyses, see Figure 21.

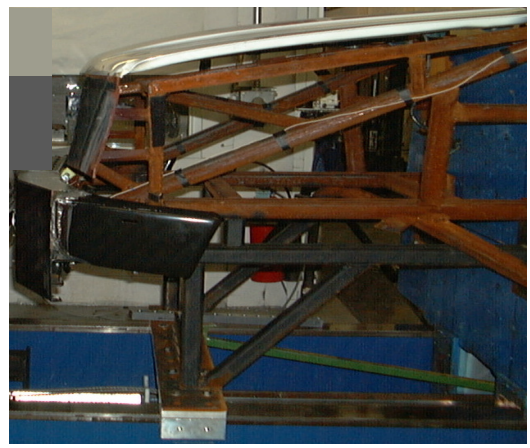

Figure 19. SUV-type buck on the VIA sled.

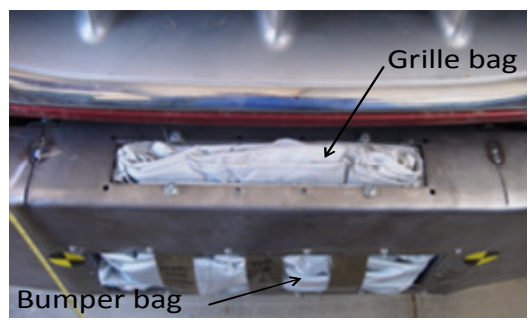

Figure 20. Housed airbags module.

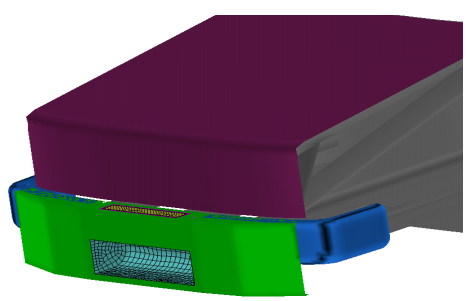

Figure 21. CAE model of the bullet buck.

VIA sled test-setup

Figure 22 shows the VIA sled experimental set-up for evaluating the external airbags concept in side impact. It can also be used for baseline testing in which the striking buck has no external airbags. The stationary Target vehicle used in this VIA sled series was a mid-size sedan. The bullet vehicle was simulated by an SUV-type rigid buck mounted on the sled that can be given an initial velocity to impact the Target vehicle. The buck had a rigid vertical plate attached to the front bumper beam. The inflatable structure (airbags) and the inflator(s) were integrated into a mechanical module or canister packaged through an opening at the center of this rigid plate. This plate is also used to act as a reaction surface for the bumper airbag to enhance stability and performance and to prevent the airbag from rolling under and behind the bumper beam.

Figure 22. VIA sled side impact test set-up .

The Target vehicle contained a belted, instrumented SID-H3 dummy for the driver. The driver seat was at the mid-position and the driver airbag was not activated. The Target vehicle and the Bullet Buck weights are listed in Table 1. Accelerometers were mounted at the armrest to calculate door velocity at discrete locations. Two types of bumper airbag venting mechanisms, rupture disc and discrete, were used in sled tests (see Table 1).

Table 1.
Test set-up characteristics

		BASELINE	RUPTURE DISC	DISCRETE VENT
Buck Speed	Km/h	48	48	48
Target Speed	Km/h	0	0	0
Buck Weight	Kg	1825	1833	1826
Target Weight	Kg	1818	1805	1803

Finite element model of the VIA sled test setup

Reliable finite element models of the passenger vehicle were required to enable reasonable predictions of structural performance. In this study, the passenger vehicle model was the same as that used by Barbat et. al. [6], in their CAE-based methodology analyses of front-to-side vehicle-to-vehicle impact. This FE model was constructed and correlated to physical FMVSS 214 and vehicle-to-vehicle front-to-side crash tests.

FE models were developed and side impact simulations were executed to guide the test plan and provide an initial performance assessment of the inflatables devices. Figure 23 shows the initial set-up of the FE model simulating a 48 kph perpendicular impact of the SUV-type rigid buck, with mounted bumper and grille airbags, against a stationary mid-sized passenger car equipped with the SID-H3 dummy in the driver seat. FE models of the inflatable structure (external airbags) were also developed and an extensive number of iterations was executed to ensure their validity before executing the side-impact VIA sled simulations. In the simulation, the airbags were pre-inflated, deployed and in position prior to contact with the target vehicle. The buck construction was modeled as rigid material, because no deformation in the buck was observed in the baseline (no airbags) impact test against a passenger car at 48 kph. The reaction plate in which the airbags were mounted was modeled with elastic shell elements (Poisson's ratio of 0.3, Young's modulus of 200 GPa).

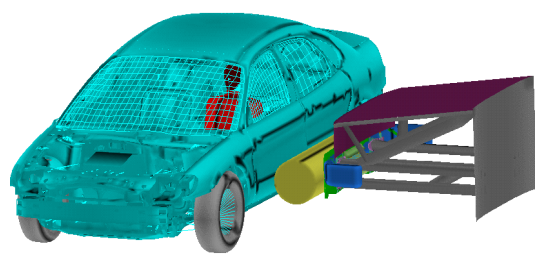

Figure 23. CAE model of VIA sled test simulation.

VIA SLED TEST AND RESULTS

The main purpose of this test series was to evaluate the bumper and grille airbag prototype assemblies for their capability to deploy the inflatable device and absorb energy in a simulated vehicle-to-vehicle collision using VIA sled. The VIA sled results obtained from the

buck impacting the side of the 4-door passenger car, both mounted on the sled, verified the bumper and grille‘ airbags deployment times, venting mechanisms and time, coverage and integrity. The bumper airbag had initial pressure of 105 KPa, peak pressure of 172 KPa, and a 150 mm diameter rupture disc vent. The grille airbag had an initial pressure of 3.44 KPa, and no vents. The airbags were instrumented with pressure transducers and were fully inflated prior to the tests. The dimensions of the circular cylinder airbags were 36.8 cm diameter and 122 cm length. Bumper airbag's deployment characteristics were deemed acceptable and the bumper airbag was compressed 90 - 95%. Bumper airbag integrity was maintained with no tears. Bumper airbag peak pressure reached 243 KPa, lower than expected. Grille airbag peak pressure reached 4.3 N/cm^2, as expected. In the test, the pre-deployed bumper airbag contacted the vehicle side at the right location, (see Figure 24 (a) and (b)).

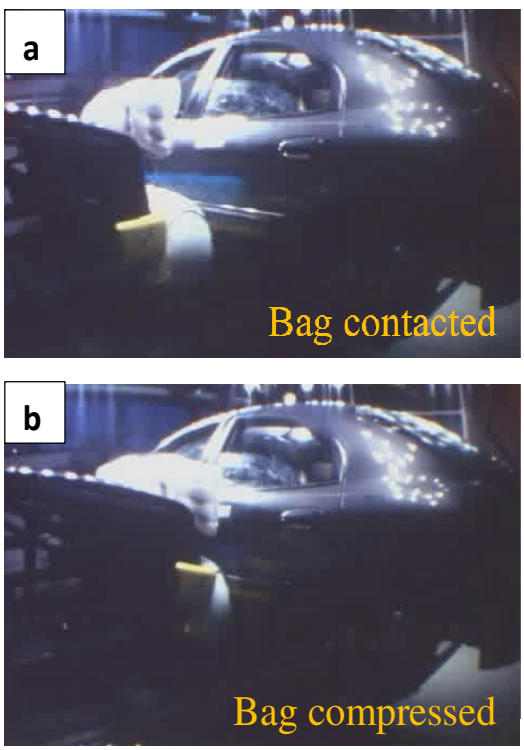

Figure 24 Bumper and grille airbag contact locations.

The grille airbag helped prevent the dummy's head from contacting the leading edge of the buck's hood (see Figure 25). The bumper airbag did not achieve the desired performance in terms of dummy responses, intrusions, and door velocity reductions. It was believed that further refinements for the bumper airbag design parameters and reaction surface design is required to achieve the desired outcome. However, the intent of the test and the current results met the objective of Phase I. Further refinements in the design of the airbags, reaction surface, and packaging are the subject of Phase II research.

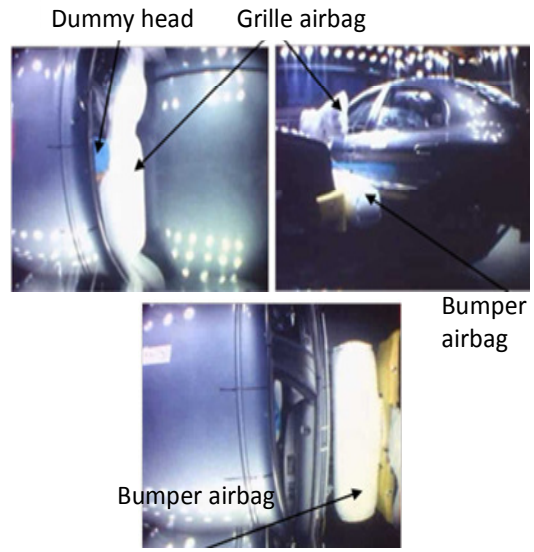

Figure 25. External airbags‘ interaction with vehicle structure and dummy head.

Model validation

Figure 26 shows the FE model that was exercised in a 48 kph side impact against a four door sedan simulating the VIA sled testing condition. Figure 27 shows an example of section taken through the dummy H-point, pointing out the importance of such models to better understand the external airbags‘ interactions with the dummy head and vehicle structure. For instance, Figure 27 shows how the bumper airbag provides a larger contact area with the vehicle side structure when it compressed.

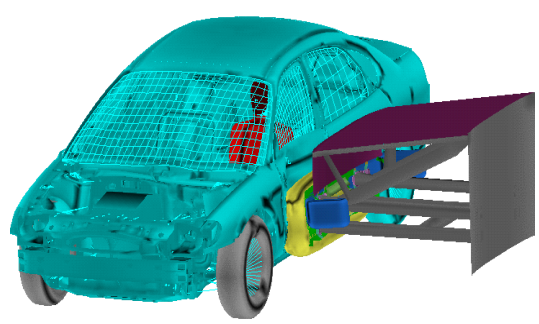

Figure 26. The CAE simulation of VIA sled test.

FE models allow for intrusions measurements and to a better understanding of the impact force distribution over a bigger contact area during the impact. The VIA sled test data and results were used to further validate the model to be used in Phase II to optimize the performance of the inflatable devices and help guide the conceptual design.

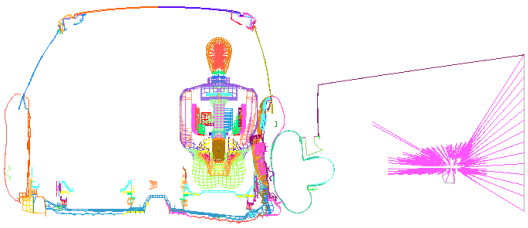

Figure 27. Section of the VIA sled simulation during impact through dummy H-Point.

Discussion of results

<u>Bumper airbag effect on bullet and target decelerations</u> Figure 28 shows the maximum deceleration measured at various locations of the bullet buck's bumper, buck's C.G. and the carrier. Data collected represented those of the three tests: baseline test with no external airbags, test with discrete vented bumper airbag and test with rupture disc vented bumper airbag.

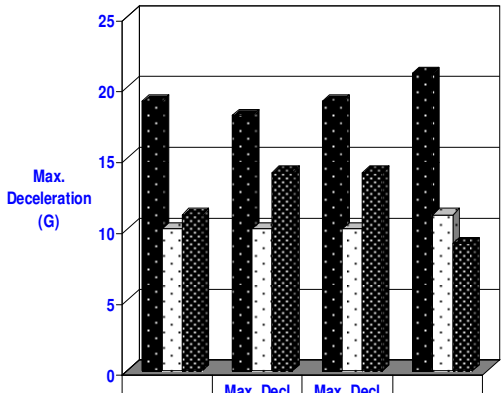

	Max. Decl @Buck	Max. Decl @Right Bumper	Max. Decl @Left Bumper	Max. Decl @Carrier
BASELINE	19	18	19	21
RUPTURE DISC	10	10	10	11
DISCRETE VENT	11	14	14	9

Figure 28. Maximum deceleration at various striking buck locations.

When the striking buck contacted the Target passenger car, the B-Pillar and the body side of the Target vehicle quickly accelerated to match the velocity of the striking bullet. The test with the rupture disc bumper airbag reduced the maximum deceleration of the striking buck by approximately 50%, compared to baseline results. The Target vehicle's accelerations were also reduced with the use of bumper airbag compared to those of the baseline (Figures 29 and 30). In these tests, the conceptual bumper airbag managed to absorb part of the impact energy and reduced the impact forces.

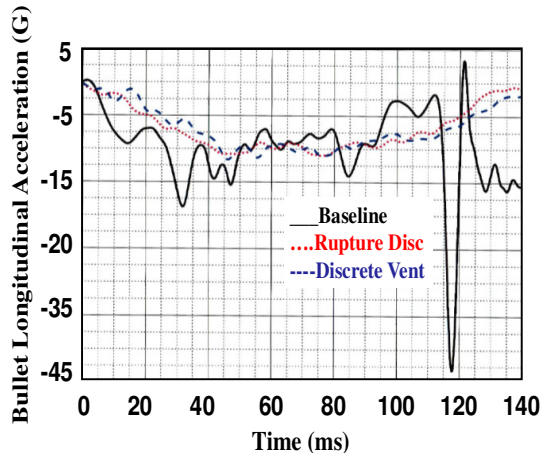

Figure 29. Deceleration time-history curves of the striking buck.

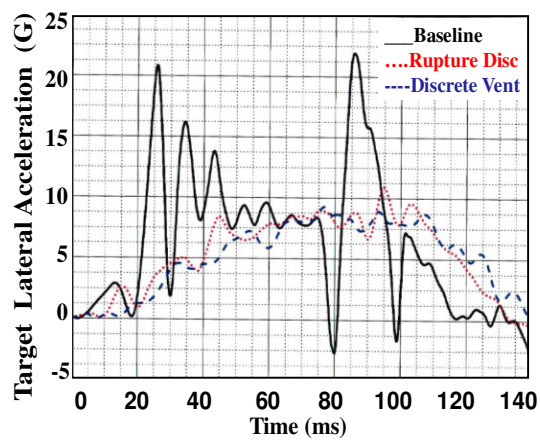

Figure 30. Deceleration time-history curves of the Target vehicle.

<u>Bumper airbag effect on armrest lateral velocity</u> The acceleration pulses at the armrest location, collected during the VIA sled test, were integrated to obtain the lateral velocity at that location. The results of the armrest lateral velocities obtained from impacts by the bullet buck with and without external airbags are presented in Figures 31 to 33. The test with the rupture disc bumper airbag provided lower lateral velocity on the armrest compared to the other tests.

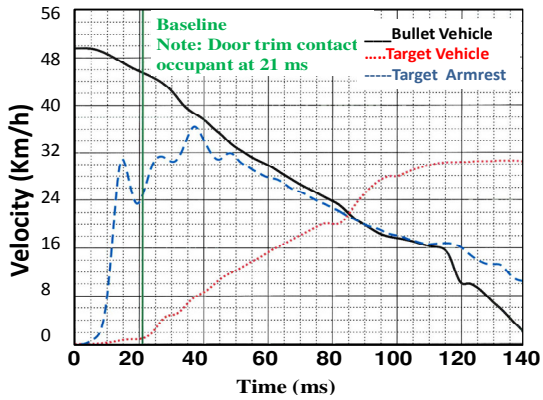

Figure 31. Armrest lateral velocity in the baseline test with no bumper airbag.

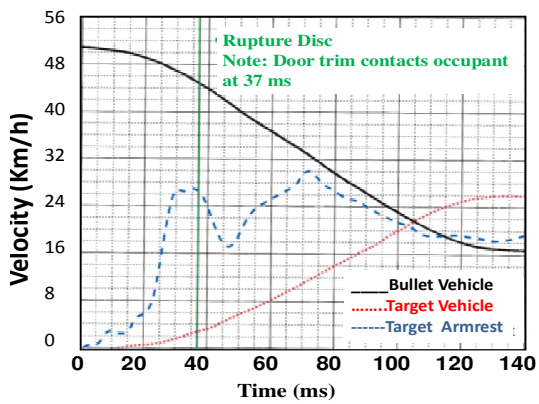

Figure 32. Armrest lateral velocity in the test with rupture disc vent bumper airbag.

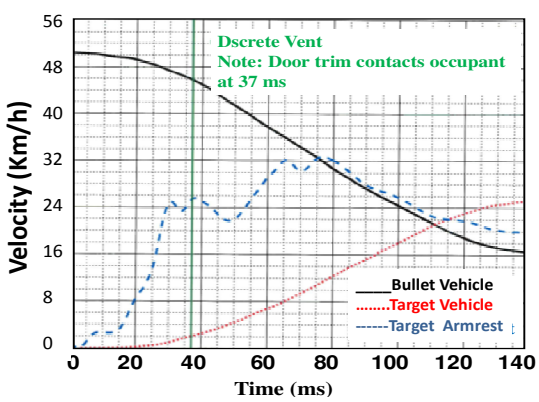

Figure 33. Armrest lateral velocity in the test with discrete vent bumper airbag.

<u>Bumper airbag effect on selected dummy responses</u> The effect of the bumper and grille airbags concept on SID-H3 responses is shown in Figure 34. The selected Head Injury Criteria (HIC), Thoracic Trauma Index (TTI), and Pelvic acceleration (G) were normalized by their corresponding values obtained from the baseline test with no external airbags. The rupture disc vent type of bumper airbag and the grille airbag reduced the HIC by 24% and the TTI by 6%, but did not improve the Pelvis response. In the case of the discrete vent type of bumper airbag, a negative impact was observed on the TTI and Pelvis responses while it provided a 17% reduction in the HIC value. This consistent trend shows that for the design considerations in the next Phase II of the study the venting mechanism of the bumper airbag will be that of the rupture disc type. However, at the same time results pointed out that there are other important considerations that need to be taken into account in addition to the airbag design.

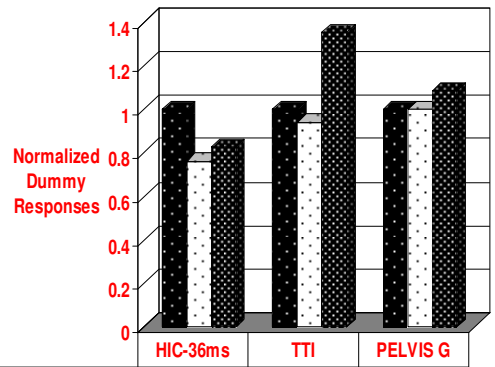

	HIC-36ms	TTI	PELVIS G
BASELINE	1	1	1
RUPTURE DISC	0.76	0.94	1.00
DISCRETE VENT	0.83	1.35	1.08

Figure 34. SID-H3 dummy responses in the target vehicle.

Altering the bumper airbag height was not considered in this test series. FE simulations indicated that aligning the bumper airbag more with the rocker, which is a major load path in side impact, may have the potential to provide further enhancement in the reduction of dummy responses and structural side intrusions. This task was deferred to Phase II in which a new design of the airbags, reaction surface and heights for rocker alignment were considered and are presented in a different paper.

CONCLUSION

- Analytical, numerical, and hardware testing methods were successfully developed and used to help set the initial design parameters for the external airbags concept
- Simplified spring-mass models were developed to set the bumper and grille airbag stiffness targets
- Computer simulations and physical testing were conducted on component, subsystem and sled testing levels to evaluate the performance of inflatable bumper system concept

- The following tasks were successfully achieved:
  - Fabric material testing, evaluation and selection
  - Inflator selection for bumper and grille airbag inflation
  - Airbag sewn construction technique and seam type evaluations
  - Design and fabrication of overall inflatable structure and canister
  - Component testing and simulations under approximate loading and boundary conditions with parallel rigid plates
  - Sled test with 48 kph striking Bullet sled against a Target sliding sled to evaluate the conceptual inflatable bumper design, integrity and vent type performance
- VIA sled test performance evaluation indicated that the rupture disc provided better performance related to energy management and reduced dummy responses
- The concept design of the initial prototype bumper and grille airbags was successfully demonstrated through a remote deployment in a VIA sled of an SUV-type buck-to-Passenger car perpendicular side crash tests at 48kph
- Head Injury Criteria (HIC), Thoracic Trauma Index (TTI), and Pelvic acceleration of the SID-H3 dummy were used as performance metrics for the bumper and grille airbags
- Bumper and grille external airbag FE models and a sled test to evaluate performance were developed
- The Phase I VIA sled test identified the areas of research for Phase II: designing a more efficient reaction surface, considering airbag chambering for stability, engaging the bumper airbag with the rocker, and further tuning of airbag parameters
- This research provided lessons learned and help set direction for future research and development of external airbags
- However, there are major limitations which may hinder making this concept production feasible such as packaging of the airbags, inflators, reaction surface. Most importantly, the airbag deployment is irreversible and requires very reliable and robust pre-crash sensors in all weather conditions and day or night. Currently, these types of pre-crash sensing systems are not available for the automotive environment
- An additional requirement is that the bumper airbag system functions in a frontal barrier impact and does not compromise any other FMVSS 208 test results

ACKNOWLEDGEMENTS

The authors would like to acknowledge the contributions made by the BF GOODRICH's Automotive (currently out of business) team members whom had worked with the authors on this project.

REFERENCES

[1] Hollowell, W.T. and Gabler, H.C.; "NHTSA's Vehicle Aggressivity and Compatibility Research Program", 15th ESV Conference, Paper No 96-S4-O-01, Melbourne, Australia, 1997.

[2] Summers, S., Hollowell, T., Prasad, A.; "NHTSA's Research Program for Vehicle Compatibility", 18th ESV Conference, Nagoya, Japan, 2003.

[3] Arbelaez, R. B., Baker, B. C., Nolan, J. M.; "Delta VS for IIHS Side Impact Crash Tests and Their Relationship to Real World Crash Severity", 19th ESV Conference, Paper 05-0049, 2005.

[4] Nolan, J., Powell, M., Preuss, A., and Lund, A.; " Factors Contributing to Front-Side Compatibility: A Comparison of Crash Test Results", Stapp Conference, 99SC02, 1999.

[5] Lugt, D.V., Connoly, T., and Bhalsod, D.; "Vehicle Compatibility – Analysis of the Factors Influencing Side Impact Occupant Injury", SAE 1999-01-0067, 1999.

[6] Barbat, S., Li, X., Prasad, P.; " Front-To-Side Crash Compatibility Analysis Using A CAE Based Methodology", 20th ESV Conference, Lyon, France, Paper 07-0347, 2007.

[7] Gabler, H.C.; "The Evolution of Side Crash Compatibility Between Cars, Light Trucks and Vans", SAE Paper 2003-01-0899, 2003.

[8] US Patent No. 7, 036, 844, "Bumper Airbag with Multiple Chambers".

[9] US Patent No. 6, 923, 483, "Bumper Airbag and System".

[10] US Patent No. 6, 950, 014, "Method for Operating a Pre-Crash Sensing System in a Vehicle Having External Airbags".

[11] US Patent No. 6, 757, 611, "Adaptive Safety System for a Bumper-Bag Equipped Vehicle".

[12] Clarke, C.; "The Crash Anticipating Extended Airbag Bumper"., 14th ESV Conference, 1994.

[13] Clarke,, C., William, Y. A.; "Airbag Bumper just Inflated Before the Crash", SAE Conference, Paper 941051, 1994.

[14] Clarke, C., William, Y. A.; "Car Crash Theory and Tests of Airbag Bumper Systems", SAE Conference, Paper 951056, 1995.

[15] Barbat,S., Li, X., and Prasad, P.; "Bumper and Grille Airbags Concept for Improved Vehicle Compatibility in Side Impact: Phas II", 23th ESV Conference, Paper 0140. 2013.

[16] RADIOSS Crash Code, Altair.

[17] M. M. Jayasuriya & N. K. Saha, "Local structural force evaluation of a vehicle in side barrier impact", International Journal of Crashworthiness, 2005 Vol. 10, No 5 page 451.

[18] Barbat, S., Mehall, M., Nayak, R., Nusholtz, G., S., Olds, N., Shi, Y, Stanko, B., Wang, J., T., Weerappuli, P., Xu, L., Yalamanchili, K.; "Idealized Vehicle Crash Test Pulses for Advanced Batteries"; SAE conference, paper 2013-01-0764, 2013.

A Study on the severity of the proposed Korean NCAP AE-MDB side impact test.

Gu Han
Kyehyeok Lee
Junho Lee
Juyup Seok
David Snyder
Kwanho Seo
Dongseok Kim
GM Korea Company
Korea
Paper Number 13-0156

ABSTRACT

Since 2003, the Korean NCAP(New Car Assessment Program) has included side impact tests. In these tests, a 950 kg moving barrier is collided into the driver side of the test vehicle at 55kph, in a direction perpendicular to the longitudinal center line of the test vehicle.[1] The Korean NCAP has recently investigated using the AE-MDB (Advanced European Mobile Deformable Barrier) in their testing to better represent the population of the vehicles on the road in Korea. It is necessary to improve. side moving deformable barrier characteristics to reflect real world side collisions.

The purpose of this study is to evaluate and compare the severity of the proposed Korean NCAP AE-MDB test at both 1300 kg and 1500 kg, relative to the current 950 kg. barrier test. Large-size, mid-size and small-size cars were tested.

INTRODUCTION

The European Enhanced Vehicle-safety Committee (EEVC) and International Harmonized Research Activities (IHRA) have studied and developed a side moving deformable barrier that attempts to match the trend in front structure stiffnesses.[2] This new barrier is called the Advanced European Mobile Deformable Barrier (AE-MDB) Korean NCAP has proposed to use this new barrier starting in 2015 but has not decided whether it should be 1300 or 1500 kg. The AE-MDB barrier face was developed to have a similar shape to that of vehicles within the current fleet. The following figure shows overlays of the progressive MDB and AE-MDB barriers with fronts of the cars which are used in this study: Large-size, Mid-size, Small-size vehicles. The AE-MDB barrier face matches the shapes of these vehicles better. Refer to the following figure 1.

(a) Progressive MDB with Study Vehicles

(b) AE-MDB with Study Vehicles

Figure1. Barrier Overlays to study vehicles

In the previous research, the center line of the AE-MDB is perpendicular to that of the target vehicle and is aligned 250mm rearward of the target vehicle's R-point. This was set to load both front and rear seat occupants and represent a moving car to moving car side impact; where the initial contact point is aimed at the driver seat Reference Point (R-point). The same condition was adopted in this study for both front and rear seat occupant consideration [3].

Korea Automobile Testing & Research Institute (KATRI) researched the status of car registrations to investigate vehicle weight in Korea [4]. The vehicle weight has been increased continuously. 37 percent of the 2010 registered cars weighed between 1.2ton and 1.6ton and 24 percent of the cars weighed between 1.4ton and 1.6ton. Refer to the following figure 2 for 2010 car registration status in Korea.

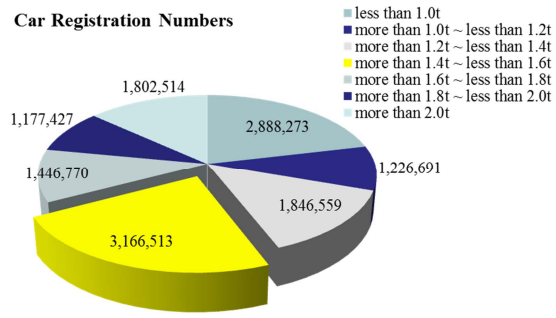

Figure2. Car registration number and weight distribution in Korea

Test Condition

In this study, one large-size, one mid-size and one small-size car were used as the struck car. The striker (Progressive MDB, 1300kg AE-MDB and 1500kg AE-MDB) impact velocity was 55kph.

In the test configuration, the progressive MDB was according to current Korean NCAP test procedure with ES2 dummy placed in driver seat. In AE-MDB tests, the center line of the 1300 kg and 1500 kg barriers were aligned to 250mm rearward from the driver seat Reference Point (R-point) with an ES2 dummy placed in front driver seat and a SID2s dummy placed in rear passenger seat. Refer to the following figure 3 for test configuration.

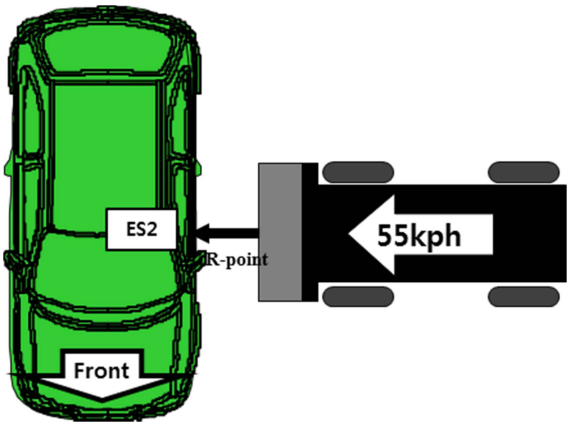

(a) Progressive MDB side impact procedure

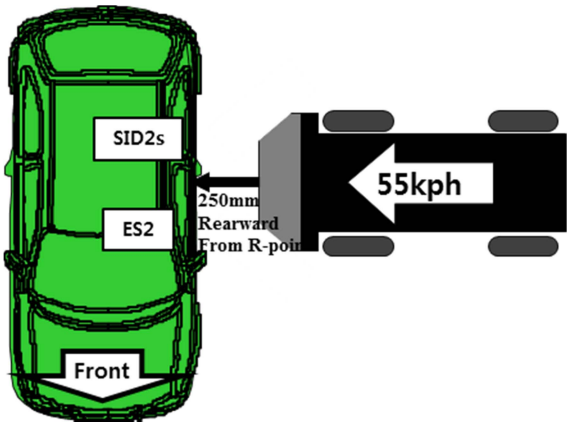

(b) AE-MDB side impact procedure

Figure3. Test configuration

According to the test configuration, the progressive MDB was not overlapped to the target vehicle rear wheel house area, whereas the right corner of AE-MDB was overlapped due to 200mm wider length in barrier face and 250mm rearward position from R-point of vehicle. Refer to the following figure 4-1 & 4-2 for MDB dimension comparison and figure 5 which represents MDB positions relative to the sides of the study vehicles.

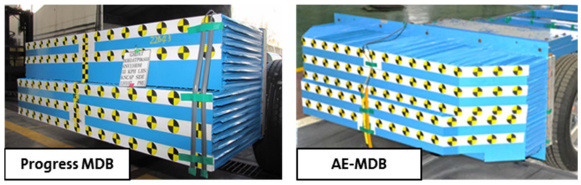

Figure4-1. Barrier shapes between Progressive MDB and AE-MDB

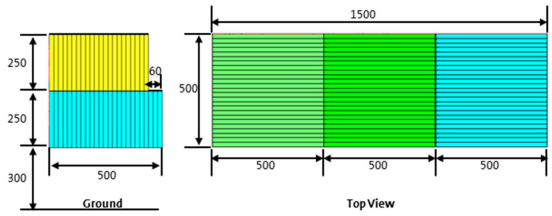

(a)Progressive MDB dimension

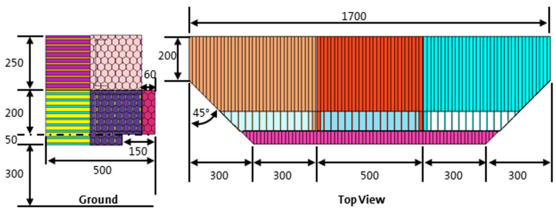

(b) AE-MDB dimension

Figure4-2. Comparison MDB dimension between Progressive MDB and AE-MDB

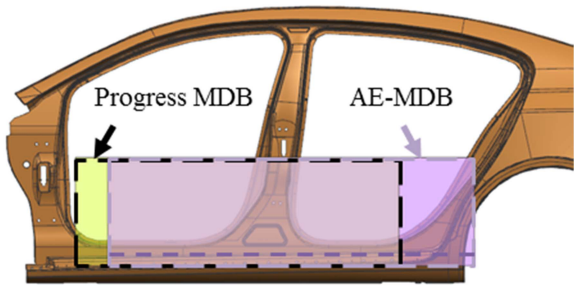

(a) Large-size Car

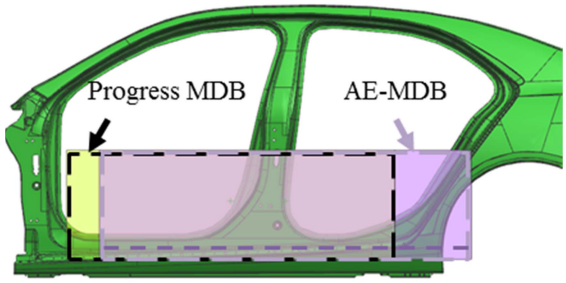

(b) Mid-size Car

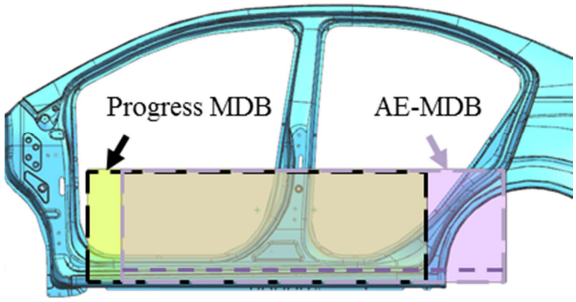

(c) Small-size Car

Figure5. Comparison MDB position between Progressive MDB and AE-MDB

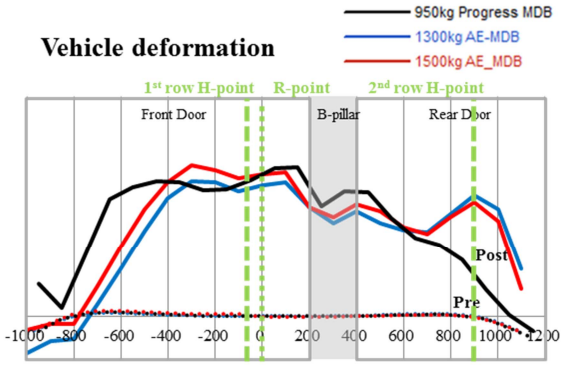

(a) Large-size Car

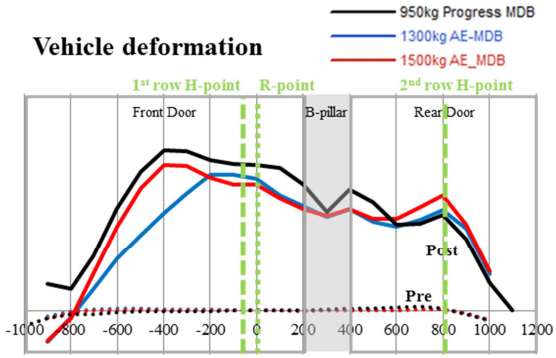

(b) Mid-size Car

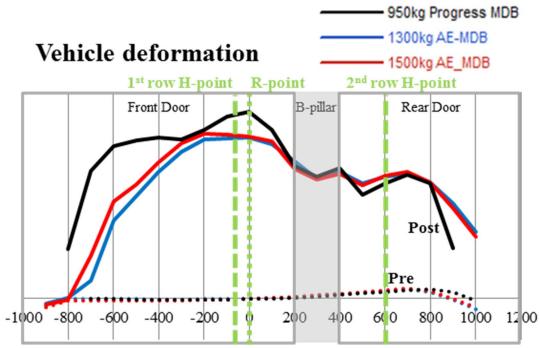

(c) Small-size Car

Figure6. Vehicle side door X-position relative to the R-point (0, 0)

Test Result

<u>Vehicle deformation</u>

1) Vehicle side outer and B-pillar deformation
After the barrier collision tests, the target vehicle's outer lines were measured along the outer surface of door in longitudinal direction. The deformed shape of the vehicles at the height of front driver seat reference point (R-point) was influenced by the different shapes of the progressive and AE barriers. Refer to the following figure 6 for vehicle deformation at driver R-point height.

The vehicle deformations at driver R-point height are different between the progressive MDB and AE-MDB tests, but are quite similar between 1300kg and 1500kg AE-MDB tests. The front door and b-pillar deformation were measured in outer panel and this data indicate less intrusion comparing progressive MDB test data. Refer to following figure 7 for B-pillar deformation measurement.

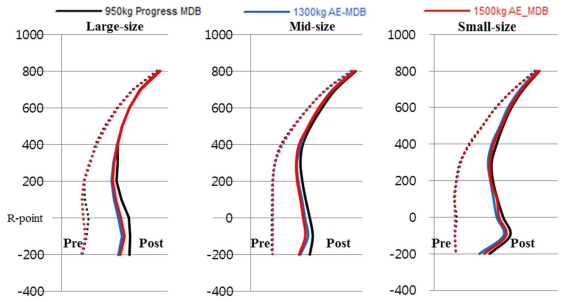

Figure7. B-pillar outer panel deformation of all cases of the crash vehicles

B-pillar deformation was less than progressive MDB in both 1300kg and 1500kg AE-MDB despite the heavier weight and higher B-pillar velocity at beltline height of impact side. This result was caused by barrier alignment which made more overlap vehicle rear wheel house.

After the test, a B-pillar investigation was conducted and the welds remained intact and there was no tearing of the sheet metal. High strength material was used in B-pillar structure of these target vehicles and they were able to withstand the heavier barrier. Refer to the following figure 8 for B-pillar inner panel post photos..

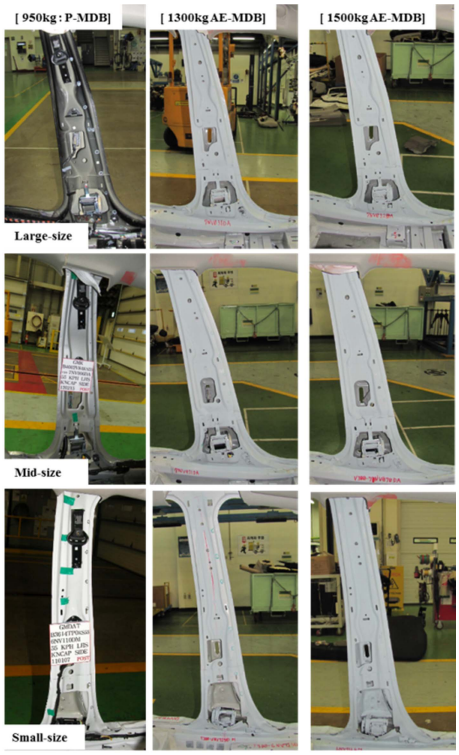

Figure8. Struck side B-pillar inner panel (the welds remained intact and there was no tearing of the sheet metal)

2) C-pillar deformation

The C-pillar wheel house areas were investigated and the welds remained intact and there was no tearing of the sheet metal. Refer to the following figure 9 for C-pillar outer panel post photos after 1500kg AE-MDB test. The C-pillar outer panel also measured except in progressive MDB and refer to the following figure 10 for C-pillar outer panel deformation measurement in both 1300kg and 1500kg AE-MDB. There are no significant differences between them.

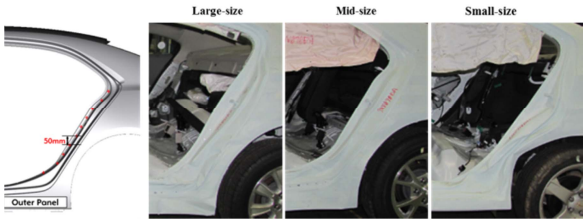

Figure9. C-pillar outer panel measuring points and post photos in 1500kg AE-MDB test

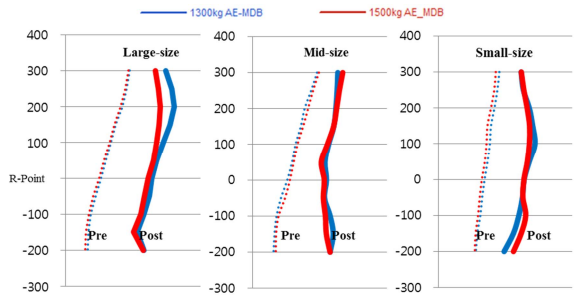

Figure10. C-pillar outer panel deformation measurement

Vehicle dynamics

During the impact, the struck cars in the AE-MDB test were rotated more than in the progressive MDB test due to impact point change. Nevertheless vehicle rotation was not much different during injury event timing up to 80ms. Refer to Figure 11. It didn't affect the occupant injury performance.

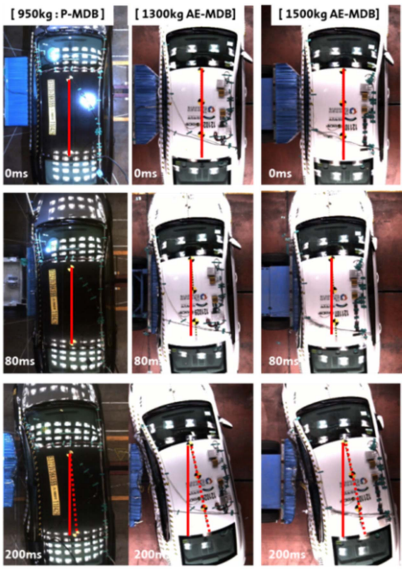

(a) Large-size car

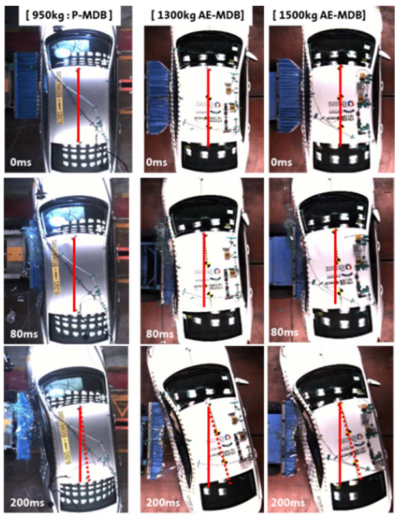

(b) Mid-size car

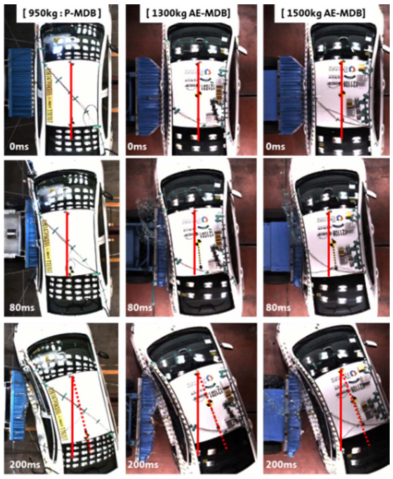

(c) Small-size Car

Figure11. Vehicle dynamic movement

The struck side B-pillar velocity was measured using an acceleration sensor on B-pillar inner panel at beltline height. Initial velocity just after barrier impact was much higher in AE-MDB test than in the progressive MDB. It could be caused by higher barrier weight, 50mm reduction at bottom of front bumper beam which made less overlap with side rocker structure. Then the B-pillar velocity increased steeply until 30ms and at that time non-struck side B-pillar velocity almost reached 15kph which is half of struck side B-pillar velocity. After that, relative velocity between struck side B-pillar and non-struck side B-pillar was decreased. Refer to the following figure 12 for struck side B-pillar velocity at beltline height and figure 13 for B-pillar relative velocity between struck side and non-struck side at beltline height and mid height.

Heavier weight and the front bumper beam area which is a new and stiffer part compared to progressive MDB causes much higher initial B-pillar velocity when the barrier impacts the target vehicle during initial 10ms. After that, the struck side B-pillar velocity decreased when the barrier contacted the rear wheel house area. The B-pillar velocity then increased again, deforming the vehicle. In this situation, the rear wheel house area could help reduce the B-pillar intrusion by distributing the barrier energy.. There was no tearing of the sheet metal in B-pillar and C-pillar area.

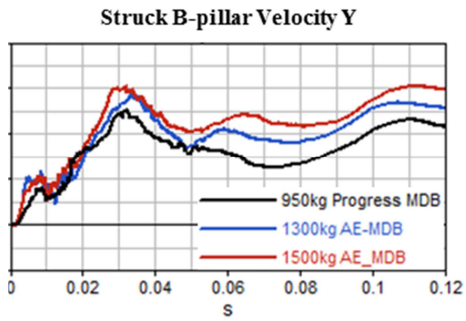

(a) Large-size car

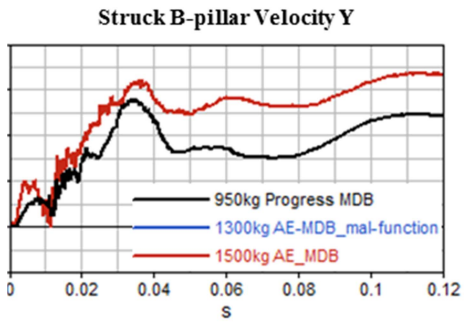

(b) Mid-size car

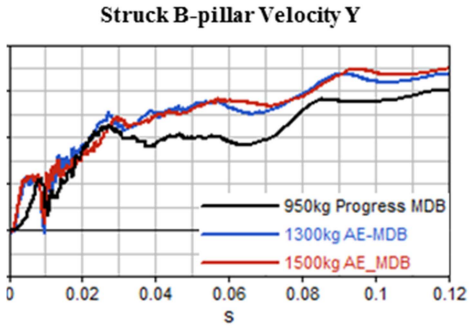

(c) Small-size car

Figure12. Struck side B-pillar velocity at beltline height of all cases of the crash cars

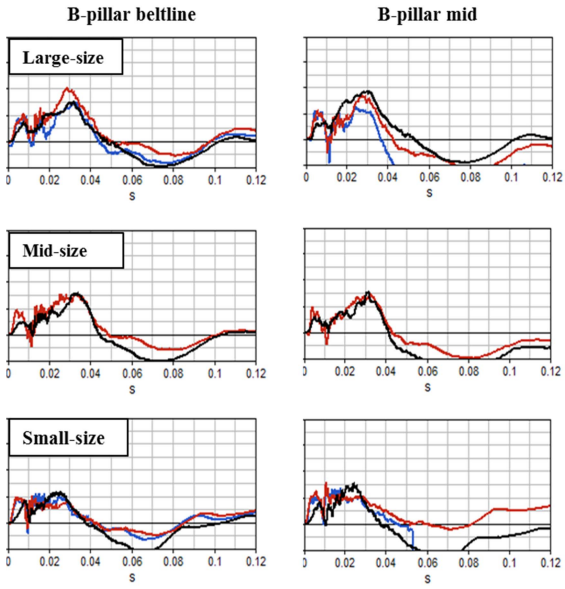

Figure13. B-pillar relative velocity at beltline and mid height between struck side and non-struck side of all cases of the crash cars

Dummy injury criteria

1) Front driver seat dummy

In the front driver seat, an ES2 dummy was positioned. Among the tests, the AE-MDB test injury result was more severe than the progressive MDB. Based on Korean NCAP high performance value as 100% (which is 5% probability of AIS 3 injury) [5], individual relative injury percent values were charted in figure 14.

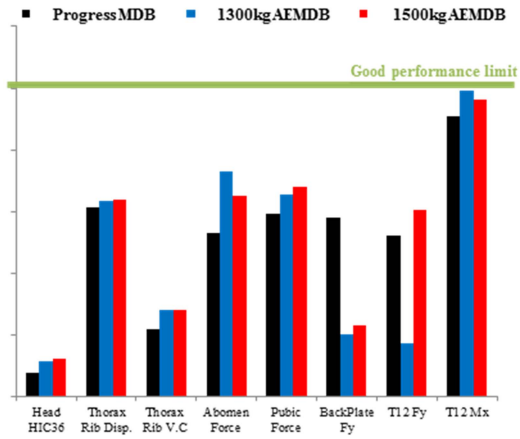

(a) Large-size car

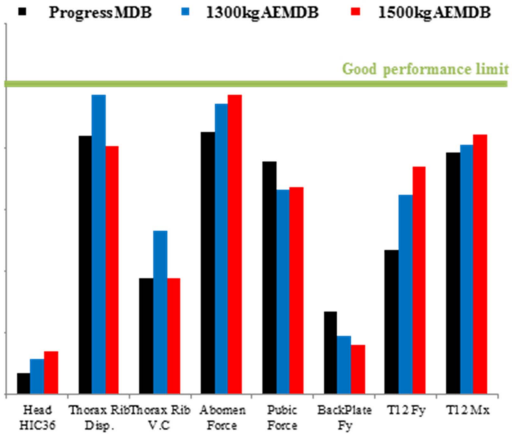

(b) Mid-size car

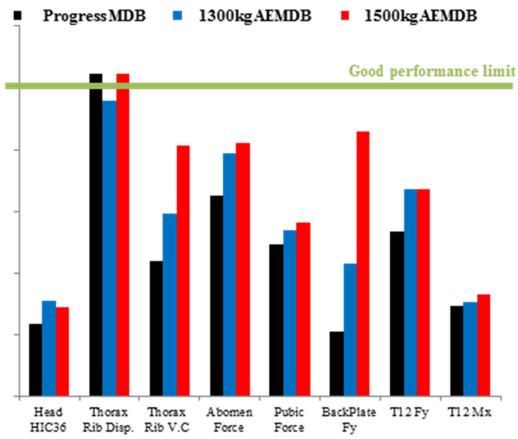

(c) Small-size car

Figure14. Front driver ES2 dummy relative injury value based on Korean NCAP high performance value as 100%

In chest injury, lower rib deflection was the worst case value in progressive MDB but upper rib deflection is the worst case value in AE-MDB. Moreover it has 2nd peak during the time between 50ms and 70ms and maximum injury value was occurred at that time. It was caused by the side airbag bottoming out due to higher vehicle speed and intrusion at initial impact time. A side airbag that stayed inflated longer could potentially improve occupant performance.

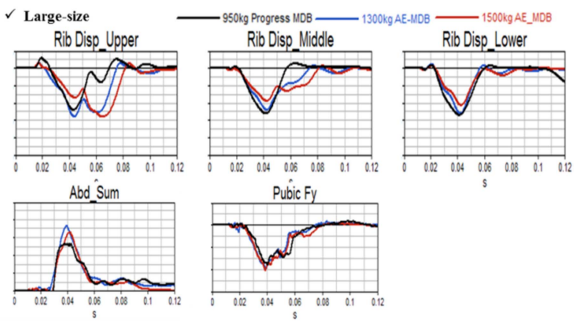

(a) Dummy injury in large-size car

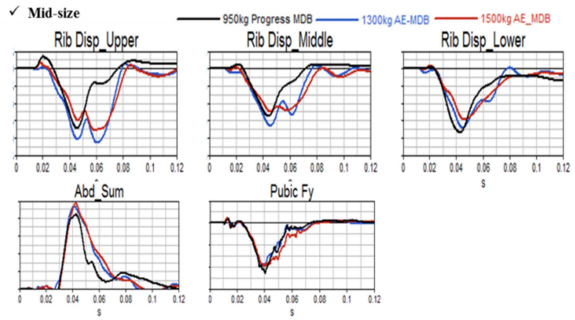

(b) Dummy injury in mid-size car

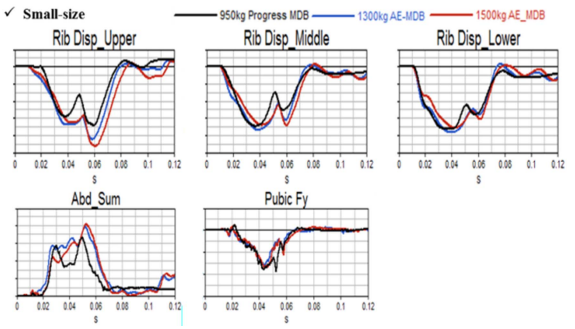

(C) Dummy injury in small-size car

Figure15. Front dummy injury pulse

In abdomen and pelvis, the AE-MDB test result was more severe than the progressive MDB especially in the abdomen area. The heavier weight of the AE-MDB and the stiffer AE-MDB bumper, which is 50mm shorter than the progressive MDB bumper, produces a faster initial B-pillar velocity and leads to earlier contact and bottoming out of side airbag. It causes higher abdomen, pelvis and 2nd peak rib deflection injuries.

2) Rear passenger seat dummy

In the rear passenger seat, a SID2s dummy was positioned. Among the tests, there is no comparable data so the AE-MDB test injury results were evaluated by using IIHS injury limit[6] in figure 16 except femur injury which is not considered in this present study.

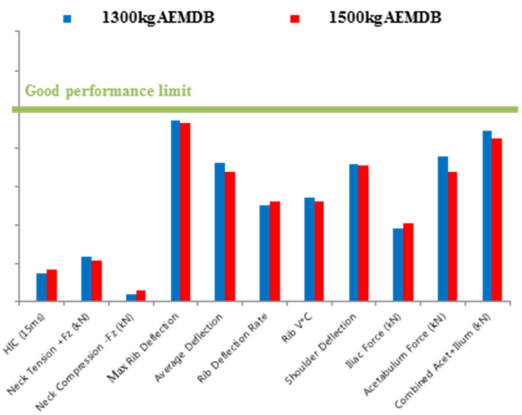

(a) Large-size car

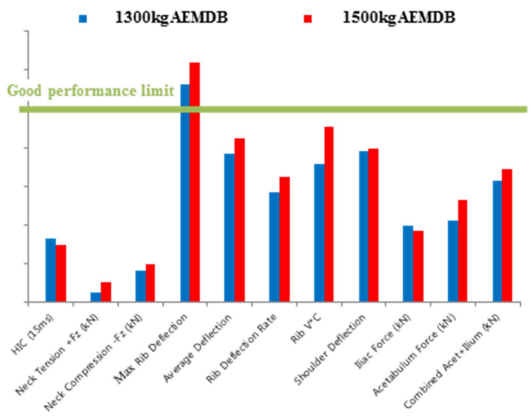

(b) Mid-size car

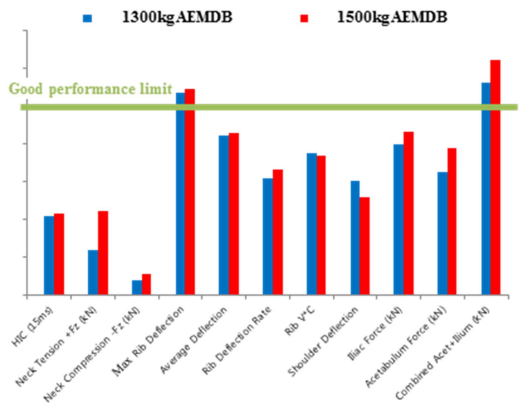

(c) Small-size car

Figure16. Rear passenger dummy injury value based on IIHS good performance limit as 100%

In the thorax area, IIHS considers only average rib deflection as 34mm for a good performance rating but this study considered not only average rib deflection but also maximum rib deflection value with a good performance limit of 34mm. In large-size and mid-size vehicles, maximum rib deflection was the highest injury value and in small-size vehicle maximum rib deflection and combined acetabulum and ilium force were the highest injury values. In mid-size and small-size vehicles rib deflection, deflection rate and viscous criteria were increased, especially in maximum rib deflection in thorax ribs, but still had a good performance rating in average rib deflection. Shoulder rib deflection also increased significantly in all of the cars; mid-size and small-size cars.

In pelvic area, iliac and acetabulum force increased with small-size vehicle. Iliac injury is the most increased value and then the total pelvic force was largely increased. This result made small-size car rating downgraded to acceptable in 1300kg and marginal in 1500kg AE-MDB although mid-size car still had good performance without a rear side airbag. This result could relate to the mid-size car being more spacious and having a larger seat bolster which is better to protect pelvic area.

DISCUSSION

1) In AE-MDB tests, the injury values measured in front driver ES2 dummy was higher than progressive MDB. AE-MDB brings the vehicle structure higher intrusion speed although B-pillar and outer door measuring data indicate less intrusion than progressive MDB. It caused airbag bottoming out and chest, abdomen and pelvic injury area increased. The target vehicles used in this study have high strength material for the B-pillar structure which can help reduce the B-pillar structure intrusion.

2) In rear passenger SID2s dummy, there was no injury data from the progressive MDB testing to compare to the AE-MDB test results. Thorax and pelvic injury area were higher than good performance limit of IIHS injury in the AE-MDB tests of the small-size vehicle. C-pillar intrusion in the AE-MDB tests was much higher than in progressive MDB tests. As well as the B-pillar structure, The target vehicles which were used in this study have high strength material for C-pillar reinforcement and also have no ruptures in this area.

3) In this study, the target vehicles are mid-size and small-size segment cars. The smallest vehicle had the highest injury values for both front and rear seat occupants. But mini-size cars have not yet been studied and more study considering the mini-size car is needed.

CONCLUSIONS

The AE-MDB barrier is heavier and positioned 250mm rearward in than the progressive MDB and contacts the vehicle rear wheel house area. The further rearward impact point reduces B-pillar deformation assuming that the B-pillar, C-pillar and rear wheel house area do not rupture. The heavier weight of the AE-MDB increases deformed structure velocities leading to higher injury values. Nevertheless, the test results showed similar front driver occupant injury values. The 2nd peak in the driver chest deflection curves in the AE-MDB tests(50ms~70ms) is caused by bottoming out of the side airbag due to the higher intrusion speeds. To improve this performance, the side air bag should potentially have a longer deployment duration or additional energy absorption capability. For the rear passenger dummy, the AE-MDB produces a more severe impact to the thorax and pelvic areas due to higher intrusion speeds. In the large-size and mid-size vehicles, occupant injury values met the IIHS "Good" occupant performance criteria, but not in the small-size vehicle. A rear side airbag or energy

absorbing system could be helpful to improve rear passenger's thorax and pelvic injuries, especially in small-size vehicles.

Globally, the trend is that the ES2 dummy will be replaced with the World SID dummy. World SID dummy has wider chest and pelvic area, which could reduce the space that the side airbag has to absorb the impact energy. A future study using the World SID dummies in these test configurations is recommended.

ACKNOWLEDGEMENT

This study project was carried out under contract between the Ministry of Land, Transport and Maritime Affairs and Korea Automobile Testing & Research Institute.

The authors are indebted to Mr. Chang Hyungjin and Kim Deaup, Korea Automobile Testing & Research Institute (KATRI), for their valuable assistance in the moving deformable barrier-to-car tests.

REFERENCES

[1] Ministry of Land, Transport and Maritime Affairs, Korean New Car Assessment Program, www.car.go.kr

[2]Advanced Protection Systems (APROSYS) EC 6th Framework Project FP6-PLT-506503 www.aprosys.com

[3]Marie-Laure Roussarie, 'Enhancement of side impact protection using an improved test procedure', 20th International Technical Conference on the Enhanced Safety of Vehicles (ESV), Paper number 07-0245

[4] Doyup Kim, 'Characteristics of Vehicle Structure Deformation and Body Injury caused by Side Impact Test Using AE-MDB', Annual Conference Proceedings, KSAE

[5] KNCAP high performance value which is 5% probability AIS3'

[6] Insurance Institute for Highway Safety, IIHS

A STUDY ON ENERGY ABSORPTION CHARACTERISTIC AND HEAD INJURY PERFORMANCE ACCORDING TO THE CHARACTERISTIC OF COUNTERMEASURES AND SPACE BETWEEN INTERIOR AND BODY STRUCTURES

Jongsoo Lim
GM Korea
Republic of Korea
Sungbin Park, Jaewoo Lee, Dongseok Kim
GM Korea
Republic of Korea

ABSTRACT

It is important to adopt proper countermeasure strategies, i.e. energy absorbers (EA), in order to meet the Upper Interior Head Impact requirements of FMVSS201 S6.2 (FMVSS201U) which assesses head injury by impacting a Free Motion Headform (FMH) to upper interior parts. The understanding of the energy absorbing characteristic for each kind of countermeasures is a stepping stone to optimize the head injury performance. This paper reviews general features of foam and plastic types of countermeasures with respect to raw material and manufacturing process, and highlights merits and demerits from the point of view of design flexibility. Energy absorbing characteristics based on static component crush testing are considered and these characteristics are also compared quantitatively by investigating energy absorbing efficiency of the countermeasures.

Lastly, sensitivity analysis is conducted to study the relationship between the space and head injury performance according to types of energy absorbers using finite element analysis (FEA).

Range of Types of Energy Absorber to be Considered

Types of foam and plastic energy absorbers are mainly used as a countermeasure for improving FMH performance, and EA countermeasures that use metal such as corrugated tubes and stamped sheet metal are excluded from this paper.

Categorizing EA as raw material and manufacturing process

There are mainly two kinds of foams, molded type and expanded. An example of the former is Polyurethane (PU) foam that is mixed and injected directly into a mold. The final products are obtained after curing in a high temperature oven.
For the latter case, using polystyrene as a raw material, the manufacturer provides a fixed size of plank by expanding process then final products are obtained by wire cutting the plank as its shape.
In addition, there are other types of EAs using plastic resin as a raw material and adopting thermoforming or injection molding as the manufacturing process. In the thermoforming process, desired EA structures are procured by heating up a sheet of polypropylene plastic, for example, then vacuum forming over a die. The final component is then die cut to the final shape. Lastly an energy absorber that has thin walled structure, usually lattice shape, is obtained by conventional injection molding process using polypropylene or other plastic resins.

In the following sections, the merits and demerits of each EA countermeasure type are reviewed.

Type 1. Molded PU Foam
The design flexibility of final parts is one of the merits of molded PU foam as a result of the molding process. Mechanical properties are generally uniform throughout the part. Prototype parts may be cut or machined from larger molded blocks without necessitating prototype tooling. However PU foam does have limited range of crush load, as compared to other EA countermeasures. In addition, when the mold tooling is set, modification of the tooling is limited.

Type 2. Expanded Polystyrene Foam
A significant advantage of expanded Polystyrene is that it provides high energy absorbing efficiency and stable crush properties along the axis of extrusion. The wire cut process requires no tooling to produce final production parts. However complex 3D geometry is not feasible with a wire cut process. In addition, the cost per part is dependent upon the number of parts cut per plank. The number of parts obtained per plank is highly dependent on the part size and geometry. Therefore, the cost per part can significantly increase as overall part yield decreases.

Type 3. Thermoformed Plastic
In contrast with the molded foam type of EA, thermoformed plastic geometries can provide a good range of crush load. The typical forming process,

vacuum forming, has positive and negative design attributes. The process enables various nominal thickness of the raw sheet material with minimal tool changes. However, this process does have limits in the amount of curvature of the base geometry. In addition, the variation of thickness in height direction is not uniform so the exact thickness distribution must be estimated or measured off or tooled parts.

Type 4. Injection Molded Plastic

Like the thermoformed plastic, injection molded EA countermeasures also have a range in adjustment of crush load and very little limitation on parts design except manufacturing requirements such as minimum thickness and draft angle. But tooling needs long lead time, carving the tool into the shape of lattice is time consuming work, and tool modification is very restricted.

The summarized characters for each kind of EAs are summarized on the Table 1. And typical shapes of each type of EAs are shown in figure 1.

Table 1.
Summary of EA as raw material and manufacturing process

	Type 1	Type 2	Type 3	Type 4
Raw Material	PP/EPP	Poly-styrene	PP	PP/ABS
MFG Process	Molding	Extruding & Wire cut	Thermo-forming	Injection Molding
Tooling Lead time	'+'	N/A	'0'	'-'
Flexibility Medication of Tooling	'0'		'0'	'-'
Flexibility Part design	'+'	'-'	'0'	'+'

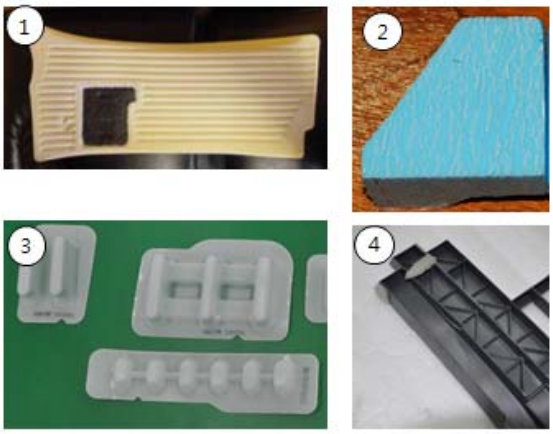

Figure 1. Types of Countermeasure
1. Molded PU Foam, 2. Extruded Poly-styrene Foam, 3. Thermoformed Plastic, 4. Injection Molded Plastic

Energy Absorbing Characteristics and Efficiency

To examine energy absorbing characteristics of the four types EAs, quasi-static crush tests were performed. The size of the test specimen for type 1 and 2 are 30x30x50 (mm) and 30x30x60 (mm), respectively. Figure 2 shows nominal stress and strain. Both EAs show densification. Stress increases quickly as the foam becomes dense at 0.68~0.78 range of strain. We define a design stress, as a stress level whose value is maintained steady state. Type 1 has 20% variations, while type 2 has 70% variations in both product families. This means that type 2 EA gives more options to choose from a crush load perspective.

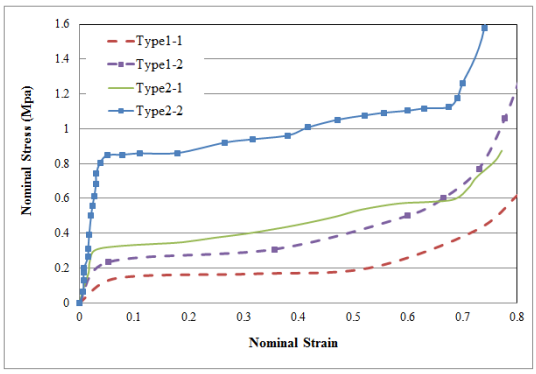

Figure 2. Nominal Stress vs Strain (Type 1, 2)

Figure 3 shows the energy absorbing feature of plastic EA's (type 3 and 4) crushed with a rigid plate. The crush loads are normalized with each peak force and are considered to identify the energy absorbing characteristic for the case of the EAs that do not have uniform cross sections.

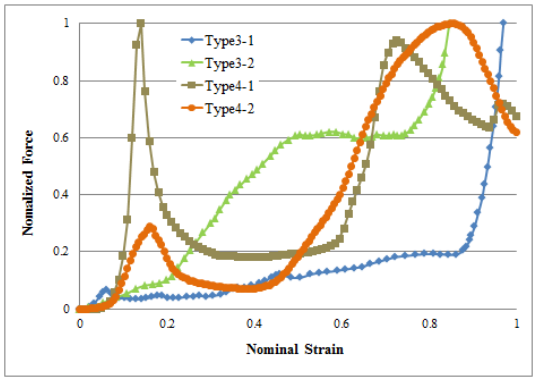

Figure 3. Normalized mean force vs Strain (Type 3, 4)

Critical strains at densification and design forces can vary drastically according to its geometry, even for the same types of EA. Type 4 shows a characteristic that exhibits a high force level at the beginning of deformation and then decreases by more than 50%

when fracture occurs.

Until now it has been observed that EAs have their own crush characteristic according to their raw material and geometry; therefore, it is necessary to evaluate the characteristic quantitatively. In previous research, G.G Lim et al. suggested Pulse Waveform Efficiency defined as a ratio of maximum to net area of a load-displacement curve derived from deceleration and time, shown in equation 1. The concept defines the efficiency; however, it gives only the ratio of total absorbed energy to an ideal amount; it does not explain the relationship between the efficiency and the amount of deformation, that is when maximum efficiency is achieved and the densification occurs as a part is deformed.

So equation 2 and 3 show the definition of modified parameter in terms of stress and strain, and equation 2-1 and 3-1 in terms of force and strain. Equation 3 and 3-1 show that the design values are updated with current ones if the current values exceed initial design ones. The efficiencies calculated based on equation 3 or 3-1are show in figure 4 for each type of EAs.

$$\eta_1 = \frac{\int_o^{t\,max} f\,du}{f_{max} u_{max}} \qquad (1).$$

$$\eta_modi = \frac{\int_o^t \sigma_{design} d\varepsilon}{\sigma_{design} \cdot \varepsilon} \qquad (2).$$

$$\sigma_{design} = \sigma \; if \; \sigma_{design} \geq \sigma \qquad (3).$$

$$\eta_modi = \frac{\int_o^t f_{design} d\varepsilon}{f_{design} \cdot \varepsilon} \qquad (2\text{-}1).$$

$$f_{design} = f \; if \; f\sigma_{design} \geq f \qquad (3\text{-}1).$$

Type 2, having rectangular cross section with polystyrene, shows good energy absorbing efficiency. More than 60% of its efficiency is reached within 0.11 strain, and the efficiency continues to increase to 80% until 0.67 range of strain. Meanwhile the maximum efficiency and the critical strain of type 1 are 80% and 90% compared to type 2 EA's, respectively under the same cross section condition.

Type 3, adopting thermoforming process using PP as raw material, shows various energy absorbing behavior according to its structures and 35 to 39% level of efficient until 0.6 strain range. Type 4 also shows a wide range of behavior similar with type 3 EA. The maximum efficiency is reaches 47 to 60% of strain.

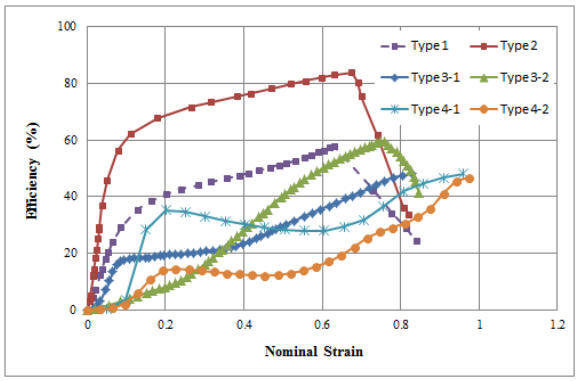

Figure 4. Energy of Absorbing Efficiency acc. to types of EAs

Considerations on the Efficiency

The efficiencies in figure 4 show only examples of each type of EAs with similar cross sections to introduce energy absorbing efficiency so the behaviors and efficiencies do not fully represent the full range of each type of EA countermeasure.
And the efficiency does not explain the absolute value of crush load, which is an important factor considering head injury performance because it is expressed as ratio. These factors, geometry and crush load of EA, are considered on the following topic.

Reviewing FMH behavior and Sensitivity Study with Full Vehicle CAE Analysis

Head injury and head form behavior are compared for 6 cases of EAs on a B-pillar upper roof area as per the protocol of FMVSS 201u with LS-DYNA 971 r511. Case 1 through 4 have same figure of solid block while case 5 and 6 have thin walled structure, however, all cases have the same coverage volume. The load deflection characteristic and efficiency are shown in figure 6 and 7. This crush characteristic of each EA is obtained with rigidly modeled FMH under the same condition of FMVSS201u testing. An example of the setting up configuration is shown on figure 5.

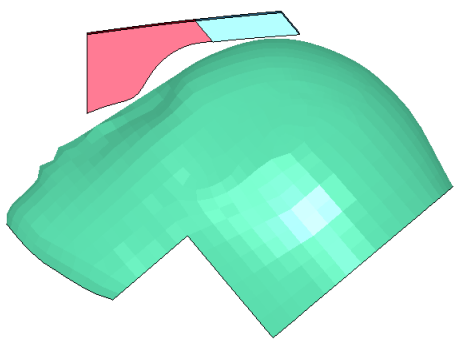

Figure. 5 Configuration for crush characteristic analysis

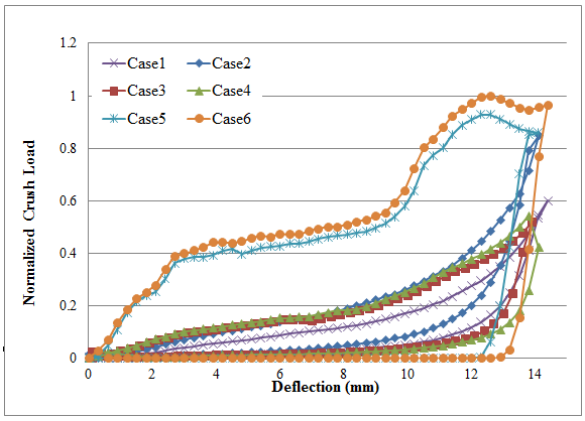

Figure. 6 Normalized crush load and deflection characteristic

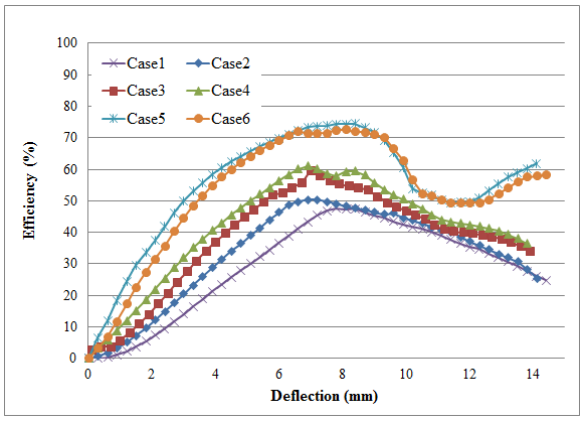

Figure. 7 Energy Absorbing Characteristic

EAs of Case 5 and 6 EA show higher energy absorbing efficiency and also higher crush load than the other cases as shown in table 2. But the foam, FMH in case 6 has the least amount of intrusion due to high crush load and results in a higher HIC(d) result. Table 2 shows normalized HIC(d) response according to efficiency and crush load.

Table 2. HIC(d) according to types of EA

	Mean Efficiency	Crush Load (%)	HIC(d) (%)
Case 1	21.6	23.3	110
Case 2	24.7	27.6	104
Case 3	31.2	27.6	101
Case 4	30.	32.0	100
Case 5	52.7	82.9	101
Case 6	49.3	100	113

To investigate head injury variation in reducing countermeasure space for the types of EAs, a sensitivity study is performed. The space is reduced by 25% and 50% to current gap by offsetting head liner surface. To minimize re-modeling of head liner, only the forehead area of surface is modified. Figure 8 shows the profile of modification. The impact conditions such as the position of FMH and impact location is adjusted as the headliner offset as per FMVSS201u targeting process. The height of EAs are also modified to accommodate the gap

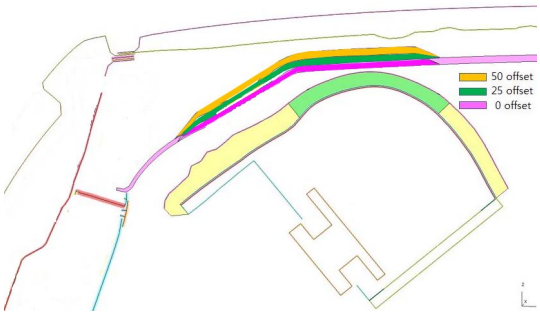

Figure.8 Section of Vehicle lateral direction

Table3. HIC(d) variation according to Energy Absorbing Space

	Baseline (0 offset)	25% offset	50% offset
Case A	100	110	116
Case B	100	116	126
Case C	100	122	134
Case D	100	123	143

Foam types of CMs, case A and B, show less variation than plastic types', case C and D. The case D, which has thin walled structure shows up to 43% more sensitive response than the others.

CONCLUSION

1. Manufacturing process and advantages and disadvantages in accordance with the process are reviewed for foam and plastic type of energy absorbers as a stand point of FMVSS201u.
2. Energy absorbing efficiency is presented as a parameter to evaluate load-deflection characteristic of examples of each type of EA countermeasure.
3. Energy absorbing efficiency and crush load should be considered together when assessing head injury performance.
4. Plastic type of EA shows sensitive response as the countermeasure space reduced.
5. This study has a limitation as below and further studies are required to cover the below topics;
 - Many different design elements affect the energy absorbing characteristic such as various geometry, wall thickness and wall pattern and are not fully considered in this paper.
 - The phenomenon that different efficiency and

crush load achieve similar HIC(d) values is not fully explained and does require further study.

References

1) Federal Motor Vehicle Safety Standard :49 CRF PART 517) "FMVSS 201u - Occupant protection in interior impact"

2) G. G. Lim, C. C. Chou, R. N. Patel, S.A. Shahab, and P.J. Patel "Estimating the Minimum Space to Meet Federal Interior Head Impact Requirement", SAE 950333

3) LS-DYNA User's Manual, Version 971, Livermore Software Technology Corporation (LSTC), May 2007.

REDUCING ALL TERRAIN VEHICLES (ATVs) INJURIES AND DEATHS - A WAY AHEAD

George Rechnitzer
Raphael H. Grzebieta
Andrew S. McIntosh
Keith Simmons
Transport and Road Safety (TARS) Research, University of NSW
Australia
Paper Number 13-0213

ABSTRACT

The use of ATV's both recreationally and in the workplace (particularly on farms in Australia), continue to be major contributors to fatal and serious injuries both in the USA and Australia.

This paper firstly presents the findings from the authors' 2003 study into ATV safety and potential countermeasures [1], and secondly, some 10 years later, leads into the current major test program being undertaken for the WorkCover Authority of NSW on ATV (Quad Bikes and Side by Side Vehicles) stability and crashworthiness at UNSW.

The 2003 study was carried out at the request of the Victorian WorkCover Authority and the State Coroner to provide a review of previous research relating to ATV fatalities and serious injuries and to examine the feasibility of fitting effective occupant protection systems, particularly regarding rollover.

While current prevention strategies continue to focus on lower order risk controls such as rider training and administrative controls, the authors consider that the very successful passenger vehicle NCAP type test and rating program could also be applied to improve ATV safety.

INTRODUCTION

Advances in vehicle safety have had a much checkered history, with periods of significant resistance to safety development, followed by major and profound advances. This is well illustrated by advances in automobile safety on many fronts: moving from largely a 'blame the driver' approach to a holistic 'safe system approach' bringing together 'safe drivers on safe roads in safe vehicles' [2].

Moving on from the days of Ralph Nader's revolutionary critique of auto safety in 1965 'Unsafe at any Speed' [3] onto the USA FMVSS auto standards in the early 1970's and then onto NHTSA's creation of NCAP in 1979. As quoted in the history of NCAP [4] "*In 1979, NHTSA created the New Car Assessment Program (NCAP) to improve occupant safety by developing and implementing meaningful and timely comparative safety information that encourages manufacturers to voluntarily improve the safety of their vehicles*".

The NCAP program has been successfully adopted in many regions including Europe, Australia, Japan and Asia, for example.

No one involved in transport safety can be in any doubt of the dramatic improvements in vehicle safety and crashworthiness, from the high road toll decades of the 1960's and 1970's to the much lower tolls in the developed world in the 1990's through to the current decade. Many vehicles now have multiple airbags, greatly improved crashworthy structures and handling assistance (ESC, pre-brake, etc.).

Notably, however, through this time the auto industry, in many cases (with well known notable exceptions, of course) seemingly and often actively resisted development and implementation of many safety technologies which are now not only standard but ubiquitous (e.g. airbags). Yet, today the auto industry can proudly boast of its great technological and safety advances, and the great benefits in terms of reduced community trauma.

Thus advances in safety were not inhibited by lack of engineering know how, but rather by lack of 'will' or incentive. Incentives for the auto industry have come in many forms, e.g. regulations (mandatory national vehicle safety standards), comparative consumer testing (NCAP), market competition, and perhaps even product liability litigation.

Of particular significance was the requirement for vehicles to meet minimum crashworthiness 'performance' standards based on set injury

criteria, such as in FMVSS 208 frontal impact standards, offset frontal impact and side impacts.

Handling improvements such as ABS and ESC (and all types of other driver assist systems) complement the improved vehicle crashworthiness through crash prevention measures.

And of course measures relating to improved driver action (drink driving); speed enforcement and road design all contributed significantly, and form part of the safe system approach to road safety [2].

This leads to consideration of the current status of ATV safety, the decades long apparent 'impasse', and in the author's opinion, a possible way ahead.

Before presenting material on ATV safety, some discussion is necessary concerning the use of the terminology 'All Terrain Vehicles'. In Australia, the term for vehicles commonly used on farms over rougher terrains is Quad Bikes (Figure 5) or Side by Side Vehicles (Figure 8) depending on their size and farming task. Both an Australian Coroner and US Consumer Product Safety Commission have indicate that the term all terrain vehicles (ATV) is misleading and may result in false assumptions as to the terrain that Quad Bikes can safely traverse [5,6]. Nevertheless, while the authors sympathise with this perspective, throughout this paper the term ATV will be used to represent Quad Bikes unless otherwise indicated in the text that the ATV vehicle is a Side by Side.

ATV SAFETY - AN OVERVIEW FROM THE 2003 MUARC STUDY

The follwing summary is taken from the MUARC study [1].

This study was carried out at the request of the Victorian WorkCover Authority and the State Coroner with the aim of presenting a review of previous research relating to ATV fatalities and serious injuries and to examine the feasibility of fitting effective occupant protection systems, particularly regarding rollover.

The study involved three main activities:

1. A review of the epidemiology of ATV related fatalities and serious injuries in Australia, USA, UK and New Zealand;
2. A detailed literature review examining previous research on ATV safety and proposed improvements to handling and fitment of Rollover Protective Systems;
3. The design and evaluation of a proposed Rollover Protective System (ROPS) comprising a protective structure and occupant restraint system (seat and 4-point seatbelts), considering both moderate and severe lateral rollovers.

The main findings from the study were:

- ATV rollovers are the major cause of fatalities in Australia, with crushing of the rider by the ATV, or ejection with impact with the ground or objects being the primary injury causal mechanism. Most serious incidents occur in agricultural settings.

- ATVs although based on motorcycle structures with two extra wheels added, have significant differences in handling, usage and collision modes. Despite these major differences, ATV safety philosophy retains and promotes, *quite inappropriately*, a motorcycle based and rider-centred perspective on safety, rather than a vehicle one. That is, ATV safety is considered to depend on rider separation from the vehicle and the addition of protective clothing and helmet. Simply put, such safety philosophies are ill conceived and dangerous for ATV riders. They do not offer any protection in the most common modes of injury with ATVs – rollovers, nor collisions.

- The design of ATVs in terms of their short wheel base, relatively narrow track and high centre of gravity positions, and lack of a differential, result in adverse handling characteristics, which are intended to be compensated by active-riding techniques. Such techniques require shift in position of the rider's body to increase stability during manoeuvring. Stability analyses of the benefits of active riding show these to have quite limited benefit (about 20% or less), and overall would appear to be overrated as a means of enhancing the control of ATVs.

- Virtually all of the previous international research on fitting Rollover Protective Systems on ATVs to date has been predicated on having an unrestrained (or ineffectively restrained) rider so as to maintain active riding. This has

led to Protective Structure designs with very poor effectiveness and in many cases designs that could well increase severe injury risk. Similarly, the Rollover Protective Structure designs suggested through the New Zealand (NZ) ROPS guide and those of United Kingdom Health and Safety Executive (UK HSE) are ill conceived, totally inadequate, indeed dangerous, as they provide inadequate survival space and do not require proper restraint systems.

- To ascertain the benefits and feasibility of fitting an effective Rollover Protective System, three crash scenarios were modelled, with and without the Rollover Protective System. The first scenario was an ATV travelling at 7km/h across a 30-degree slope in which the ATV rolls due to hitting a rock. The second scenario involved the ATV travelling at 30km/h across a 30-degree slope and rolling due to hitting a rock. The third scenario was the same as the second, but with the ATV travelling at 20km/h. In the case of the ATV without the Rollover Protective System, in the first scenario, the ATV rolled onto the rider, and in the second and third scenarios the rider was ejected striking the ground resulting in severe injury levels (fatal in the 2nd scenario). In the three scenarios where the ATV was fitted with the Rollover Protective System, the occupant received low injury levels.

- It is possible to design a practical rollover protection system for an ATV that will protect a rider against serious injury in a rollover, and other collision modes. Such a system requires a lightweight but high strength structure that protects the occupant survival space, together with a high backed seat with side bolsters, and seatbelt system to effectively restrain the occupant within the protected zone.

- The provision of Rollover Protective Systems on currently designed ATVs will result in reduced stability. To regain the original stability ratings, such ATVs would require either increased track width or lowering of centre of gravity height.

Comments on MUARC study and ATV ROPS

The MUARC report proposed a ROPS system for ATVs as shown in Figure 1. This was based on fundamental crashworthiness principles on what would be required *ideally* for effective rider protection both in a rollover and in collisions. From this perspective, the deficiencies of other ROPS systems such as the rear single post or similar (as in NZ) were considered by the authors at the time as quite deficient, and even potentially dangerous.

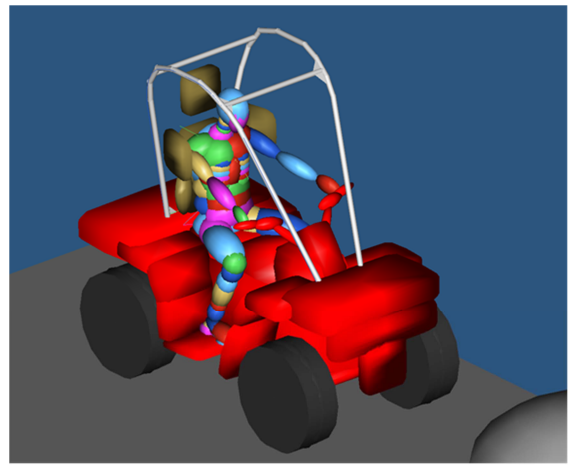

*Figure 1***.** Proposed MUARC ROPS for ATV, with 4-point seatbelt;winged seats. MADYMO model analysis.

While such a perspective may have appeared justified at the time, in hindsight, a more incremental approach based on 'harm minimisation' now appears to be pragmatically more appropriate. The 'all or nothing' approach does not reduce injuries in the interim. For example, 2-post ROPS were encouraged to be retrofitted to older tractors in Victoria without seatbelts being mandated also - despite the knowledge that a risk of ejection from the tractor with out seatbelts was still possible. Overall, this would be regarded as an effective pragmatic safety outcome for older tractors [7].

On the other hand the MUARC ROPS (and indeed any ROPS) was also strongly opposed by the ATV industry, and regarded by them as being more injurious than not having such a system. Such a claim was based on computer simulations by Zellner et al, and strongly questioned by the authors and others [8-10]. The industry still opposed ROPS and CPDS (Crush Protection Devices) of all types claiming these do more harm than good [11, 12].

ATV INJURY

Lower et a [13] presented data on the 127 quad bike deaths in Australia between 2001 and 2010:

"*It examines differences between causes of death occurring through use of the machine in farm/non-farm settings and during work/non-work operation. Data were extracted from the National Coroners' Information System (NCIS). In total, 65% of fatalities occurred on-farm, with 45% of incidents being work-related and 46% involving rollovers of the quad bike.*"

They report notes that "*A study of trends in farm deaths in Australia found that while deaths from tractor rollovers had decreased by 74% between 1982–84 and 2001–04, deaths associated with quad bikes had increased nearly 13-fold. … Massive increases in occupationally related incidents have also been reported in the United States of America (USA)*".

Lower quotes USA data "*Between 2000 and 2007 in the USA there was an average of 723 deaths per annum attributed to quad bike use.*"

In regard to injury mechanisms, rollovers predominate [13]: "*Analysis of the nature of the crash event highlights the leading mechanisms of injury as: collision with stationary object (34), rollover with no load or attachments (33), collision with other vehicle (10) and rollover with spray tank (9). Rollover of the quad bike attributed to 46% of all deaths where the mechanism of injury was known. Additionally, where the work status and mechanism were known, rollovers accounted for 58% of deaths.*"

The report identifies the incidence of thorax injuries and asphyxia in rollover cases, and the potential benefits of Crush Protection Devices [CPDs] for prevention: *The significant variation in the primary cause of death between rollover and non-rollover events is a crucial finding. With 53% of rollover deaths involving the thorax, asphyxiation and drowning alone, the potential benefits of any crush protection device to prevent entrapment are clearly apparent. In addition, it can be reasonably contended that a sizeable number of head (24%), neck (14%), abdomen (4%) and multiple injuries (4%) incurred in rollovers could be averted by such a device".*

ATVS and CRUSH PROTECTION DEVICES

In response to the incidence of fatal and serious injury rollovers involving ATVs, and lack of any industry response to provision of rollover protection systems on ATVs (who maintain that such systems are hazardous), CPD systems have been developed by Trax LifeGuard (Figure 2 and 3) [14], and Quadbar (Figue 4) [15].

Figure 2. TRAX LifeGuard CPD system [14].

Figure 3. TRAX LifeGuard CPD system, showing deformable characterstics [14].

Figure 4. Quadbar CPD system [15].

While in principle it is clear that such systems will have a protective benefit, it is also clear that they cannot be effective in all rollover situations, as ejection still occurs and crush by stiff areas on

the ATV may still result. The research on the level of effectiveness has yet to be done.

Industry criticism of CPDs

Most ATV manufacturers have strongly opposed the introduction of CPDs or other ROPS systems: "*Australia's peak body for the automotive industry, the Federal Chamber of Automotive Industries (FCAI) together with the Australian All Terrain Vehicle (ATV) industry, comprising the leading distributors, have today called for proposals for the use of rollover devices on ATVs to be rejected.*" [11]

The FCAI statement notes that "*Reports released last week by Dynamic Research Inc. (DRI), an internationally recognised firm specialising in applied research in the areas of vehicle dynamics and controls, simulator technology and accident investigation, confirmed that Rollover Protection Systems (ROPS) and Crush Protective Devices (CPDs) on ATVs can cause unacceptably high levels of harm in comparison to their benefits.*

Updated research into one type of locally-produced CPD found that it caused more harm than it prevented in the sample of overturns examined, regardless of whether a helmet was worn"

The referenced report by Zellner et al [8] involved "*Approximately 3,080 computer simulations were run, with the baseline ATV and the Quadbar ATV, using 110 "low energy" overturn types, and six additional variations of each overturn type in order to reduce the sensitivity of the results to the details of any single overturn type, for the helmeted condition and for the unhelmeted condition.*"

The report concludes that: "*The overall updated results were that in the helmeted condition the Quadbar had an injury risk/benefit percentage of 108% [69%, 168%]; and a fatality risk/benefit percentage of 134% [79%, 219%]. ….. In extending this sample estimate to the population of overturns, these confidence intervals indicate that the injury risks and fatality risks of the device are not statistically significantly different from the injury benefits and fatality benefits of the device, respectively, i.e., for the population of overturns, the Quadbar would cause approximately as many injuries and fatalities as it would prevent.*"

Of course there have been significant criticism and disagreements with the methodology used in such analysis by Zellener et al and others, and indeed vice-versa [9, 10, 12, 16-18].

Thus it appears there is little agreement on the way forward in improving ATV safety, particularly in regard to rollover [11]. The industry position remains focused on rider training, administrative controls and PPE: "*Unfortunately, while the focus remains on rollover devices, real solutions will continue to be ignored. Attention should instead be maintained on helmet use, training and keeping children off full-size ATVs.*"

In contrast, users of ATVs and farm industry groups and safety regulators, and safety researchers, see from the history of safety advances in transport that design countermeasures are possible but that the ATV industry continues to negate promotion of or indeed adequately research any solutions.

Hence the decades long impasse on advancing ATV safety, and the need for a new approach, is set out in this paper as a way ahead to reduce ATV trauma.

THE CURRENT QUAD BIKE AND SIDE BY SIDE VEHICLE PERFORMANCE TEST AND RATING PROJECT

To help over come this 'impasse' in progressing ATV (Quad Bike) safety, The WorkCover Authority of New South Wales (Australia) has funded the *Quad Bike Performance Project*. This major project is also strongly supported by the State Government of New South Wales (NSW), and is based at the Transport and Road Safety (TARS) Research unit at the University of NSW, with the project led by the authors of this paper. The project commenced in September 2012, with completion towards September 2013.

The Project aims are:

1. Establishment of stability ratings and crashworthiness ratings for the selected Quad Bike models;
2. Development of an NCAP type testing and rating system (NQDAP) for rollover stability and rollover crashworthiness.

The main project stages are:

1. Selection and purchase of 15 new representative Quad Bikes and SSV (Side by Side Vehicles) as shown in Figures 5 to 9;
2. Biomechanics analysis: further detailed identification of injury mechanisms related to rollover, especially crush and asphyxiation; and development of related crashworthiness test methods;
3. Series of static stability tests for lateral rollover and forward and rearward pitch, based on tilt table tests, with and without rider (Hybrid III Anthropomorphic Crash Test Dummy: ATD); and with typical fitment and combinations of accessory loads on the front and rear. Effect of a selected sample of CPD (crush protection type devices) on stability will also be tested [see Figure 10];
4. Series of crashworthiness tests related to lateral rollover and front and rear pitch, to determine serious injury risk with and without CPDs;
5. Establishment of stability ratings and crashworthiness ratings for the selected Quad Bike and SSV models;
6. Development of an NCAP type testing and rating system New Quad Assessment Program (NQDAP) for rollover stability and rollover crashworthiness.

In addition the project is currently seeking additional funding to include dynamic handling tests as part of the stability evaluation and include such performance in the NQDAP rating. Improvements in Quad Bike and SSV handling has been highlighted by authors such as Roberts [19] and others as being practical means to reduce crash and rollover risk.

The testing program is being undertaken at the Crashlab test facility in Sydney, Australia.

The vehicles selected for testing include eight Quad Bikes typically used in the work place, particularly on farms [see Figures 5 & 7], three sports/ recreational type Quads [see Figure 6], and four side by side utility style off-road vehicles used in the workplace/farms [see Figures 8 & 9]. The three sports/recreational Quads were added to the project and funded by the Australian Competition and Consumer Commission (ACCC).

In addition to the multi-disciplinary research team undertaking the project, the project is also supported by a highly experienced Project Reference Group, which includes a worldwide range of experts in Quad Bike vehicle safety issues. The Reference Group includes ATV industry representatives, farming groups, safety regulators, university researchers, and safety consultants.

Figure 5. One of the "workplace' Quad Bike at Crashlab.

Figure 6. A sports/ recreational Quad Bike at Crashlab.

The outcome of the Project is to provide a clear 'way ahead' to improve the safety of Quad Bikes and SSV type vehicles used in the workplace /farm (and recreationally) by providing consumers with a NCAP style performance based safety rating system to help identify appropriate vehicles for their use.

Figure 7 One of the "workplace' Quads at Crashlab, with a Hybrid III ATD 'rider', and other Quad Bikes and SSVs at Crashlab.

Figure 8. One of the SSVs at Crashlab, awaiting testing.

Figure 9. Another SSV style vehicle at Crashlab.

The outcome of the Project is to provide a clear 'way ahead' to improve the safety of Quad Bikes and SSV type vehicles used in the workplace /farm (and recreationally) by providing consumers with a NCAP style performance based safety rating system to help identify appropriate vehicles for their use.

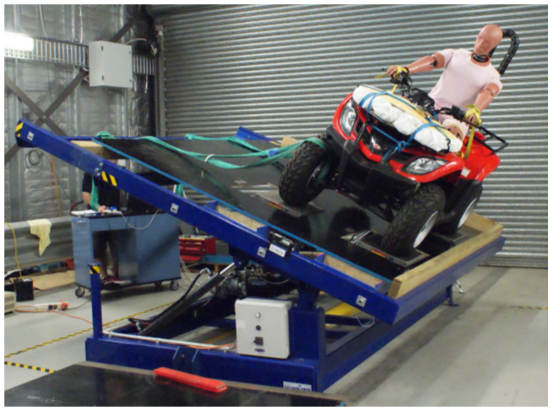

*Figure 10***.** ATV tilt table static stability test being carried out at Crashlab, UNSW-TARS project, Feb 2013. Quad Bike loaded with rider (95th % Hybrid III ATD, with front load and rear Quadbar CPD fitted.

Such a rating system is intended to help provide incentives to manufacturers and consumers to drive competition for improved safety for such vehicles, in a similar way to what has been achieved for automobile safety.

By focusing on a performance based system, rather than by prescription (e.g. prescribed fitment of CPDs), leaves open a wider range of vehicle design enhancements in relation to crash prevention (handling improvements, electronic controls, etc.) and crashworthiness (rider/ occupant protection) in a crash.

An additional further intended outcome of the Project is the development standards for improved handling and reduced risk of rollover through of performance requirements for lateral stability, and lateral, front and rear pitch crashworthiness.

CONCLUSIONS

ATV rollover crashes represent a major mechanism in fatal and serious injuries for ATV users, particularly in the farming sector.

Currently little progress has been made in reducing such rollovers incidents or severity with a strong community and regulatory push for CPD type devices which is being opposed by the ATV manufacturers as unsafe. To help overcome this impasse on improving Quad Bike safety, the authors consider that ATV vehicle safety can be improved by drawing on the successful methods developed in the NCAP programs which use crash and other performance based tests to provide

consumers with vehicle safety ratings, rather than prescriptive approaches.

This paper has outlined a major testing and rating project being undertaken at the University of New South Wales and Crashlab to develop the NQDAP (New Quad Assessment Program), and performance standards aimed at reducing the incidence and serious/fatal injury risk resulting from ATV rollovers.

ACKNOWLEDGEMENTS

The Authors would like to gratefully acknowledge: the Victorian WorkCover Authority for funding the original MUARC work; WorkCover Authority of NSW for funding the current Quad Bike Performance Project, in particular Tony Williams and Diane Vaughan for their assistance; and the Australian Competition and Consumer Commission (ACCC) for contributing funding for testing the recreational/sport Quad Bikes. The Authors are also grateful to Ross Dal Nevo, Drew Sherry and staff from Crashlab, Roads and Maritime Services, for their assistance with testing, and to Dr. Rebecca Mitchell, Dr. Tim White, Nick Pappas, Declan Patton, David Hicks and Mario Mongiardini for their assistance with various tasks including administration, data collection and technical assistance. The members of the Project Reference Group are also acknowledged for their valuable input into the Quad Bike Performance Project.

REFERENCES

[1] Rechnitzer G, Day L, Grzebieta R, Zou R & Richardson S, (2003). *All Terrain Vehicle Injuries and Deaths*, Monash University Accident Research Centre.

[2] Australian Transport Council (ATC), (2011). *National Road Safety Strategy*, 2011-2020.

[3] Nader R, (1965). *Unsafe At Any Speed: The Designed-In Dangers of the American Automobile*.

[4] NHTSA, (2007). *The New Car Assessment Program Suggested Approaches for Future Program Enhancements*; DOT HS 810 698.

[5] Olle J, (2009). *Investigation into deaths of Vince Tobin, Joseph Jarvis Shepherd, Jye Kaden Jones, Peter Vaughn Crole, Thomas James Scutchings, John Neville Nash, Patricia Murray Simpson, Elijah Simpson with inquest*, Melbourne: State Coroner Victoria, Australia.

[6] Elder J, Leland E, (2006). *CPSC Staff Response Regarding Follow-Up Questions from Commissioner Moore after the June 15, 2006, ATV Safety Review Briefing*, in editor: http://www.cpsc.gov/LIBRARY/FOIA/FOIA06/brief/atvmoore.pdf

[7] Day L & Rechnitzer G, (1999). *Evaluation of the Tractor Rollover protective Structure Rebate Scheme*, Monash University Accident Research Centre, Report 155.

[8] Zellner JW, Kebschull SA, Van Auken RM, Lenkeit JF, Broen PC, (2004). *Review And Analysis Of MUARC Report "ATV Injuries And Deaths," And Additional Simulation And Initial Testing of MUARC ATV Rollover Protection System (ROPS), Volumes I to III*, Report submitted to Victorian Coroner Inquest into ATV deaths, Dynamic Research Inc.

[9] Rechnitzer G, Richardson S, Grzebieta RH, (2004). *Review of Report by Dynamic Research: Review and Analysis Of MUARC Report "ATV Injuries and Deaths," and Additional Simulation and Initial Testing of MUARC ATV Rollover Protection System (ROPS), Volumes I & II*, Report submitted to Victorian Coroner Inquest into ATV deaths, DVExperts International Pty Ltd.

[10] Grzebieta RH, Rechnitzer G, Richardson S, (2004). *Review of Report by Dynamic Research: Review and Analysis Of MUARC Report "ATV Injuries and Deaths," And Additional Simulation and Initial Testing of MUARC ATV Rollover Protection System (ROPS), Volume III*, Report submitted to Victorian Coroner Inquest into ATV deaths, DVExperts International Pty Ltd.

[11] FCAI, (2012). *ATV industry opposes rollover devices on safety rounds,* http://www.fcai.com.au/news/news/all/all/311/atv-industry-opposes-rollover-devices-on-safety-grounds. 13 August.

[12] Zellner JW, Kebschull SA & Van Auken RM, (2006). *Updated Injury Risk/Benefit Analysis Of Quadbar Crush Protection Device (CPD) For All-Terrain Vehicles (ATVs)*; DRI-TR-12-06.

[13] Lower T, Herde E and Fragar L, (2012). *Quad bike deaths in Australia 2001 to 2010*, Journal of Health Safety Environment, 28(1), pp. 7-24.

[14] TRAX Lifeguard CPD; http://www.traxequipment.co.nz/lifeguard.php

[15] Quadbar CPD; http://www.quadbar.com.au/

[16]Grzebieta RH and Achilles T, (2007). *Report on Quad-bar in Relation to ATV Rollover Crashworthiness*, submitted to Victorian Coroner Inquest into ATV deaths, Dept. Civil Engineering, Monash University, Victoria, Australia.

[17]Wordley S and Field B, (2012). *Quad Bike Safety Devices: A Snapshot Review*, Department of Mechanical and Aerospace Engineering, Monash University, Victoria, Australia, February.

[18] Zellner JW, Kebschull SA & Van Auken RM, (2012). Comments On Monash/ISCRR Report By Wordley And Field Entitled "Quadbike Safety Devices: A Snapshot Review", DRI-TR-12-10

[19] Roberts A, (2009). *Dynamic Analysis of Side-by-Side Utility and Recreational Vehicles*, Proc. 21st International Safety Conference on the Enhanced Safety of Vehicles, Stuttgart, Germany, June, Paper No.09-0260-O.

A COMPARISON STUDY OF TWO SIDE IMPACT DUMMIES BASED ON THE PROBABILITY OF INJURY RSIK CURVES

Younghan Youn
Korea University of Technology and Education, Korea, Republic of
Eun-Dok Lee, Dae-up Kim
Korea Automotive Testing and Research Institute, Korea, Republic of
Paper Number 13-0487

ABSTRACT

In recent years, WorldSID dummy has been continuously developed and investigated to better represent biofidelic ATD as well as a device for replacement of the current existing ES-2 side impact dummy.

In Korea, the side impact type traffic accident is one of the major sever accidents in terms of numbers of accidents and fatality. Since 2003, 50kph 90 degree side crash test has been initiated as a safety standard with ES-1 at the first stage and also same time 55 kph impact speed test has been conducted as a part of KNCAP program. Currently only ES-2 is accepted as a regulatory tool for vehicle certification and KNCAP.

In spite of the introduction of side impact regulation and NCAP test procedures for the protection in lateral collisions during the last 10 years, injuries in this accident type still constitute a significant category of road traffic injuries. The fatality from side impact accidents has not been successfully decreased as expected. The head injury is major sources of fatality in side impact crash accidents in Korea.

In 2009, for further enhancing the protection of side collision, the perpendicular 29 kph pole side impact test with ES-2 dummy has been introduced as an optional test in KNCAP. The main objective of the optional pole side impact test was to promote installation of side curtain airbag in the vehicle fleet as a standard option.

In this study, injury outcome from WorldSID and ES-2 were evaluated with the two different types of vehicle sizes, small and medium size vehicles crash tests. Also, the computer simulations were performed.

In this simulation matrix, impact speeds (50 kph, 55 kph), MDB types (MDB and AE-MDB) were considered as variables.

In fact, WorldSID 50th male dummy's injury risk criteria limits are not finalized yet. Only the injury criteria categories have been just defined in the informal meeting as head injury criteria (HIC36), shoulder performance criteria (shoulder force: Fy), thorax performance criteria (thorax rib deflection), abdominal performance criteria (abdominal rib deflection and T12 resultant acceleration) and pelvis performance criteria (peak pubic symphysis force) Also the injury criteria and dimension of body structures between ES-2 and WorldSID cannot match each other.

In this study, in steads of direct comparison between two dummy's performances, the percentages of injury risk probability were compared with each individual body parts. ES-2 shows higher thoracic rib deflection compared with WorldSID for compact size vehicle. But mid-size case, two dummy's injury risk probability are same levels. The abdomen injuries from two dummies were similar but WorldSID showed lower pelvic injuries. In this study, only 2 different types of vehicles were tested with ES-2 and WorldSID. A small amount of rib deflection from the WorldSID may due to the upper body rotation during the impacts. From this study, the injury patterns are similar between two dummies. However, the probability of injury risk in the thoracic body was not higher than the ES-2 for small size vehicle.

INTRODUCTION

Development of the WorldSID 50th percentile male dummy began in June 1997 with a resolution by the International Organization for Standardization (ISO) ISO/TC22/SC12/WG5 to establish a task group. This task group consisted of many government and industry organizations worldwide. Through this collaboration, the group conducted extensive testing and evaluation, and prepared the drawings and user's manual.

In 2008, the task group finished the biofidelity assessment. They are currently working on risk curves for the injury measures and a practical seating procedure. The WorldSID 50th percentile male dummy has a standing height of 1,753 mm, seating height of 911 mm, and a mass of 77.3 kg. It has symmetrical response (left/right) and is able to be used in side impacts up to ±30° from the pure lateral impact direction.

In terms of global regulatory process, at the 148th session of WP.29 of June 2009, the importance of harmonizing test tools was discussed and there was general agreement to explore opportunities to complete the development of the world side impact dummy (WorldSID) 50th percentile male and 5th percentile female side impact dummies. At the 149th session of WP.29 of November 2009, the representative of the United States of America submitted in an informal document proposing the establishment of an informal group to focus on the development of the two WorldSID dummies. Since the first meeting held in November 2009, the latest meeting, the 11th informal group meeting was in January 2013. Korea has been also regularly participated in this informal group as well as informal group of pole side impact GTR.

WORLDSID VS. ES-2 DUMMIES SIDE IMPACT TEST

The total 4 vehicles were tested according to KMVSS 102 which similar to UN R94 with 2 different dummies, WorldSID 50%tile and ES-2. In the test, two different types of vehicles were selected as mid-size and small compact size vehicle to evaluate structural performances. AE-MDB was used in the test with 50kph impact speed. The test specification was shown in shown figure 1. The Both cars were equipped with thorax and curtain airbags.

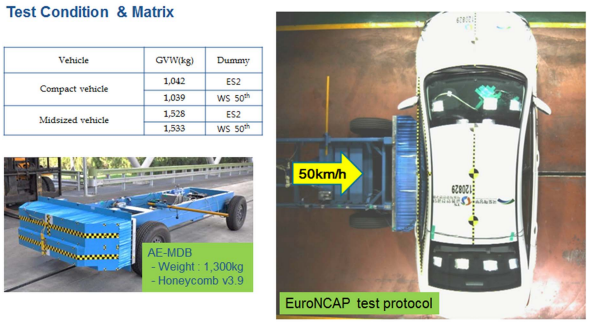

Vehicle	GVW(kg)	Dummy
Compact vehicle	1,042	ES2
	1,039	WS 50th
Midsized vehicle	1,528	ES2
	1,533	WS 50th

Figure 1. AE-MDB side impact test

In this test, each of dummy was seated in the driver to evaluate dummy kinematics and injury patterns especially thoracic and pelvic parts. The dummies seated in the cars shown in figures 2 and 3.

Figure 2. Dummy seated in the compact size car

Figure 3. Dummy seated in the mid-size car

The test results are shown in Table 1. In the compact car, the rib defections of WorldSID are significantly lower than those of ES-2 dummies. It may be caused by more rotational behavior in WorldSID than ES-2. In the ES-2 dummy, while the upper rib deflection was the maximum value, the lower rib had a largest deflection in the WorldSID. But reversely, mid-size care case, WorldSID rib

deflection is larger than ES-2. The public forces from the WorldSID are lower than ES-2 in both vehicles. The thorax rib deflections and pubic forces are shown in figures 4 and 5.

Table 1. Injury outcomes from side impact tests

			Compact vehicle		Midsized vehicle	
			ES2	WS 50th	ES2	WS 50th
Head	HIC 36	-	84.03	62.93	63.15	96.2
	Peak resultant Acceleration	g	37.33	27.79	26.23	29.33
	3ms	g	29	23.09	25.41	27.05
Shoulder	Shoulder Rib Deflection(1)	mm	-	20.12	-	38.7
Thorax	Upper Rib Deflection(2)	mm	32.4	7.09	12.3	6.13
	Middle Rib Deflection(3)	mm	22.1	7.57	10.0	9.6
	Lower Rib Deflection(4)	mm	22.5	11.89	15.7	18.3
Abdominal & Pelvis	Abdomen Rib1 Deflection(5)	mm	-	16.66	-	20.6
	Abdomen Rib2 Deflection(6)	mm	-	31.03	-	21.9
	Pubic Symphysis Force(Fy)	kN	2.11	1.2	2.48	1.37

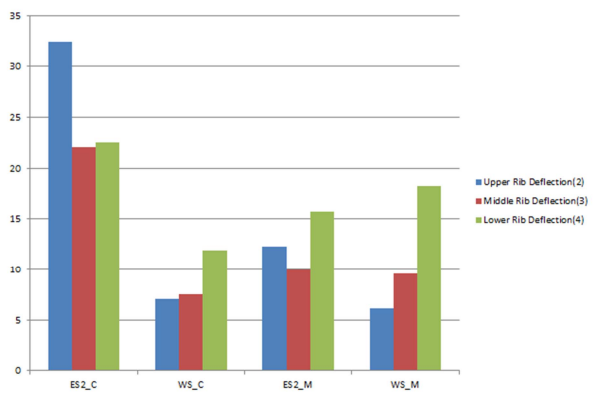

Figure 4. Thorax rib deflections

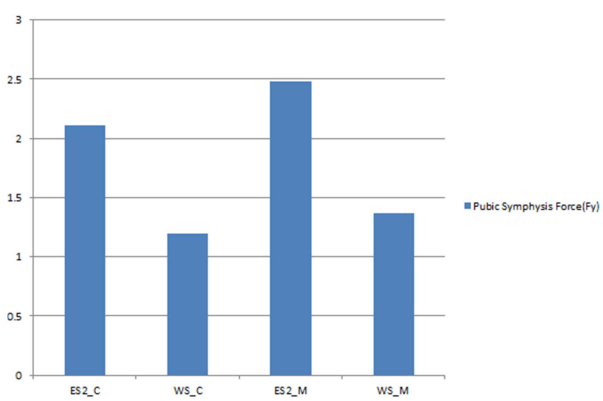

Figure 5. Pubic symphysis forces

However the injury criteria for the WorldSID 50%tile dummy is not finalized yet. In steads of direct comparison, the relative injury risks are examined by IARV's criteria. In general, injury risk curves can be expressed by the logistic regression equations. But in these comparisons, the injury risk rations were simple calculated by the linear relationships. As shown in Table 2, pelvis injury performance, pubic force, are similar in the both dummies. The thorax injury risk ratios for the WorldSID is relatively lower than ES-2.

Table 2. Injury ratios between two dummies in the compact car

Compact Car Injury Performances

ES-2	Injury	Unit	Injury value	IARV's	Ratio
Thorax Ribs	Deflection	mm	32.4	44	73.6%
Pubic	Force	kN	2.11	6.0	35.2%

WorldSID	Injury	Unit	Injury value	IARV's	Ratio
Thorax Ribs	Deflection	mm	11.89	[55.4]	21.5%
Pubic	Force	kN	1.2	[3.365]	35.7%

For the mid-size car, the both thorax and pelvis injury ratios are similar as shown in Table 2.

Table 3. Injury ratios between two dummies in the mid-size car

Mid-size Car Injury Performances

ES-2	Injury	Unit	Injury value	IARV's	Ratio
Thorax Ribs	Deflection	mm	15.7	44	35.7%
Pubic	Force	kN	2.48	6.0	41.3%

WorldSID	Injury	Unit	Injury value	IARV's	Ratio
Thorax Ribs	Deflection	mm	18.3	[55.4]	33.0%
Pubic	Force	kN	1.37	[3.365]	40.7%

A SERIES OF SIMULATIONS RESULTS

Since the side impact tests were limited, the series of the computer simulation were conducted to evaluate two dummies with the different impact speeds and side structural integrities. In the simulation, LS-Dyna with FE WorldSID and ES-2 dummy models were used. The generic mid-size vehicle was modeled without airbags to eliminate effects of airbags.

WorldSID vs. ES-2 Dummies

As a first analysis model, injury outcomes of

two dummies were compared with 55 kph impact speed in 1,300 kg AE-MDB. The dummies kinematics and injury results were shown in figure 6 and Table 4.

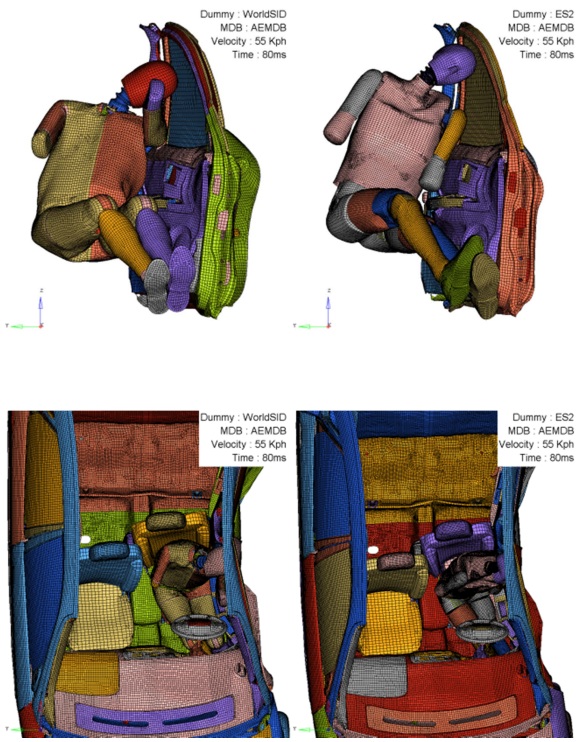

Figure 6. WS and ES-2 kinematics

Table 4. Injuries between two dummies in the mid-size car simulations

WorldSID				ES2			
Shoulder (KN)		-1.29		Clavicle (KN)		-0.46	
Rib def. (mm) /acc. (G)	U	Ax	107.6	Rib def. (mm) /acc. (G)	U	Ay	172.0
		Ay	274.5			def.	-45.2
		Az	111.2		M	Ay	183.3
		def.	-28.1			def.	-49.7
	M	Ax	108.9		L	Ay	110.9
		Ay	192.7				
		Az	60.6				
		def.	-23.6				
	L	Ax	54.8				
		Ay	149.7				
		Az.	56.8			def.	-53.7
		def.	-13.6				
T12 (G)		Ay	68.6	Lower spine acc. (G)		Ay	6.64
		AR	69.1				
Pubic symphysis Shear-s (KN)		1.68		Pubic symphysis Shear-s (KN)		3.25	
Abdominal def. (mm)		Upper	-12.1				
		Lower	-59.2				

As indicated in figures and Table 4, the rib deflections of WorldSID are lower than ES-2. It can be due to the rotation of dummy during the impact. In the ES-2 dummy, x, z directions rib acceleration sensors are not available. However, in WorldSID, as shown in Table 4, x, y directional acceleration values are significant. It means that the deformation of rib cage is influenced by x, z directional forces and generating acceleration in these directions.

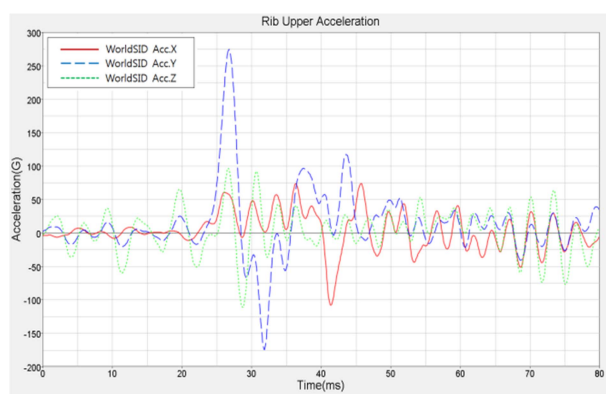

Figure 7. WS50 upper rib accelerations (x, y, z)

In figure 7, it displays the rotation of rib cage. Each individual rib can be deformed and rotated independently. But in the ES-2, whole rib cage is moved as one part as shown in figure 8.

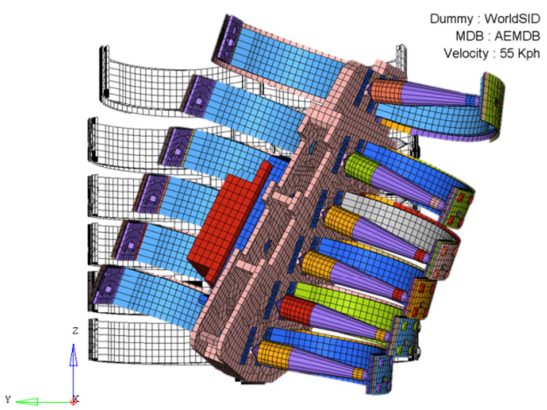

Figure 7. Deformation shape of WordlSID

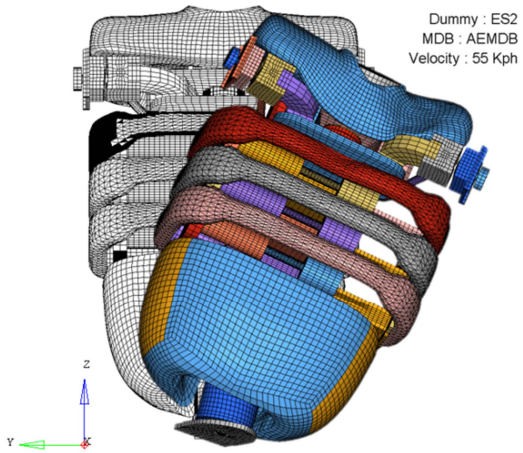

Figure 8. Deformation shape of ES-2

AE-MDB vs. R95 MDB in WorldSID and ES-2

Results from two different MDBs, the injury levels are similar in WS 50 and ES-2 dummies as shown in Table 5 and 6. The impact speed was 55 kph in both cases.

Table 5. Injury comparison with AE-MDB and R95 MDB in WS50 dummy

	MDB	
	AEMDB	R95
Shoulder load cell (KN)	-1.29	-1.63
Thorax rib upper displacement (mm)	-28.06	-30.60
Thorax rib middle displacement (mm)	-23.60	-22.46
Thorax rib lower displacement (mm)	-13.59	-13.51
Abdomen rib upper displacement (mm)	-12.07	-16.36
Abdomen rib lower displacement (mm)	-59.22	-60.70
Abdomen T12 resultant accel. (G)	69.09	82.76
Pubic load cell (KN)	-0.63	-0.67

Table 6. Injury comparison with AE-MDB and R95 MDB in ES-2 dummy

	MDB	
	AEMDB	R95
Clavicle load cell (KN)	-0.46	-0.64
Thorax rib upper (mm)	-45.18	-41.03
Thorax rib middle (mm)	-49.72	-42.36
Thorax rib lower (mm)	-49.72	46.00
Pubic load cell (KN)	5.75	7.45

50 kph vs. 55 kph impact with AE-MDB in WorldSID and ES-2

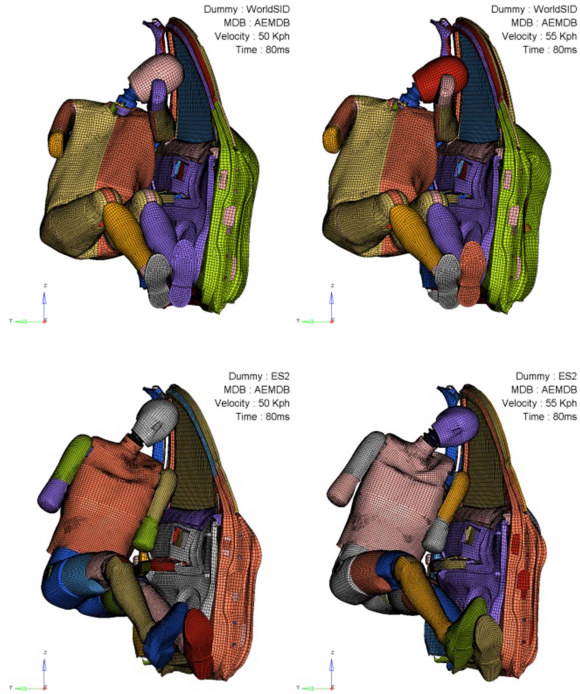

Figure 8. Kinematics of WS50 and ES-2

As shown in figure 8-9 and Table 7-8, the higher

impact speed increased injury values in both two dummies. But the difference is not significant for WS50 dummy. For the 50 kph case, the maximum rib deflection was 23.46 mm at the upper rib. Increasing impact speed to 55 kph, the maximum rib deflection is increased 19.6%, 28.06 mm. The following figures represent upper rib deflection, lower abdomen deflection and pubic force comparisons.

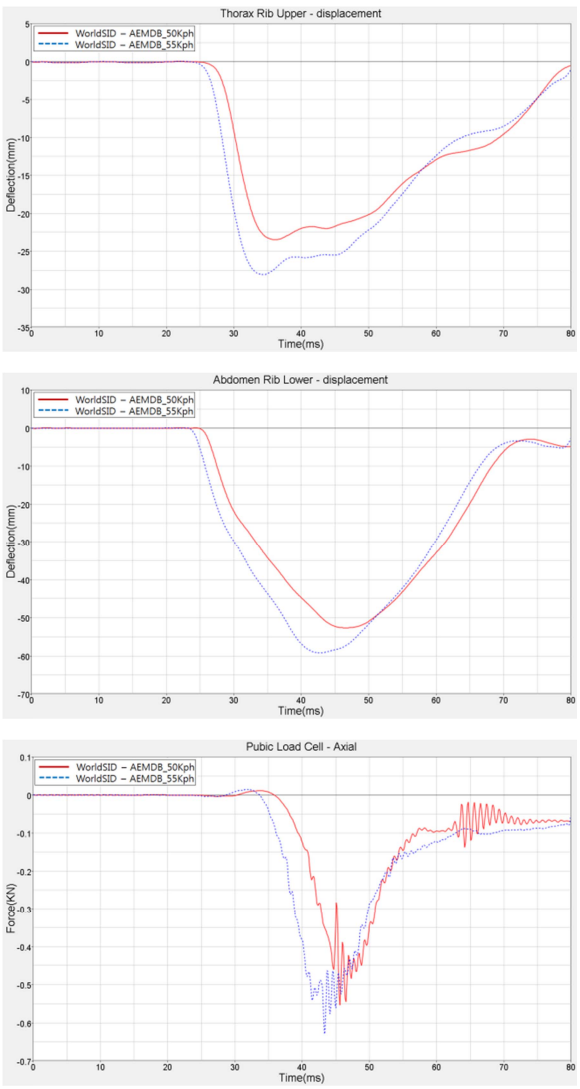

Figure 8. Injury comparison 50, 55 kph in WS50

Table 7. WS50 Injury comparison with different impact speeds, 50, 55 kph

WS 50 /AE-MDB	Velocity (Km/h)	
	50Kph	55Kph
Shoulder load cell (KN)	-1.16	-1.29
Thorax rib upper displacement (mm)	-23.46	-28.06
Thorax rib middle displacement (mm)	-18.10	-23.60
Thorax rib lower displacement (mm)	-11.16	-13.59
Abdomen rib upper displacement (mm)	-9.31	-12.07
Abdomen rib lower displacement (mm)	-52.64	-59.22
Abdomen T12 resultant accel. (G)	57.95	69.09
Pubic load cell (KN)	-0.55	-0.63

For the ES-2 dummy, increasing impact speed to 55 kph, the maximum rib deflection is increased only 6.7%, 53.67 mm. The following figures represent lower rib deflection, and pubic force comparisons.

9.6%

Table 8. ES-2 Injury comparison with different impact speeds, 50, 55 kph

	Velocity (Km/h)	
	50Kph	55Kph
Clavicle load cell (KN)	-0.63	-0.46
Thorax rib upper displacement (mm)	-43.35	-46.18
Thorax rib middle displacement (mm)	-45.35	-49.72
Thorax rib lower displacement (mm)	-50.26	-53.67
Pubic load cell (KN)	4.34	5.75

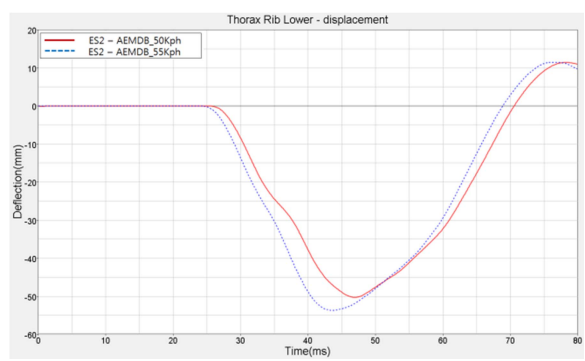

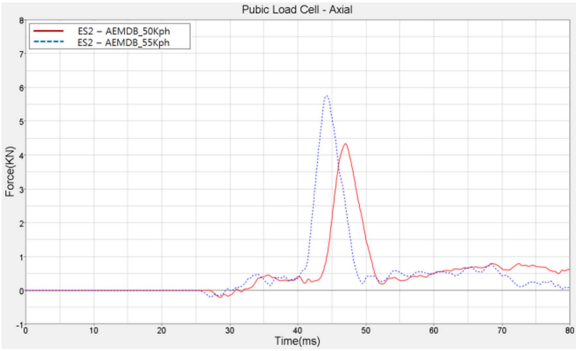

Figure 9. Injury comparison 50, 55 kph in ES-2

CONCLUSIONS

With impact tests and computer simulations, two different side impact dummies, WS50 and ES-2 have been evaluated in terms of dummy kinematic and injury outcomes. In general, WS50 dummy shows lower thorax rib deflection than ES-2. It may be caused by rotational behaviors in WS50 dummy. Since WS50 dummy is designed for ability to be used in side impacts up to ±30° from the pure lateral impact direction. Also, the way of construction of rib cage which more flexible and independently movable each rib part. Therefore, the resultant deflection of WS rib and abdomen should be counted in steads of only y directional deflection to consider rotational behavior of dummy.

Since injury criteria for WS50 is not established yet, IARV's values of each dummy were compared. In general, injury risk curves can be expressed by the logistic regression equations. But in these comparisons, the injury risk rations were simple calculated by the linear relationships. The pelvis injury performances, pubic force, are similar in the both dummies. The thorax injury risk ratios for the WorldSID is relatively lower than ES-2.

REFERENCES

ISO/TC22/SC12/WG5, Technical Report 9790 – Road Vehicles – Anthropomorphic Side Impact Dummy – Lateral Impact Response Requirements to Assess the Biofidelity of the Dummy, 2000.

WorldSID Informal Group Document, WS-08-04, https://www2.unece.org/wiki/pages/viewpage.action?pageId=3178648

FTSS FE Model Development Technical Report, "World SID 50th (ver. 2.0) and World SID 5th ", (ver 1.0), 2007.

Maltese, M., Eppinger, R., Rhule, H., Donnelly, B., Pintar, F., & Yoganandan, N. (2002). Response corridors of human surrogates in lateral impacts Stapp Car Crash Journal 46:321-351.

Miller, C.S. and Rupp, J.D. (2011). PMHS impact response in low and high-speed nearside impacts. UMTRI Report 2011-10. University of Michigan Transportation Research Institute, Ann Arbor, MI.

Newland, C. 2005. "International Harmonised Research Activities Side Impact Working Group Status Report.", ESV 2005 IHRA status report on behalf of the IHRA Side Impact Working Group. conference paper 05-0460

Pintar, F. A., Yoganandan, N., Hines, M. H., Maltese, M. R., McFadden, J., Saul, R., Eppinger, R., et al. (1997). Chestband Analysis of Human Tolerance to Side Impact. Society of Automotive Engineers, Warrendale, PA.

CRASH DAMAGE PATTERNS ASSOCIATED WITH CHEST INJURIES IN FAR-SIDE ROLLOVERS

Kennerly Digges
Fadi Tahan
The George Washington University, National Crash Analysis Center
USA

Raphael Grzebieta
Michael Bambach
Garrett Mattos
Andrew McIntosh
University of New South Wales, Transport and Road Safety Research
Australia
Paper Number 13-0066

ABSTRACT

The NASS/CDS formed the initial basis for investigating the vehicle damage patterns associated with serious chest injuries suffered by belted occupants in far-side rollovers. MAIS 3 or 4 lung contusions were the most frequent severe chest injury. Unilateral left and right lung contusions and bilateral lung contusions were all observed in the population of injured occupants. The lung injury sources most frequently designated by the NASS investigators were the side interior and the shoulder belt. The crash tests and simulations indicated that ground impact with a lateral component produced roof and front fender damage patterns like those observed in cases with chest injuries. The observed damage patterns suggested the following as possible sources of injury causing environments for belted drivers: (1) lateral loading the roof pillars and left front fender during the third and possibly the seventh quarter-turn, and (2) rebound loading induced by the suspension system during the fourth or eight quarter-turn. Other mechanisms may also be possible in complex rollovers.

INTRODUCTION

The purpose of this study was to better understand the events in rollover crashes that are most likely to cause chest injuries among belt restrained occupants. This paper was restricted to the causes of chest injuries suffered by occupants seated on the far-side of the rollover. The data source for the investigation was NASS/CDS. The research objective was to determine the occupant to vehicle interactions that cause chest injuries. An essential and unique approach to achieve this goal was to determine vehicle damage patterns among rollovers with serious chest injuries and to reconstruct cases in order to determine the event in the crash that most likely produced the injury. A purpose of the research was to determine the requirements for a dynamic rollover test that can be used to evaluate countermeasures to reduce chest injuries.

METHODS

Rollovers frequently involve planar impacts prior to the rollover. Earlier studies have shown that these multiple crash events increase the risk of injury, when compared to a rollover without prior crash events [Digges et al 2005]. An increase in the extent of the damage from the planar impact was found to be related to an increase in injury risk. In order to study the cause of chest injuries that occur during the rollover event, only pure rollovers (without prior impacts) were considered.

Initially the NASS/CDS was examined to determine the frequency of serious (AIS 3+) injuries and the nature of the serious chest injuries. Case studies of NASS crashes with serious chest injuries sustained by belted drivers seated on the far-side of the rollover were then undertaken and damage patterns were determined. Vehicle rollover tests with dummies were examined to determine occupant motion in crashes with damage similar to that observed in the NASS cases. Computer simulations were performed to further explore factors that could contribute to chest injury.

RESULTS – NASS DATA ANALYSIS

A study of tripped single vehicle rollovers in NASS/CDS 2000-2010 examined the distribution of seriously injured belted adult occupants by injured body region [Mattos et al 2012]. The results are displayed in Figure 1. In this study, rollovers with involvement of embankments and fences were excluded. The query produced 13,387 weighted cases (124 raw).

A second CDS query identified 857,216 (n unweighted= 1676) restrained and contained

occupants involved in single-vehicle pure rollover crashes between 2000 and 2009 (inclusive) [Bambach et al 2012]. These included injured and non-injured occupants of age 16 years and older.

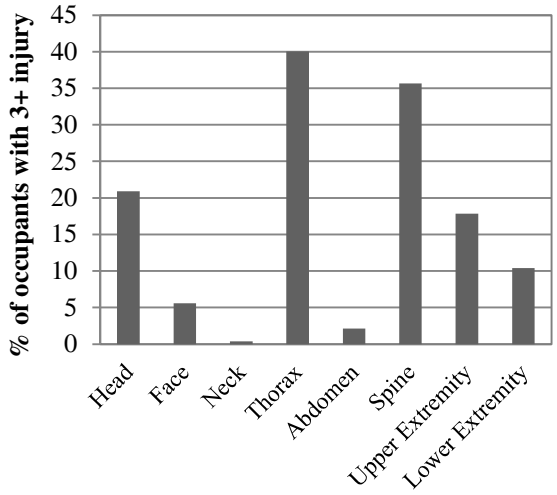

Figure 1. Distribution of occupants with serious injuries by AIS body region [Mattos et al 2012].

The number of quarter turns the vehicle underwent during the single-vehicle pure rollovers experienced by the occupants are plotted in Fig. 2 [Bambach et al 2012]. The plot indicates that the majority of vehicles were either on their wheels or on their roof post-crash, as opposed to on their side. The percentages of occupants that were in vehicles that rolled 8 quarter-turns or less were 99% and 93.9%, for all occupants and seriously injured occupants, respectively. It may be noted that injury peaks occur at 4 quarter-turns and 8 quarter-turns. The 8 quarter-turn event is particularly notable because it portrays 5% of the rollovers but 18% of the serious injuries. These results suggest a more detailed investigation of crashes with 4 quarter-turns and 8 quarter-turns.

Of the belted occupants in pure rollovers, 17,368 (n unweighted= 194) received serious injury (AIS≥3) and of these seriously injured occupants 6356 (n unweighted= 64) received a serious thoracic injury (36.6%) [Bambach et al 2012].

For some occupants, more than one chest injury was recorded. Of the occupants that received serious thoracic injury, the proportions of AIS3, AIS4, AIS5 and AIS6 injuries were 61%, 34%, 3% and 2%, respectively. The total number of weighted injuries was 35,788.

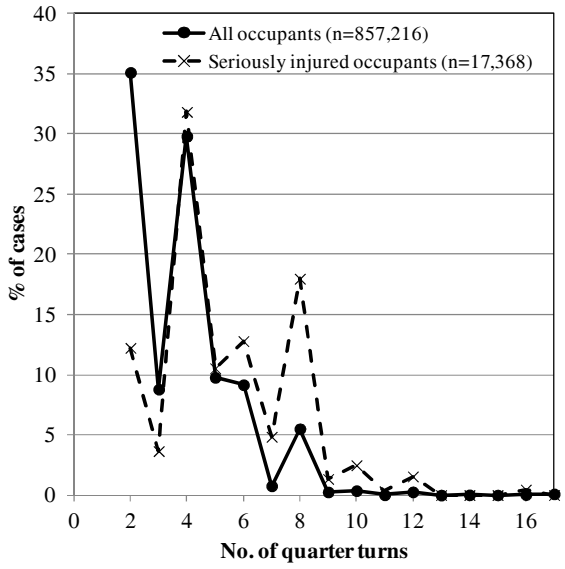

Figure 2. Number of quarter-turns experienced by restrained and contained occupants in single vehicle contained rollover crashes [Bambach et al 2012].

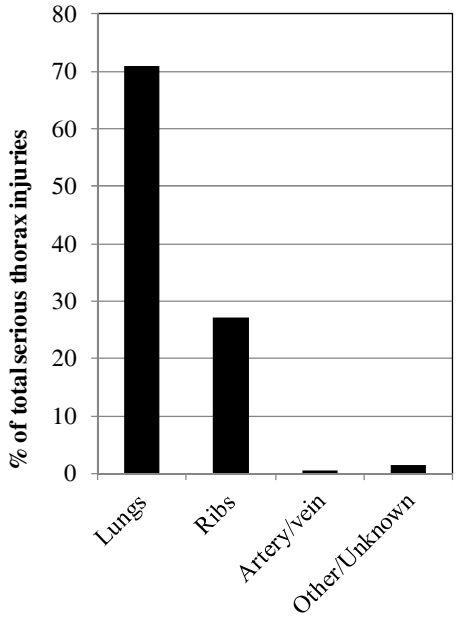

Figure 3. Distribution of serious chest injuries by organ/bone injured [Bambach et al 2012].

The distribution of thoracic injuries by organ/bone injured is shown in Figure 3. It is evident that the lung and rib injuries are predominant.

Figure 4 shows that lung contusions were the principle lung injury with unilateral more frequent than bilateral. In Figure 4, the populations of lung injuries and rib injuries each add to 100%.

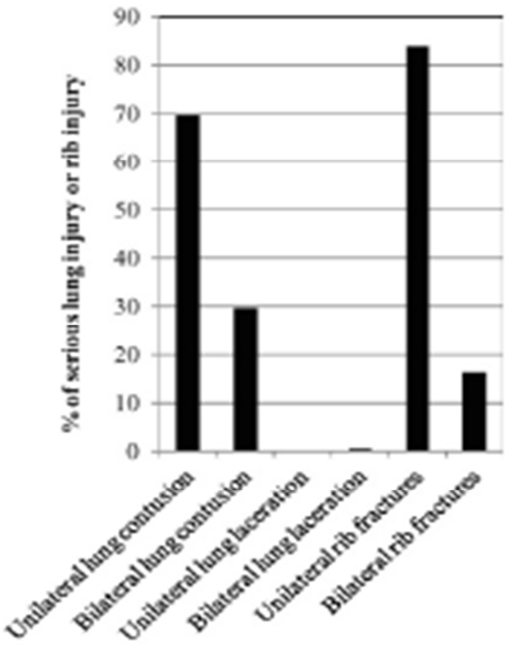

Figure 4. Distribution of serious chest injuries by aspect of the injury [Bambach et al 2012].

The distribution of serious lung injuries suffered by occupants in far-side rollovers is displayed in Table 1. The unweighted number of cases for this distribution was 48.

Table 1.
Distribution of serious lung contusions in among belted occupants in far-side rollovers (NASS 2000-2009 unweighted data)

Lung Injury Type	Percentage
Unilateral -door side	42%
Unilateral -console side	19%
Bilateral	40%

RESULTS – CASE STUDIES

The approach to develop a better understanding of chest injury causes involved a case review of NASS rollovers with AIS 3+ thoracic injuries. The review examined the damage pattern of the rollover cases to determine the direction and sequence of the crash forces that might contribute to the injury. In order to improve the chance of accurately analyzing the cases, it was desirable to select cases in which the chest injury was the most serious injury and it was not caused by confounding factors such as interactions with other occupants in the vehicle.

The selection criteria for cases of far-side belted occupants with AIS 3+ chest injuries to be examined were filtered by the following criteria:

- Passenger car, pickup or SUV
- A single vehicle without other crashes before, during or after the rollover
- Driver only or with right front passenger with no or minor injuries not related to driver injury
- Right side leading rollover (Driver on the far-side of the rollover)

Sixteen cases met the initial criteria. Upon examining the cases, additional criteria were needed to exclude cases that were not possible to reconstruct. Two cases were so severe that the damage to the vehicle was so extensive that crash forces could not be determined. Occupants in five of the cases sustained more severe roof contact brain injuries than their thorax injuries. One case did not document the damage to the vehicle.

These eight cases were removed and the damage patterns of the remaining eight cases were analyzed.

Table 2.
Vehicles and rollover severity of selected cases with serious chest injuries

Case Nr.	PSU	NASS Case	1/4 Turn	MY	Model
1	48	248K	4	1996	Explorer
2	41	176K	4	1994	Explorer
3	74	86A	6	2002	Explorer
4	12	135J	6	2006	G6
5	48	114J	7	2006	Tacoma
6	48	180J	8	2001	Rodeo
7	48	5J	8	2002	Montero
8	78	45C	9	2002	Malibu

A list of the eight cases and significant characteristics is included in Table 2. It is interesting to note that half of the cases were on their wheels at the completion of their rollover.

For the eight cases under study, Table 3 displays the injuring contact, the type of chest injury and the vehicle damage that was used to define the force direction during the rollover. The injuring contact in the table is based on the NASS documentation.

An additional damage pattern that was noted on 5 of the 8 cases was upward damage of the roof at the center or on the near-side of the rollover. This roof

tenting suggested a lateral force component on the roof during the rollover.

Table 3.
Occupant contacts, injuries and vehicle damage that defined the roll motion for cases in the study

Case Nr.	Occupant Contact	AIS Injury	Vehicle Damage
1	Belt	4 Bilateral Lung	Side Left Fender
2	Left Interior	4 Bilateral Lung	Top/side Left Fender
3	Belt	4 Bilateral Lung	Lower Left Rear
4	Left Interior	4 Bilateral Lung	Side Left Fender/Wheel
5	Belt	3 Right Lung	Top/side Left Fender
6	Left Interior	3 Left Lung	Top/side Left Fender
7	Seat Back	3 Right Lung	Rear C-pillars
8	Left Interior	4 Bilateral Lung	Side Left Fender/Wheel

The four cases that were upright at the termination of rollover exhibited some similarities in their damage patterns. These four cases are: 1, 2, 5 and 6. To truncate the presentation of results, the reconstruction was focused on these cases and they are addressed in this paper. These four cases are summarized in the subsections to follow.

Case 1 - 2006 41 176

Case 2006 41 176 was a 1996 Ford Explorer that rolled 4 quarter-turns, passenger side leading. The vehicle is shown in Figure 5. There were three occupants, two of which suffered no injuries. The driver was a belted 38 year old male. There was no air bag deployment.

While negotiating a turn, the Explorer departed left, steered right and crossed the highway. The vehicle departed right and rolled on the grass shoulder.

The 38 year old male driver sustained an AIS 4 bilateral lung contusion and AIS 3 bilateral rib fractures, all attributed to the safety belt. He also had 4 AIS 1 skin abrasions to the chest and abdomen and an AIS 1 heart contusion attributed to the belt. There was an AIS 1 right back skin abrasion attributed to the seat. There were 2 AIS 1 lower extremity skin injuries caused by the knee bolster and 2 AIS 1 facial injuries caused by the roof side rail and flying glass.

Figure 5. Case 1 – Ford Explorer – 4 quarter-turns.

Case 2- 2005 48 248

Case 2005 48 248 was another Explorer with more extensive roof damage. This 1994 model, shown in Figure 6, was subjected to a 4 quarter-turn trip-over, passenger side leading. There was no air bag deployment.

Figure 6. Case 2 – Ford Explorer – 4 quarter-turns.

In addition to the 54 year old male belted driver, the Explorer in Case 2005-48-248 contained a 52 year old female right front passenger who sustained a single AIS 1 skin abrasion to the arm.

The vehicle departed the roadway to the right and rolled along the shoulder and in the roadway.

The 54 year old male driver sustained an AIS 4 bilateral lung contusion attributed to the left interior. Also coded were 2 AIS 3 left arm fractures attributed to the roof, an AIS 2 head injury attributed to the roof

and one AIS 1 skin abrasion of the abdomen attributed to the belt. There were no AIS 1 or 2 level injuries from left interior.

Case 5- 2004 48 5

Figure 7. Case 5 — Isuzu Rodeo - 8 quarter-turns.

Case 2004-48-5 involved the 2001 Isuzu Rodeo shown in Figure 7. This vehicle was subjected to an 8 quarter-turn trip-over, passenger side leading. The sole driver was a 26 year old female. She was belted and the air bag did not deploy.

A non-contact vehicle, in lane two, changed lanes to its right into the Rodeo's travel lane. To avoid a collision the Rodeo departed the right road edge. The right wheels descended a negative slope (-8/122), and the driver steered left to correct. The front wheels went left and the rear wheels went down the slope. The Rodeo tripped and rolled eight quarter-turns. The vehicle came to rest from the rollover on its wheels in lane one facing southeast. The vehicle's engine was still running and in gear and it began moving forward into the median.

The driver sustained an AIS 3 unilateral left lung contusion and an AIS 1 chest skin contusion attributed to the left interior. There were 2 other AIS 1 leg injuries attributed to the knee bolster. The roof was the contact for AIS 1injuries to the head, cervical spine and upper extremity.

Case 6- **2002 48 180**

Figure 8 shows a 2002 Mitsubishi Montero that was subjected to a trip over with 8 quarter-turns, passenger side leading. The driver was a 23 year old male. He was belted and the air bag did not deploy.

Figure 8. Case 6 –Mitsubishi Montero - 8 quarter-turns.

There was also a right front passenger with unknown age, gender but with no injuries.

2002 Mitsubishi Montero, was travelling west on a four lane, dry, level (-0.016 slope) interstate highway divided by a grassy median. There was a very slight curve to the right. The vehicle went off the left side of the roadway, came back onto the road and crossed both travel lanes. When the vehicle reached the right side shoulder it began to rollover. After rolling eight quarter-turns, the Montero came to final rest partially on the shoulder and partially on the grassy roadside.

The driver sustained a right lung contusion, AIS 3, attributed to the seat, back. He also had an AIS 2 cervical vertebral fracture caused by the roof. There were four AIS 1 facial and scalp lacerations attributed to the roof.

RESULTS - ROLLOVER TEST

A rollover test of a Ford Expedition conducted by Transportation Research Center for Vehicle Research and Test Center (VRTC) (NHTSA test number 6960), was analyzed to determine occupant motion during an 8 quarter-turn rollover. The damaged vehicle is shown in Figure 9. This test was a soil tripped rollover crash that was conducted to investigate the dynamics of belted occupants during rollover crashes. The Expedition was translated laterally on a test cart at 48.8 km/h (30.3 mph). It was released with its roll axis perpendicular to the direction of the soil trip area. The vehicle contained a belted Hybrid III dummy on the far-side of the rollover. Videos were available showing the dummy motion and the external vehicle position during the rollover.

The three videos from the rollover test were superimposed and synchronized in order to examine

the driver dummy motion at various times of the rollover. Critical conditions showing dummy motion that could contribute to chest injury are shown in Figures 10, 11 and 12. The dummy motion is shown in the left side of the figures. The top right graphic is from the downstream high speed video and the lower right graphic shows the real time video.

Figure 9. Damaged Ford Exposition after a rollover test with 8 quarter-turns.

Figure 10. Dummy and vehicle position during the third quarter-turn.

Figure 11. Dummy and vehicle position prior to completion of the eighth quarter-turn.

Figure 12. Dummy and vehicle position during the completion of the eighth quarter-turn.

DISCUSSION

Analysis of the videos from the Expedition rollover tests indicate that for an 8 quarter-turn rollover there were at least two opportunities for far-side belted occupants to incur serious chest injuries. The first occurred during the third quarter-turn and the second at the eighth quarter-turn.

The damage patterns for the 4 quarter-turn cases analyzed (cases 1 and 2) and the 8 quarter-turn case (case 6) all display lateral damage to the left front fender. This damage and the tenting of the roof suggest that lateral forces were applied to the vehicle during the third quarter-turn. Computer simulation of 4 quarter-turn cases confirmed this hypothesis [Tahan et al 2013]. The computer simulations further indicated that the dummy impacts the center console during the fourth (final) quarter-turn. This impact was induced by the rebound of the suspension system. Damage to the left front fender in cases 1, 2 and 5 suggest that there was an off-axis roll component or a wobble in the rollover. Simulation indicated that increases in the wobble increase the severity of the occupant impacts to the door and to the center console.

The 8 quarter-turn rollover test of the Expedition showed similar opportunities for chest injuries to those discussed above. Figure 10 shows the dummy impacting vehicle side during the third quarter-turn. In this test, an air curtain protects against head injury. A less severe impact with the door was noted at the seventh quarter-turn. The driver in case 5 sustained a left lung contusion attributed to the left interior, suggesting that the injury occurred during the third quarter turn.

Figures 11 and 12 show how the dummy moves rapidly from the exterior of the vehicle (Figure 11) to the interior (Figure 12) in less than 200 milliseconds. This motion occurs rapidly during the rebound of the suspension system. In the Expedition test vehicle,

the center console was removed and consequently the dummy head excursion shown in Figure 12 may be greater than in the unmodified vehicle. The chest injury induced by this upper body motion could originate from the seat belt that crosses the lower chest. In real world rollovers the driver's right side chest injury could also be caused by impact with the center console, the seat back or other objects or passengers located to the right of the driver.

The vehicle in case 6 sustained lateral damage to the left front fender and the left rear upper quadrant. This damage pattern suggests a more extreme wobble than existed in the other cases. The driver in case 6 sustained a right lung contusion attributed to the seat back. Based on the motion shown in Figures 11 and 12, it is probable that this injury occurred during the eighth quarter-turn. It is also possible that in case 6, a rearward component from the upper quadrant impact may have increased the severity of occupant interaction with the vehicle.

Other injury mechanisms may exist in rollovers, especially those with added complexity and those that do not terminate on the vehicle's wheels.

The vehicles analyzed in this study were all SUV's. Further analysis of passenger cars and pickups will be required to determine the extent to which the observations from the SUV's can be broadly applied.

CONCLUSIONS

Chest injuries are a major source of harm to belted occupants in rollovers. The approach of reconstructing rollovers with chest injuries provides a basis for understanding these injuries and for developing rollover test procedures and countermeasures.

For NASS belted occupants with serious chest injuries incurred during exposure to far-side rollovers, lung contusions are the most frequent chest injury.

For serious lung contusions that occurred in NASS rollovers involving 4 or 8 quarter-turns, at least two opportunities for the injuries were evident. Based on NASS vehicle damage patterns and analysis of simulation and crash test data, the most probable opportunities were during the third quarter-turn and the final quarter-turn.

The crash tests and simulations indicated that ground impact with a lateral component produced roof and front fender damage patterns like those observed in NASS cases with chest injuries.

The observed damage patterns suggested the following as possible sources of injury causing environments for belted drivers: (1) lateral loading the roof pillars and left front fender during the third and possibly the seventh quarter-turn, and (2) rebound loading induced by the suspension system during the fourth or eight quarter-turn. Other mechanisms may also be possible in complex rollovers.

ACKNOWLEDGMENT

The authors would like to thank the Australian federal government's Australian Research Council for providing funds to carry out this research through the Linkage Projects grants scheme (No: LP110100069). The authors would also like to thank the industry partners for providing funding, namely, the New South Wales state government's Centre for Road Safety at Transport for New South Wales, the Victorian state government's 3rd party insurer Transport Accident Commission (TAC), the West Australian (WA) state government's Office of Road Safety at Main Roads WA, the mining company BHP Billiton Ltd, and the US Center for Injury Research (CFIR).

REFERENCES

Bambach, M.R., Grzebieta, R.H., and McIntosh, A.S, 2012; Thoracic injuries to contained and restrained occupants in single-vehicle pure rollover crashes. Accident Analysis and Prevention, 2012

Digges, K.H., Eigen, A.M., Dahdah, S., 2005; Injury patterns in rollovers by crash severity. Paper no. 355. In: Proceedings of the 19th International Technical Conference on the Enhanced Safety of Vehicles (ESV), 2005.

Mattos, G.H., Grzebieta, R.H., Bambach, M.R and McIntosh, A.S. 2012; Head injuries to restrained occupants in single-vehicle pure rollover crashes. Traffic Injury Prevention, 2012.

Tahan, F.J., Digges, K.H., Reichert R., Kan, C.D., Grzebieta, R.H. 2013; Assessing vehicle damage patterns with chest injuries in far-side rollovers, NCAC 2013-R-001 Report submitted to Transportation and Road Safety (TARS) Research University of New South Wales (UNSW), Sydney, Australia.

THE ADVANCED EUROPEAN MOBILE DEFORMABLE BARRIER SPECIFICATION FOR USE IN EURO NCAP SIDE IMPACT TESTING

Ellway, J.D
van Ratingen, M
European New Car Assessment Programme, Belgium

Versmissen, T
van Montfort, S
TNO Science and Industry, The Netherlands

Langner, T
Dobberstein, J
BASt, Germany

Goutas, P
Gay, P
Cellbond, United Kingdom

Malak, A
AFL/CT Sim, Germany

Denker, C
Hallack, J
Plascore, Germany

Odanaka, K
Ogihara, T
Showa, Japan

Paper Number: 13-0069

ABSTRACT

Past European collaborative research involving government bodies, vehicle manufacturers and test laboratories has resulted in a prototype barrier face called the Advanced European Mobile Deformable Barrier (AE-MDB) for use in a new side impact test procedure. This procedure offers a better representation of the current accident situation and, in particular, the barrier concept is a better reflection of front-end stiffness seen in today's passenger car fleet compared to that of the current legislative barrier face. Based on the preliminary performance corridors of the prototype AE-MDB, a refined AE-MDB specification has been developed.

A programme of barrier to load cell wall testing was undertaken to complete and standardise the AE-MDB specification. Barrier faces were supplied by the four leading manufacturers to demonstrate that the specification could be met by all. This paper includes background, specification and proof of compliance.

INTRODUCTION

In European New Car Assessment Programme (Euro NCAP) consumer testing, the effectiveness of improved vehicle side impact protection is assessed in two full-scale laboratory crash tests: the mobile deformable barrier (MDB) test and the perpendicular pole test. Since side barrier testing commenced in 1997, Euro NCAP has closely followed the UN-ECE Regulation 95 (R95) in terms of the test specification, the driver dummy and the injury criteria. However it has applied more demanding limits and additional requirements to promote side impact protection beyond the legal requirements.

In 2010 the safety organisation started a review of its crash procedures that have formed the backbone of its vehicle safety rating over the last fifteen years. Included in the work is an update of the MDB test which takes into account the latest injury patterns and state-of-the-art test tools. In particular, the adoption of a revised mobile crash barrier, alongside more biofidelic adult and child dummies, is considered an important new catalyst for further enhancements to vehicle side impact performance.

PREVIOUS RESEARCH

It has been well documented that the European vehicle fleet has developed since the R95 barrier was first conceived; as a result the barrier face no longer accurately represents the average passenger cars on the market, particularly in terms of the accident situation. The first concepts for an alternative barrier were developed within the European Enhanced Vehicle safety Committee (EEVC) Working Group 13 as part of a contribution to the work of the International Harmonised Research Activities (IHRA). Early prototype barrier faces were constructed by Cellbond using multiple layers of honeycomb in the same way as the R95 'Multi-2000' barriers. Both homogeneous and non-homogeneous stiffness profiles were evaluated. The barrier faces had greater geometric dimensions than that of R95, different ground clearance and trolley mass of 1500kg. Further modifications were made including the addition of a 45 degree chamfer on the edges. This work was reported by Lowne at the 2001 ESV conference [1].

Once the geometry of the barrier face had been fixed, the non-homogeneous stiffness profile was chosen as it reflected data from a number of vehicle

to load-cell wall (LCW) impacts, supporting data was provided by a series of 'baseline' car to car side impact tests. This work was reported by Roberts et al at the 2003 ESV conference [2].

The R95 barrier specification was updated to the 'Advanced 2000' barrier face in the 2002 series of regulatory amendments. The honeycomb blocks were acid etched to produce progressive stiffness as opposed to multiple honeycomb layers increasing in stiffness. A revised version of the AE-MDB was produced by Cellbond using acid etched blocks and termed Version 1. A comparison between the prototypes and Version 1 was performed to ensure that the new construction techniques did not affect the stiffness profile of the barrier face.

In 2002 the AE-MDB build specification was then updated to Version 2 following further testing which included vehicle to LCW tests and barrier to vehicle tests. It is important to note the inclusion of steps in the corridors of Version 2. These steps were incorporated as a result of the new geometry of the AE-MDB. The corridors specified by WG13 for Version 1 were based on blocks that were 500mm x 250mm, as per the R95 blocks. However, version 1 corridors did not take into account the geometry of the AE-MDB blocks which are not always 500mm x 250mm.This work was reported by Ellway at the 2005 ESV conference [3].

After 2005, accident research suggested that the side impact regulation should first be improved by the addition of a mandatory pole impact test [4]. Consequently, the involvement of EEVC WG13 in further development of the AE-MDB diminished. The work on the AE-MDB barrier development continued in the research programme supported by the European Commission, Advanced Protection Systems (APROSYS) [5]. Based on the results seen with AE-MDB Version 2, modifications were proposed to reduce the stiffness of the lower row, outer blocks. New stiffness profiles were proposed and a bumper beam element was added to the barrier face, see Figure 1. When considering any version of the AE-MDB after Version 2, it is important to note that the stiffness specifications for all later barriers use the Version 2 corridors as an initial starting point.

The development work undertaken by APROSYS is reported in the task deliverable [6]. Various iterative modifications were evaluated, focusing specifically on the lower row of three blocks. The research culminated with Version 3.9, which utilised identical upper blocks to those of Version 2 but with lower blocks of reduced stiffness to 55/60/55 percent of the outer lower blocks D and F from Version 2. It is important to note that the Version 3.9 corridors shown in the APROSYS project report do not fully account for the addition of the bumper beam, although some efforts were made to take this into consideration.

BARRIER CONSIDERATIONS

In 2011, Euro NCAP agreed to adopt the AE-MDB for future side impact testing. The side impact working group (SIWG), tasked to develop and validate the new MDB procedure, set up an ad-hoc Task Force to bring the barrier from its prototype stage to a well defined design and build specification. The SIWG and Task Force AE-MDB, agreed to the following items:

Barrier face

After consultation with experts previously involved in the development of the AE-MDB, it was agreed to adopt the Version 3.9 barrier face with a beam element as evaluated by APROSYS. Before this work began, the block E corridor was partly re-drafted to reflect the theoretical performance of the Version 3.9 barrier with bumper beam fitted. This was done by establishing the theoretical performance of the original corridor of Version 1 and applying the relevant geometry.

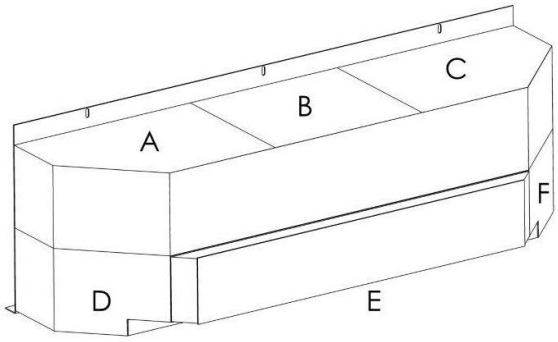

Figure 1: AE-MDB Version 3.9 consisting of six honeycomb blocks and with bumper beam fitted.

Trolley mass

The early development of the AE-MDB was part of a contribution to the work of the IHRA Side Impact Working Group. This work specified a trolley mass of 1500kg in an attempt to find global consensus. However, research conducted by the University Institute for Automobile Research (INSIA) Madrid, the German Institute for Highway Safety (BASt) using accident research (GIDAS/CCIS) data, Euro NCAP data and the European Environment Agency [7] showed that a total trolley mass of 1300kg would be more appropriate for use in Europe. Owing to the adoption of a lower trolley mass (1300kg) it was necessary to adjust the target requirements for peak dynamic displacement and static crush of the barrier face in certification load cell wall tests.

Test speed
The speed of the trolley used during the development of the AE-MDB in barrier to car impacts was 50km/h. Consideration was given to how appropriate this speed is for side impact testing. Some research has suggested that increasing the test speed to 65km/h might address a larger proportion of MAIS 3+ injuries. However, concerns were raised about the calculation method of delta V in side impacts in this study [8]. In particular the reliability was questioned in light of real world accident data which suggested similar delta V but showed considerable differences in vehicle deformation. Due to the lack of a more suitable test speed, it was agreed that the AE-MDB to car test would be run at 50km/h. This issue would be monitored in the future.

Barrier energy
Consideration was given to the amount of energy to be absorbed by the barriers during the impact. Previous versions of the barrier specification required that the barrier absorbs a total amount of energy equal to the kinetic energy of the trolley calculated using $mv^2/2$. However, there is additional energy in the rotating parts of the trolley such as wheels, hub assemblies and brakes etc. An analysis of wheel assemblies from three different test institutions suggested that, there can be up to 2kJ of additional energy provided by the rotating parts. However, it is acknowledged that not all of the rotational energy is absorbed by the barrier face.

AE-MDB to LCW testing
From previous experience, it is understood that performance corridors alone do not ensure that barriers of different suppliers behave identically. Hence, with the initial test conditions of trolley mass and speed defined, a programme was initiated to complete a full barrier build and performance specification.

The aim of this last phase was to define the construction of the AE-MDB in detail, evaluate the performance of a number of barriers constructed by multiple manufacturers and finalise the static and dynamic performance specifications. To that end, four barrier manufacturers AFL, Cellbond, Plascore and Showa agreed to construct and supply barriers for use in comparative barrier to LCW impacts.

The work began with a review of the draft build specification [5] to define the necessary materials and ensure that construction is consistent between manufacturers. Each barrier manufacturer then provided three barriers for use in the LCW evaluation tests. Testing was performed at two Euro NCAP test laboratories; BASt in Germany and TÜV Rheinland TNO Automotive International B.V. (TTAI) in the Netherlands. The LCW configurations between the two labs were different: BASt used a high resolution wall with load cells measuring 125mm x 125mm. At TNO, six plates were used that corresponded to the barrier blocks with a smaller number of load cells. Close attention was paid to the accuracy of barrier displacement measurements. High speed film was used alongside multiple accelerometer measurements due to the known errors involved with calculating displacement from accelerometer signals.

RESULTS

The results of the 12 barrier to LCW tests are shown in Figure 2. The solid black line denotes an average force for the new barriers. As the data from each barrier was normalised to 1mm incremental displacements; anomalies appeared in the region of peak barrier displacement. This was due to the variation in peak displacement between barriers; the data was subsequently cropped at this point. One of the barrier tests shows a peak displacement of 371mm, above the permitted maximum. There were concerns regarding the validity of the data used in calculating displacement of this particular barrier, this data has been excluded from any further analyses.

The dotted black line is the data from an early Version 3.9 barrier that was published within the APROSYS research. The trolley mass in this test was 1500kg, hence the additional displacement, and the data filtering was not in accordance with the draft specification. However, this data serves as a baseline for the new barriers. It is intended that the updated specification reflects the performance of the barriers evaluated within APROSYS. The corridors shown in Figure 2 are based on those published by APROSYS with the corrections to block E which account for the addition of the beam element.

Blocks A, B and C
The data from the upper row of blocks always tended to be toward the top of the corridors. This was the case for the baseline test and for the tests to the most recent barriers. The largest difference between peak values in the upper row (ignoring the baseline data) was approximately 5kN for the upper row. At the peak force, the coefficient of variance for blocks A, B and C were 6%, 6% and 7% respectively.

Blocks D and F
Although most of the block D and F traces were within the corridors, albeit towards the top, three traces for each block did exceed the corridor. The spread in peak forces of blocks D and F was

approximately 5.5kN. Previous barrier data suggests that the AE-MDB will bottom out on the LCW at approximately 380mm crush. The baseline data shows a visible imbalance between the two outer blocks; this was thought to have been caused by a misalignment of the trolley (yaw) during the impact. The latest data did not show the same high impulse as that of the baseline data in the early stages of the impact. At the peak force, the coefficient of variance for blocks D and F were both 3%.

Block E

The initial corridor modifications that accounted for the addition of the bumper beam to block E are apparent in Figure 2. As mentioned previously, this modification was based on how the honeycomb should perform theoretically and without consideration of the influence of other blocks and the beam element. Even when bearing in mind the heavy channel filtration class (CFC), the actual performance of the block produces a far smoother trace than that of the theoretical calculation.

All traces for this block were within the corridor. The peak variance between barriers was approximately 7kN with a similar coefficient of variation to that of the outer blocks.

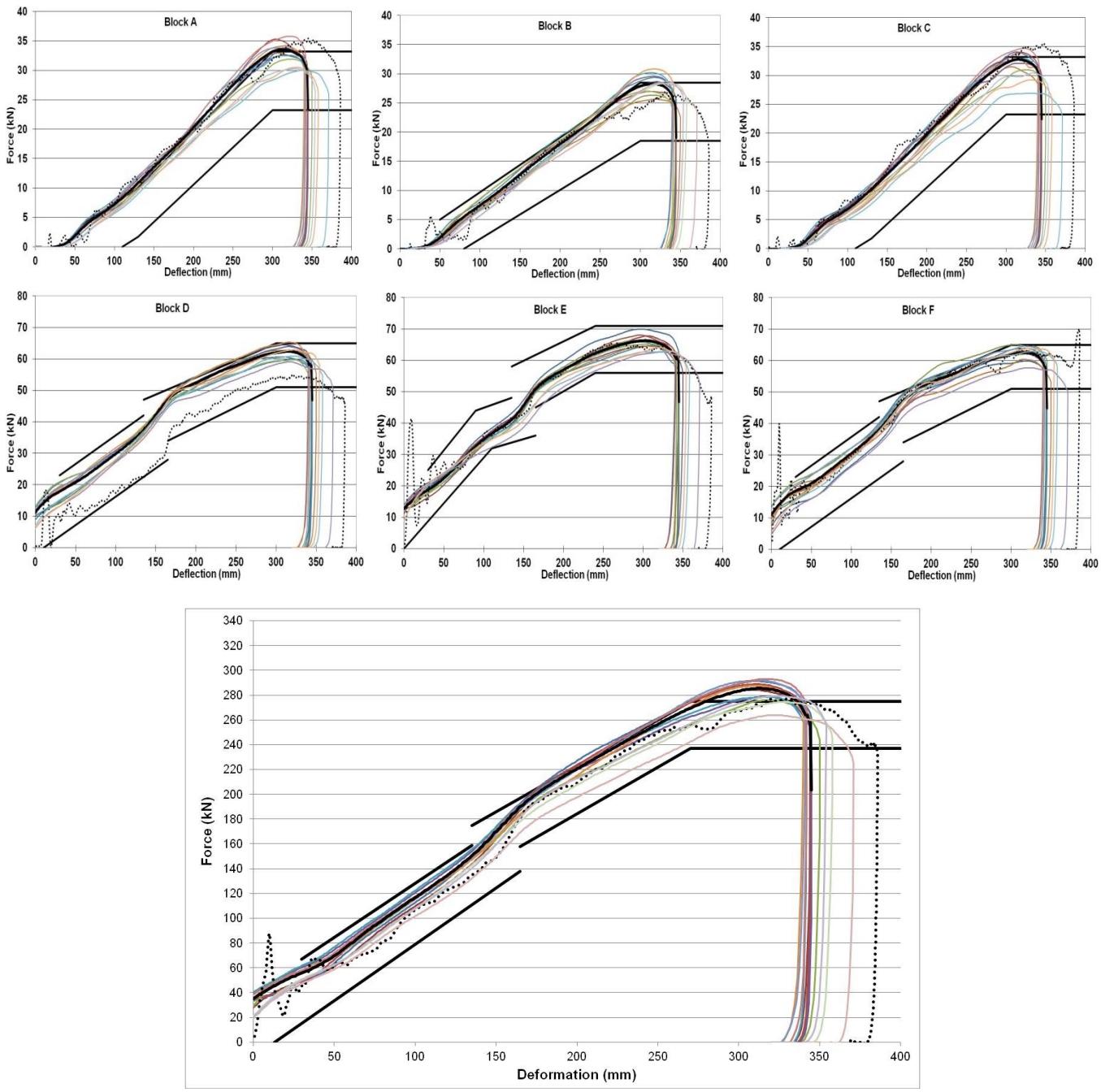

Figure 2: AE-MDB to LCW data (old corridors)

DISCUSSION

The variation of the data from the barrier to LCW tests (Figure 2) shows comparable performance between barriers of different makes tested at two different laboratories. The average data for each barrier is shown in Figure 3 along with revised corridors in solid black lines. The initial corridors are detailed as dotted black lines.

The corridor increases were based upon the difference between the average of the latest data and the theoretical trace that was used to produce the previous corridors. For example, the corridors for the upper row of blocks were increased by just under 5kN at 300mm. Proportionally smaller increases were made to the earlier parts of the corridors. This same method was applied to all of the blocks.

For blocks D and F, the initial part of the upper corridor was extended to 10mm to ensure that there is adequate control of the barrier stiffness in the early stages of barrier crush. There were initial concerns that the addition of the beam element to the lower row would result in high LCW forces in the very early stages of the impact. This was observed in the APROSYS barrier to LCW test between 0mm and 30mm of deflection. However, with correct application of the data processing and filtering requirements, detailed in the draft barrier specification, this will prevent such issues from arising.

It was also decided that the corridor for block E could justifiably be simplified. Consideration was given to using the corridor of blocks D and F for block E. However, differences in gradient in the latter part of the D and F corridor and the need for an inflection in block E at 260mm mean that this cannot be done. The principle behind block E was that it is a scaled down version of D and F, but it is important to note that the core material for block E is not the same as that used for D and F due to the very different geometry.

All of the lower corridors have been cropped at 330mm displacement as this corresponds to the smallest barrier displacement that is permitted in accordance with the energy absorption requirements.

There was no indication that any of the new barriers bottomed out on the LCW. The peak dynamic displacements of the individual barriers were all within 18mm of each other. Based on the barriers used in the evaluation, the revised AE-MDB specification details a peak dynamic displacement of 346 ±20mm and a static displacement at 340 ±20mm. The upper displacement limit is necessary to avoid the possibility of barriers being produced which are close to bottoming out.

An investigation was performed to establish the contribution of energy from the rotating parts of the trolleys. It was found that some of the barriers were absorbing up to an additional 1-2kJ above that calculated from the trolley mass and velocity ($mv^2/2$). However, the average data from all of the tests suggested that the additional energy absorbed by the barriers was not sufficiently substantial enough to warrant inclusion in the overall energy requirement. Furthermore, the overall tolerance of ±5kJ was considered sufficiently large enough to account for this energy. The reduction in trolley mass to 1300kg results in a total energy of 61.5 ±5kJ to be absorbed by the barrier.

The latest barrier to LCW tests highlighted the need for the further modification to the individual block corridors from those detailed in the APROSYS project report. It is important to note that the corridors were modified to account for the barriers that were evaluated by APROSYS and those tested in this programme of work. Therefore, any previous evaluations of AE-MDB Version 3.9 with a bumper beam are valid as those barriers would comply with this latest specification.

Data Filtering

The procedure requires that LCW data is filtered at a CFC of 60Hz. Such a ‘heavy’ filter results in LCW forces being observed earlier than physically possible. For example, the upper row does not contact the LCW until 60mm of barrier crush but forces are seen as early as 25mm crush. The filtered LCW data was correctly aligned with the displacement with the use of unfiltered data and contact switches between the barrier face and LCW. It is therefore accepted that, with filtered data, the LCW force will not be 0kN at 0mm displacement for the lower row.

Static data

In addition to dynamic performance corridors, the AE-MDB specification also details static requirements. Samples of each block were taken from the same batches used to produce barriers for use in the dynamic test and quasi-statically tested. Due to the small change in dynamic corridors, corresponding changes were also made to the static corridors. All samples tested by the barrier manufacturers met the static corridors.

With the final amendments introduced, the AE-MDB performance and build specifications have been completed. The final specification document is included in the Appendix of this paper for reference.

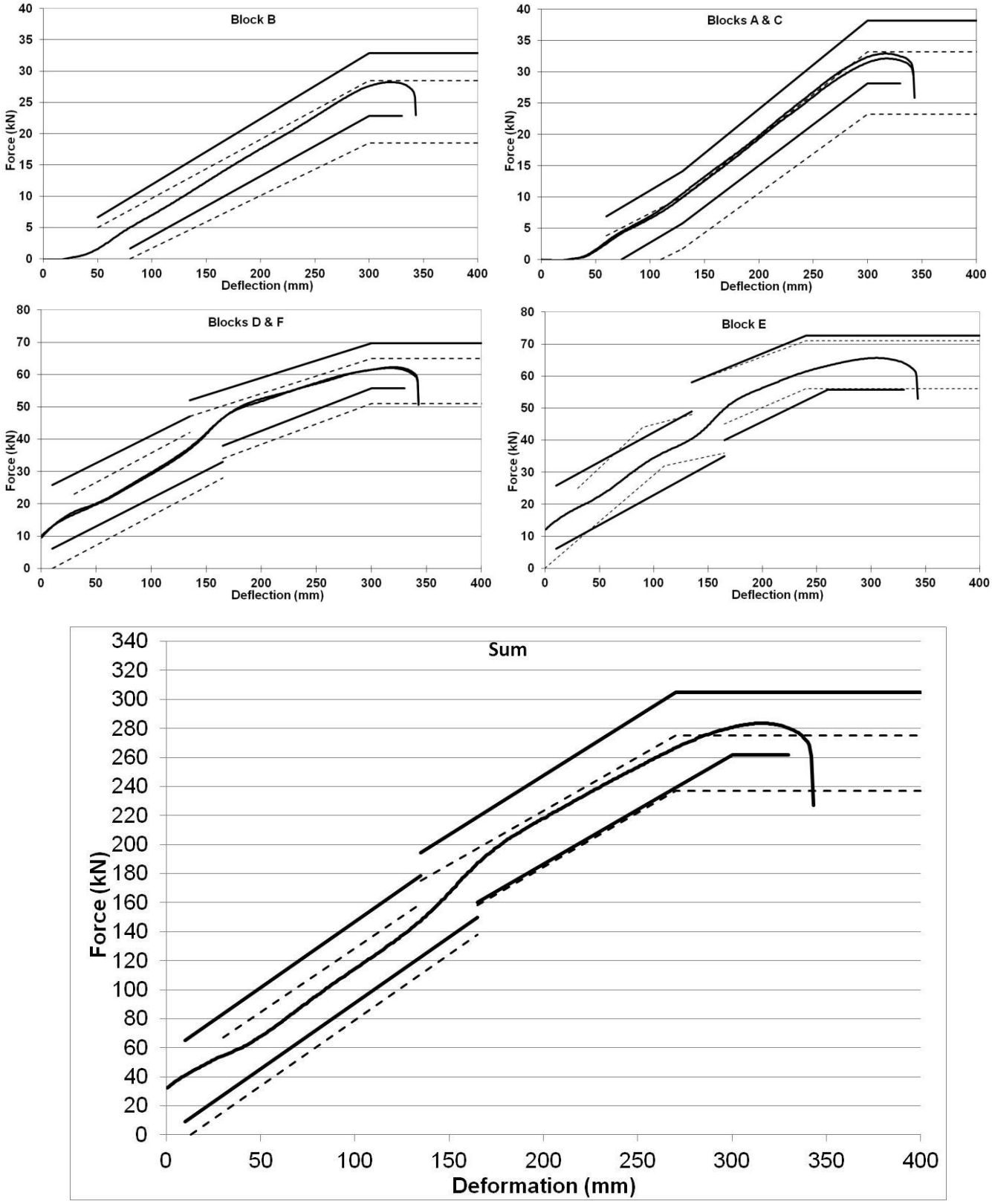

Figure 3: Modified AE-MDB Corridors

CONCLUSIONS

The aim of this work was to complete the specification for the AE-MDB for use by Euro NCAP in its revised side impact test procedures.

Based on the Version 3.9 draft specification, final build and performance specifications have been set. A series of LCW tests was performed using barriers manufactured by four independent manufacturers. Tests performed at two independent Euro NCAP test laboratories demonstrate that the results of all tests were comparable.

Revised corridors have been produced that reflect the barrier performance of both the latest barriers and those evaluated within the APROSYS project. The final AE-MDB specification is detailed in the Appendix to this paper.

ACKNOWLEDGEMENTS

Euro NCAP would like to express its thanks to Showa, Cellbond, Plascore and AFL for their support and participation in this programme and for their contribution to updating and finalising the AE-MDB specification. All drawings included in the AE-MDB specification were provided by Cellbond. The representatives of this group were:

James Ellway, Euro NCAP
Jan Dobberstein, BASt
Tobias Langner, BASt
Sjef van Montfort, TNO
Ton Versmissen, TNO

Christoph Denker, Plascore
Patrick Gay, Cellbond
Petros Goutas, Cellbond
Jason Hallack, Plascore
Arnauld Malak, AFL
Katsuhito Odanaka, Showa

Euro NCAP would also like to thank the members of the side impact working group:

Euro NCAP representatives
Michiel van Ratingen, Euro NCAP, Chairman
James Ellway, Euro NCAP, Secretary
Hans Ammerlaan, RDW
Luca Baroncelli, CSI
Aurelie Choulet, IDIADA
Tobias Langner, BASt
Jean-Philippe Lepetre, UTAC
Volker Sandner, ADAC
Richard Schram, Euro NCAP
Ton Versmissen, TNO

Industry representatives
Karsten Hallbauer, Takata
Paul Lemmen, Humanetics
Marc van Slagmaat, Autoliv
Fabien Duboc, Renault/ACEA
Erwin Segers, Honda/JAMA
Philipp Wernicke, BMW/ACEA
Christoph Weimer, HMC/KAMA

REFERENCES

[1] Lowne, R, 2001 (on behalf of EEVC WG13). Research Progress on Improved Side Impact Protection: EEVC WG13 Progress Report. ESV 2001, Amsterdam, the Netherlands.

[2] Roberts, A.K and van Ratingen, M, 2003 (on behalf of EEVC WG13). Progress on the Development of the Advanced European Mobile Deformable Barrier Face (AE-MDB). ESV 2003, Nagoya, Japan. Paper number 126.

[3] Ellway, J.D, 2005 (on behalf of EEVC WG13). The Development of an Advanced European Mobile Deformable Barrier Face (AE-MDB). ESV 2005, Washington DC, USA. Paper number 05-0239.

[4] M.J, Edwards et al, 2010 (on behalf of EEVC WG13 & WG21).
Analysis to estimate likely benefits and costs for the EU of modifying Regulation 95, EEVC WG13 and WG21 Subgroup.

[5] Advanced Protection Systems APROSYS, EC 6th Framework programme.
http://cordis.europa.eu/search/index.cfm?fuseaction=proj.document&PJ_RCN=7521834

[6] Ellway, J.D et al, 2006 (APROSYS task 1.1.1.) Development and Evaluation of the Advanced European Mobile Deformable Barrier Face Test Procedure. APROSYS deliverable 1.1.1B.

[7] European Environment Agency, 2010.
Monitoring the CO2 emissions from new passenger cars in the EU: Summary of data for 2010.

[8] M.J, Edwards et al, 2010.
Side impact safety. UK Department for Transport report: 4/12/55.

APPENDIX: AE-MDB SPECIFICATION

1. CHARACTERISTICS OF THE MOBILE DEFORMABLE BARRIER

1.1 The mobile deformable barrier (MDB) includes both an impactor and a trolley.

1.2 The total mass shall be 1300 ± 20kg.

1.3 The centre of gravity shall be situated in the longitudinal median vertical plane within 10mm, 1000 ± 30mm behind the front axle and 500 ± 30mm above the ground.

1.4 The distance between the front face of the impactor and the centre of gravity of the barrier shall be 2000 ± 30mm.

1.5 The height of the barrier shall be such that the uppermost part of the front face of the beam element (the intersection between the upper and lower row of blocks) is 550mm ± 5mm above ground level measured statically prior to impact.

1.6 The front and rear track width of the trolley shall be 1500 ± 10mm.

1.7 The wheelbase of the trolley shall be 3000 ± 10mm.

2. CHARACTERISTICS OF THE IMPACTOR

The impactor consists of six single blocks of aluminium honeycomb, which have been processed in order to give a progressively increasing level of force with increasing deflection. An additional single element is attached of 60mm depth to the front of the lower row of blocks. Front and rear aluminium plates are attached to the aluminium honeycomb blocks. The plates cover the angled surfaces.

2.1 Honeycomb blocks

2.1.1 Geometric characteristics

2.1.1.1 The impactor consists of six joined zones whose configuration and positioning are shown in Figure 4 and Figure 5. The principle dimensions of Blocks B and E are 500 ± 5mm x 250 ± 3mm and the principle dimensions and blocks A, C, D, F are 600 ± 5mm x 250 ± 3mm, Figure 5. The 500mm and 600mm should be in the W direction and the 250mm in the L direction of the aluminium honeycomb construction, see Figure 6.

2.1.1.2 The impactor is divided into two rows. Both rows shall be 250 ± 3mm high and 440 ± 2mm deep.

2.1.1.3 A 45 degree chamfer is applied to the outmost blocks on both the upper and lower rows. The chamfer is <u>not</u> applied to the facing or backing plates of the beam element. See detail A on Figure 5.

2.1.1.4 A bumper element is added to the front of the lower row, making the complete impactor 500 ± 2mm deep. The foil ribbon of this element will run parallel to the width dimension and the cell axis running parallel to the height dimension. The 1220mm should be in the W direction and the 200mm in the L direction of the aluminium honeycomb construction. See Figure 6 .

2.1.2 Pre-crush

2.1.2.1 Pre-crushing only applies to blocks A, B, C, D, E & F <u>not</u> to the bumper element.

2.1.2.2 The pre-crush shall be performed on the surfaces of the honeycomb that are parallel to the rear mounting face including the lower stepped section on Blocks D, E and F. Pre-crushing of the angled faces is not required.

2.1.2.3 All blocks (A, B, C, D, E & F) are to be pre-crushed by 10 ± 2mm on the front surface prior to testing and shaping.

2.1.2.4 The angled faces on Blocks A, C, D and F should be cut after pre-crushing.

2.1.3 Material characteristics

2.1.3.1 The expansion direction of the Aluminium Honeycomb shall be as defined in Figure 6.

2.1.3.2 The cell dimensions shall be 19mm ± 10 per cent for all blocks A, B, C, D, E & F and 6.35mm ± 10 per cent for the bumper section, see Figure 7.

2.1.3.3 All honeycomb blocks must be made of 3003 aluminium.

2.1.3.4 The aluminium honeycomb blocks (A, B, C, D, E & F) should be processed so that the force deflection-curve when statically crushed (according to the procedure defined in Paragraph 2.1.4) is within corridors to be defined for each of the six blocks in Section 5.

2.1.3.5 The aluminium honeycomb blocks for the bumper element should be processed so that the strength is 1.586 to 1.793MPa when statically crushed (according to the procedure defined in NHTSA TP-214D).

2.1.3.6 The processed honeycomb material used in the honeycomb blocks to be used for construction of the barrier shall be cleaned in order to remove any residue that may have been produced during the processing of the raw honeycomb material.

2.1.3.7 The mass of the blocks in each batch shall not differ by more than 5 per cent of the mean block mass for that batch.

2.1.4 Static tests for all blocks

2.1.4.1 A sample taken from each batch of processed honeycomb core shall be tested according to the static test procedure described in Section 5.

2.1.4.2 The force-deflection characteristic for each block tested shall lie within the force deflection corridors to be defined in Section 8.

2.1.5 Dynamic test

2.1.5.1 The dynamic deformation characteristics, when impacted, shall comply with the procedure described in Section 6.

2.1.5.2 Deviation from the limits of the force-deflection corridors characterising the rigidity of the impactor, as defined in Section 9 may be allowed provided that:

2.1.5.2.1 The deviation occurs after the beginning of the impact and before the deformation of the impactor is equal to 150mm.

2.1.5.2.2 The deviation does not exceed 50 per cent of the nearest instantaneous prescribed limit of the corridor.

2.1.5.2.3 Each deflection corresponding to each deviation does not exceed 35mm of deflection, and the sum of these deflections does not exceed 70mm.

2.1.5.2.4 The sum of energy derived from deviating outside the corridor does not exceed 5 per cent of the gross energy for that block.

2.1.5.3 The dynamic stiffness requirements for Block B is such that the force deflection curve falls between corridors of Section 9, Figure 18.

2.1.5.4 The dynamic stiffness requirements for Blocks A and C are identical. Their rigidity is such that their force deflection curves fall between corridors of Section 9, Figure 19.

2.1.5.5 The dynamic stiffness requirements for Block E is such that the force deflection curve falls between corridors of Section 9, Figure 20.

2.1.5.6 The dynamic stiffness requirements for Blocks D and F are identical. Their rigidity is such that their force deflection curves fall between corridors of Section 9, Figure 21.

2.1.5.7 The dynamic stiffness requirement for the complete barrier is such that the force deflection curve falls between corridors of Section 9, Figure 22.

2.1.5.8 The force-deflection curves shall be verified by a test detailed in Section 6 consisting of an impact of the barrier against a dynamometric wall at 35 ± 0.5km/h.

2.1.5.9 The dissipated energy against blocks A and C during the test shall be equal to 5.0 ± 1.0kJ per block.

2.1.5.10 The dissipated energy against block B during the test shall be equal to 4.6 ± 1.0kJ.

2.1.5.11 The dissipated energy against blocks D and F shall be equal to 14.8 ± 2.0kJ per block.

2.1.5.12 The dissipated energy against block E shall be equal to 17.3 ± 2.0kJ.

2.1.5.13 The dissipated total energy during the impact shall be equal to 61.5 ± 5.0kJ. The tolerance takes into account any additional energy contribution from the rotating parts of the MDB.

2.1.5.14 The maximum impactor deformation from the point of first contact, calculated from integration of the accelerometers according to Section 6.5.3 shall be equal to 346 ± 20mm.

2.1.5.15 The final residual static impactor deformation measured after the dynamic test at a height of 425mm above ground and along the MDB centreline shall be equal to 340 ± 20mm.

2.1.5.16 The amounts of energy indicated are the amounts of energy dissipated by the system when the extent to which the impactor is crushed is greatest.

2.2 Front plates

2.2.1 Geometric characteristics

2.2.1.1 The three front plates (upper, lower & bottom) shall cover the full front surface of the barrier and have a thickness of 0.5 ± 0.06mm. The three plates shall be 250mm, 200mm and 50mm wide and of the appropriate length to cover the pre-crushed and angled surfaces in a continuous length. The bottom strip (50mm wide) shall not cover the angled sides of the barrier.

2.2.1.2 When assembled the overall dimensions of the impactor shall be 1700 ± 2.5mm wide and 500 ± 2.5mm high. See Figure 5.

2.2.1.3 The upper edge of the lower front plate and the lower edge of the upper front plate shall be aligned within 4mm.

2.2.2 Material characteristics

2.2.2.1 The front plates are manufactured from aluminium of series AlMg2 to AlMg3 with elongation ≥ 12 per cent, and a UTS ≥ 175 N/mm^2.

2.3 Bumper front and rear plates

2.3.1 Geometric characteristics

2.3.1.1 The geometric characteristics shall be according to Figure 4 and Figure 5.

2.3.2 Material characteristics

2.3.2.1 The bumper plates shall be manufactured out of aluminium 5251 H22, 5052 H32 or 5052 H34. The plates have a thickness of 3mm ±0.07mm.

2.4 Barrier back plate

2.4.1 Geometric characteristics

2.4.1.1 The geometric characteristics shall be according to Section 7.2.

2.4.1.2 The upper mounting flange shall be vertical. The lower mounting flange shall be bent through 90 degrees.

2.4.2 Material characteristics

2.4.2.1 The back plate shall be manufactured from aluminium of series AlMg2 to AlMg3 with hardness between 50 and 67 HBS. The back plate is 3mm thick ±0.2 5mm. This plate shall be perforated with holes for ventilation, the location, diameter and pitch are shown in Figure 8 and Figure 10.

2.5 Location of the honeycomb blocks

2.5.1 The honeycomb blocks shall be centred on the perforated zone of the back plate.

2.6 Expanded polyester

2.6.1 Synthetic polyester thermo bonded wadding shall cover the chamfered zone of block A, C, D & F as shown in Figure 4.

2.6.1.1 The material shall have a weight of $60g/m^2 \pm 20\%$.

2.6.1.2 The material shall provide a 'soft link' between the upper and lower row of blocks. It may be added to the chamfered zone as a single piece or in multiple pieces provided that divisions are in the vertical direction only. The height of each piece is equal to that of the chamfered face.

2.7 Bonding

2.7.1 For both the front and the back plates, a maximum of adhesive film thickness of 0.5mm shall be applied evenly over the surface of the front plate. The adhesive to be used throughout should be a two-part polyurethane, (such as Ciba Geigy XB5090/1 resin with XB5304 hardener) or equivalent.

2.7.2 For the back plate the minimum bonding strength shall be 0.6MPa (87psi), tested according to Section 2.7.3.

2.7.3 Bonding strength tests

2.7.3.1 Flatwise tensile testing is used to measure bond strength of adhesives according to ASTM C297-61.

2.7.3.2 The test piece should be 100mm x 100mm, and 15mm deep, bonded to a sample of the ventilated back plate material. The honeycomb used should be representative of that in the impactor, i.e. chemically etched to an equivalent degree as that near to the back plate in the barrier but without pre-crushing.

2.7.3.3 Back plate ventilation holes should be clean and clear of bonding material to enable free flow of air.

2.8 Traceability

2.8.1 Barriers shall carry consecutive serial numbers which are stamped, etched or otherwise permanently attached, from which the batches for the individual blocks and the date of manufacture can be established.

2.9 Impactor attachment

2.9.1 The fitting on the trolley must be according to Figure 11. The fitting will use six M8 bolts, and nothing shall be larger than the dimensions of the barrier in front of the wheels of the trolley. Appropriate spacers must be used between the lower back plate flange and the trolley face to avoid bowing of the back plate when the attachment bolts are tightened.

3. VENTILATION SYSTEM

3.1 The interface between the trolley and the ventilation system should be solid, rigid and flat. The ventilation device is part of the trolley and not of the impactor as supplied by the manufacturer. Geometric characteristics of the ventilation device shall be according to Figure 12 and Figure 13.

3.2 Ventilation device mounting procedure

3.2.1 Mount the ventilation device to the front plate of the trolley;

3.2.2 Ensure that a 0.5mm thick feeler gauge cannot be inserted between the ventilation device and the trolley face at any point. If there is a gap greater than 0.5mm, the ventilation frame will need to be replaced or adjusted to fit without a gap of > 0.5mm;

3.2.3 Dismount the ventilation device from the front of the trolley;

3.2.4 Fix a 1mm thick layer of cork to the front face of the trolley;

3.2.5 Re-mount the ventilation device to the front of the trolley and tighten to exclude air gaps.

4. CONFORMITY OF PRODUCTION

The conformity of production procedures shall comply with those set out in the Agreement, Appendix 2 (E/ECE/324-E/ECE/TRANS/505/Rev.2), with the following requirements:

4.1 The barrier manufacturer shall be responsible for the conformity of production procedures and for that purpose must in particular:

4.1.1 Ensure the existence of effective procedures so that the quality of the products can be inspected;

4.1.2 Have access to the testing equipment needed to inspect the conformity of each product;

4.1.3 Ensure that the test results are recorded and that the documents remain available for a time period of 10 years after testing;

4.1.4 Demonstrate that the samples tested are a reliable measure of the performance of the batch (examples of sampling methods according to batch production are given below);

4.1.5 Analyse results of tests in order to verify and ensure the stability of the barrier characteristics, making allowance for variations of an industrial production, such as temperature, raw materials quality, time of immersion in chemical, chemical concentration, neutralisation etc, and the control of the processed material in order to remove any residue from the processing;

4.1.6 Ensure that any set of samples or test pieces giving evidence of non-conformity gives rise to a further sampling and test. All the necessary steps must be taken to restore conformity of the corresponding production.

4.2 The manufacturer's level of certification must be at least ISO 9001-2008 standard.

4.3 Minimum conditions for the control of production: the holder of an agreement will ensure the control of conformity following the methods hereunder described.

4.4 Examples of sampling according to batch

4.4.1 If several examples of one block type are constructed from one original block of aluminium honeycomb and are all treated in the same treatment bath (parallel production), one of these examples could be chosen as the sample, provided that they are not shaped and care is taken to ensure that the treatment is evenly applied to all blocks. If not, it may be necessary to select more than one sample.

4.4.2 If a limited number of similar blocks (say three to twenty) are treated in the same bath (serial production), then the first and last block treated in a batch, all of which are constructed from the same original block of aluminium honeycomb, should be taken as representative samples. If the first sample complies with the requirements but the last does not, it may be necessary to take further samples from earlier in the production until a sample that does comply is found. Only the blocks between these samples should be considered to be approved. All samples must remain unshaped.

4.4.3 Once experience is gained with the consistency of production control, it may be possible to combine both sampling approaches, so that more than one groups of parallel production can be considered to be a batch provided samples from the first and last production groups comply.

5. STATIC TESTS

5.1 One or more samples (according to the batch method) taken from each batch of processed honeycomb core shall be tested, according to the following test procedure:

5.1.1 The samples for all blocks (A, B, C, D, E and F) shall be 250mm x 500mm x 440mm.

5.1.2 The samples should be compressed between two parallel loading plates which are at least 20mm larger that the block cross section;

5.1.3 The compression speed shall be 100 millimetres per minute, with a tolerance of 5 per cent;

5.1.4 The data acquisition for static compression shall be sampled at a minimum of 5Hz;

5.1.5 The static test shall be continued until the block compression is at least 300mm for all blocks (A, B, C, D, E and F);

6. DYNAMIC LOAD CELL WALL TESTS

For every 200 barrier faces produced, the manufacturer shall make one dynamic test against a dynamometric wall supported by a fixed rigid barrier, according to the method described below.

6.1 Installation

6.1.1 Testing ground

6.1.1.1 The test area shall be large enough to accommodate the run-up-track of the mobile deformable barrier, the rigid barrier and the technical equipment necessary for the test. The last part of the track, for at least five metres before the rigid barrier, shall be horizontal, flat and smooth.

6.1.1.2 Fixed rigid barrier and dynamometric wall

6.1.1.3 The rigid wall shall consist of a block of reinforced concrete not less than 3 metres wide and not less than 1.5 metres high. The thickness of the rigid wall shall be such that it weighs at least 70 tonnes.

6.1.1.4 The front face shall be vertical, perpendicular to the axis of the run-up-tack and equipped with a minimum of six load cell plates, each capable of measuring the total load on the appropriate block of the mobile deformable barrier impactor at the moment of impact. The load cell impact plate area centres shall align with those of the six impact zones of the mobile deformable barrier face. Their edges shall clear adjacent areas by 20mm ± 2mm such that, within the tolerance of impact alignment of the MDB, the impact zones will not contact the adjacent impact plate areas. Cell mounting and plate surfaces shall be in accordance with the requirements set out in the annex to standard ISO 6487:1987.

6.1.1.5 The load cell wall must consist of at least 6 load cells, with the centre load cell having a loading surface area 500mm wide and 250mm high, and the outer load cells, covering Blocks A, C, D and F, having a loading surface area 600mm wide and 250mm high. If more than six load cells are used the aggregated area must be 500mm by 250mm at the centre and 600mm by 250mm outside.

6.1.1.6 The area surrounding the load cells (<1700mm by <500mm) must have a surface common to that of the load cell wall face for at least 150mm (>2000mm by >800mm). This is required to ensure that the barrier face is uniformly crushed and does not wrap around the edge of the load cells if the barrier impact is not in perfect alignment.

6.1.1.7 Surface protection, comprising a plywood face with a thickness of 18mm ± 5mm shall be added to each load cell plate such that no degradation of transducer responses occurs.

6.1.1.8 The rigid wall shall be either anchored in the ground or placed on the ground with, if necessary, additional arresting devices to limit its deflection. A rigid wall (to which the load cells are attached) having different characteristics but giving results that are at least equally conclusive may be used.

6.1.1.9 The load cells must align with the principle axes of the MDB face with Blocks B and E aligned with the central load cells. The intersection of all blocks must align with intersections between load cells.

6.2 Propulsion of the mobile deformable barrier

6.2.1 At the moment of impact the mobile deformable barrier shall no longer be subject to the action of any additional steering or propelling device. It shall reach the obstacle on a course perpendicular to the front surface of the dynamometric wall. The impact alignment shall be accurate to within ± 15mm.

6.3 Measuring instruments

6.3.1 Speed

6.3.1.1 The impact speed shall be 35 ± 0.5km/h the instrument used to record the speed on impact shall be accurate to within 0.1 percent.

6.3.2 Loads

6.3.2.1 Measuring instruments shall meet the specifications set forth in ISO 6487:1987

CFC for all blocks:	60Hz
CAC for all blocks:	100kN

6.3.3 Acceleration

6.3.3.1 The acceleration in the longitudinal direction shall be measured at three separate positions on the trolley, one centrally and one at each side, at places not subject to bending.

6.3.3.2 The central accelerometer shall be located within 500mm of the location of the centre of gravity of the MDB and shall lie in a vertical longitudinal plane which is within ± 10mm of the centre of gravity of the MDB.

6.3.3.3 The side accelerometers shall be at the same height as each other ± 10mm and at the same distance from the front surface of the MDB ± 20mm

6.3.3.4 The instrumentation shall comply with ISO 6487:1987 with the following specifications:

CFC 1,000Hz (before integration)
CAC 50g

6.3.4 Contact timing

6.3.4.1 Two foil contact switches shall be fitted at the outboard ends of the face of the beam element which contact the load cell wall first.

6.3.4.2 The contact switches must have a depth of 3mm or less.

6.4 General specifications of barrier and impactor

6.4.1 The individual characteristics of each mobile deformable barrier shall comply with Section 1 of this specification and shall be recorded.

6.4.2 The suitability of an impactor as regards to the dynamic test requirements shall be confirmed when the outputs from the six load cell plates each produce signals complying with the requirements indicated in this specification.

6.4.3 Impactors shall carry consecutive serial numbers which are stamped, etched or otherwise permanently attached, from which the batches for the individual blocks and the date of manufacture can be established.

6.5 Data processing procedure

6.5.1 Raw data

6.5.1.1 At time $T = T_0$, all offsets should be removed from the data. The method by which offsets are removed shall be recorded in the test report.

6.5.1.2 T0 shall be established using the two contact switches fitted to the beam element.

6.5.2 Filtering

6.5.2.1 The raw data will be filtered prior to processing/calculations.

6.5.2.2 Accelerometer data for integration will be filtered to CFC 180, ISO 6487:1987.

6.5.2.3 Accelerometer data for impulse calculations will be filtered to CFC 60, ISO 6487:1987.

6.5.2.4 Load cell data will be filtered to CFC 60, ISO 6487:1987.

6.5.3 Calculation of MDB face deflection

6.5.3.1 Accelerometer data from all three accelerometers individually (after filtering at CFC 180), will be integrated twice to obtain deflection of the barrier deformable element.

6.5.3.2 The initial conditions for deflection are:

6.5.3.2.1 Velocity = impact velocity (from speed measuring device);

6.5.3.2.2 Deflection = 0;

6.5.3.3 The deflection at the left hand side, mid-line and right hand side of the mobile deformable barrier will be plotted with respect to time.

6.5.3.4 The maximum deflection calculated from each of the three accelerometers should be within 10mm. If it is not the case, then the outlier should be removed and difference between the deflection calculated from the remaining two accelerometers checked to ensure that it is within 10mm.

6.5.3.5 If the deflections as measured by the left hand side, right hand side and mid-line accelerometers are within 10mm, then the mean acceleration of the three accelerometers should be used to calculate the deflection of the barrier face.

6.5.3.6 If the deflection from only two accelerometers meets the 10mm requirement, then the mean acceleration from these two accelerometers should be used to calculate the deflection for the barrier face.

6.5.3.7 If the deflections calculated from all three accelerometers (left hand side, right hand side and mid-line) are NOT within the 10mm requirement, then the raw data should be reviewed to determine the causes of such large variation. In this case the individual test house will determine which accelerometer data should be used to determine mobile deformable barrier deflection or whether none of the accelerometer readings can be used, in which case, the certification test must be repeated. A full explanation should be given in the test report.

6.5.3.8 T0 will be defined for both force and acceleration data using the two contact switches placed on the beam element. Due to the effects of filtering, it is expected that force levels

at T0 will be above 0kN for the lower row of blocks. Force data must NOT be shifted to establish 0kN at T0.

6.5.3.9 The mean deflection-time data will be combined with the load cell wall force-time data to generate the force-deflection result for each block.

6.5.4 Calculation of energy

6.5.4.1 The absorbed energy for each block and for the whole MDB face should be calculated up to the point of peak deflection of the barrier.

$$E_n = \int_{t_0}^{t_1} F_n \, . ds_{mean}$$

where:
t_0 is the time of first contact
t_1 is the time where the trolley comes to rest, i.e. where u = 0.
s is the deflection of the trolley deformable element calculated according to Paragraph 6.5.3.

6.5.5 Verification of dynamic force data

6.5.5.1 Compare the total impulse, I, calculated from the integration of the total force over the period of contact, with the momentum change over that period (M*ΔV).

6.5.5.2 Compare the total energy change to the change in kinetic energy of the MDB, given by:

$$E_K = \frac{1}{2} M V_i^2$$

where:
V_i is the impact velocity
M the whole mass of the MDB

6.5.5.3 If the momentum change (M*ΔV) is not equal to the total impulse (I) ± 5 per cent, or if the total energy absorbed (E En) is not equal to the kinetic energy, E_K ± 5 per cent, then the test data must be examined to determine the cause of this error.

6.6 Post test

6.6.1 The crush of the AE-MDB should be recorded after the LCW impact at a representative point on the barrier. The crush measurement shall be compared to the deflection calculated from the trolley accelerometer data. If the calculated deflection is 20mm or more below the crush measured after the impact, the individual test house will determine if any of the accelerometer data can be used, in which case, the certification test must be repeated. A full explanation should be given in the test report.

7. DESIGN OF THE IMPACTOR

All dimensions are in mm.

7.1 Barrier face

7.1.1 The tolerances on the dimensions of the blocks allow for the difficulties of measuring cut aluminium honeycomb. The tolerance on the overall dimension of the impactor is less than that for the individual blocks since the honeycomb blocks can be adjusted, with overlap if necessary, to maintain a more closely defined impact face dimension.

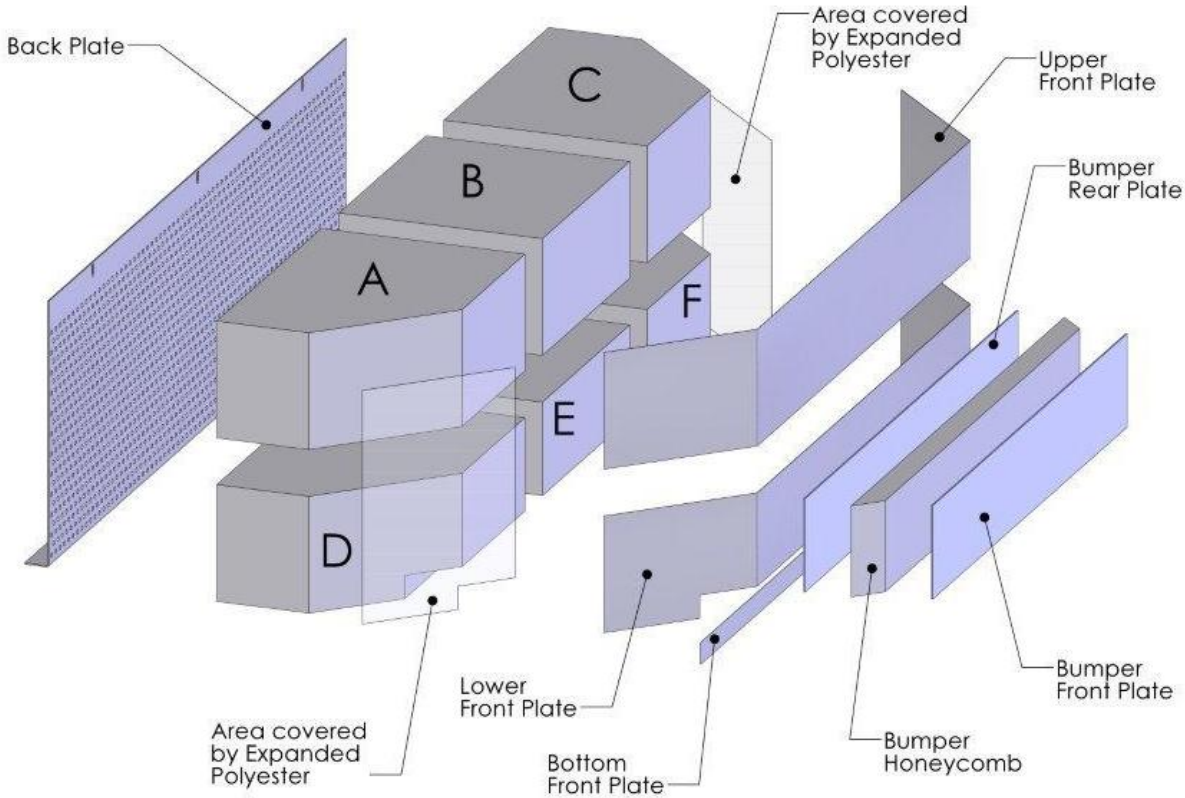

Figure 4: Exploded isometric view of AE-MDB

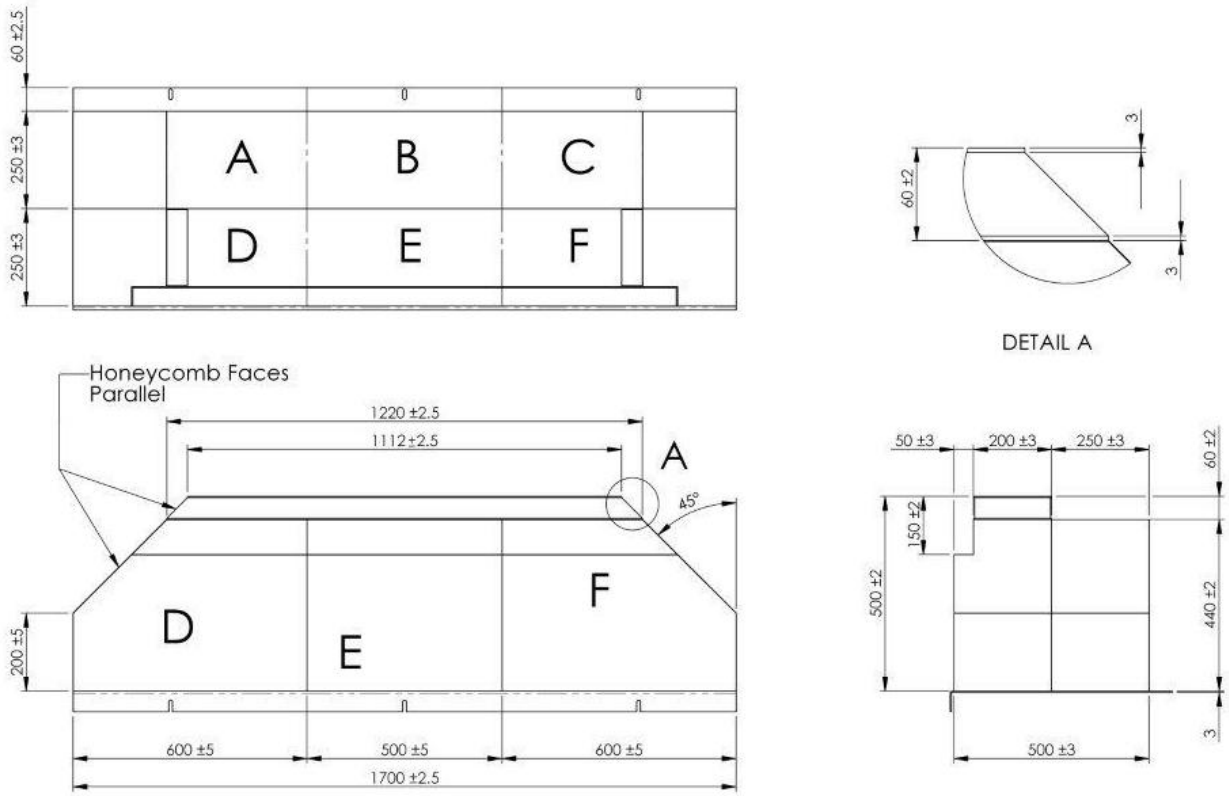

Figure 5: AE-MDB dimensions

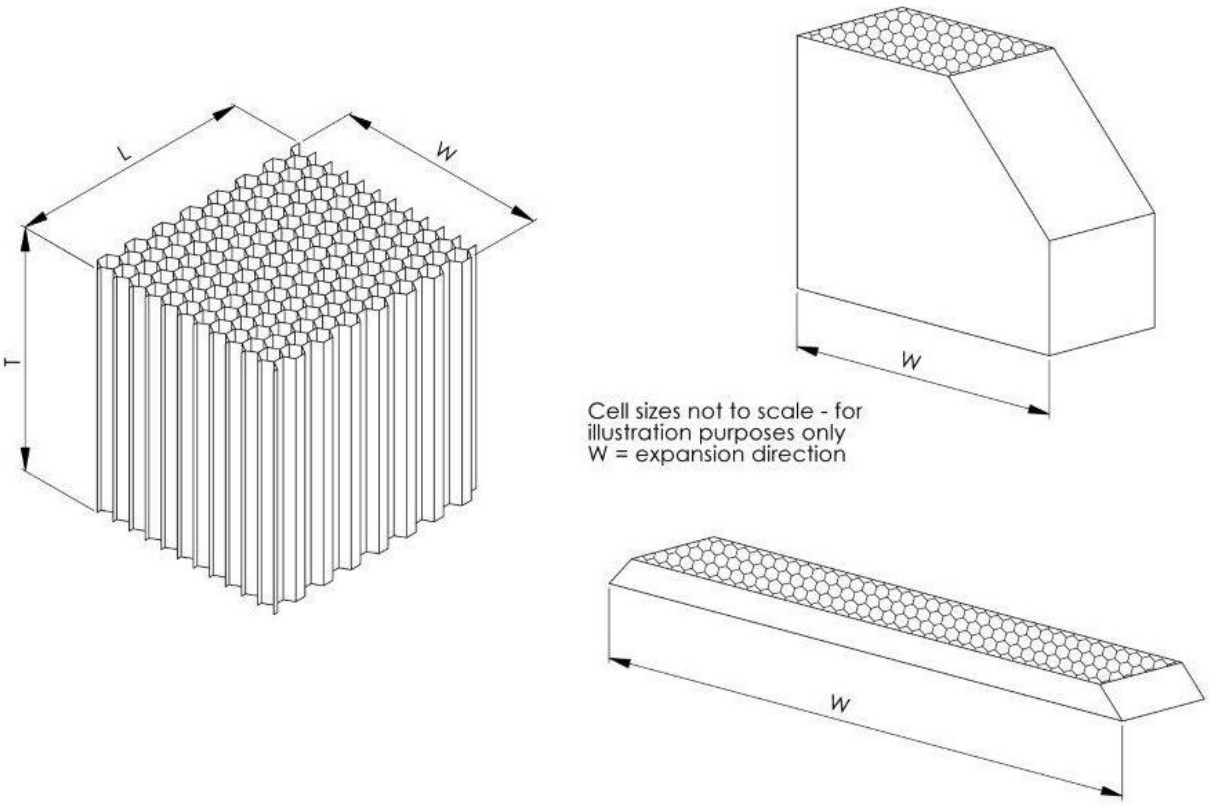

Figure 6: Aluminium honeycomb orientation

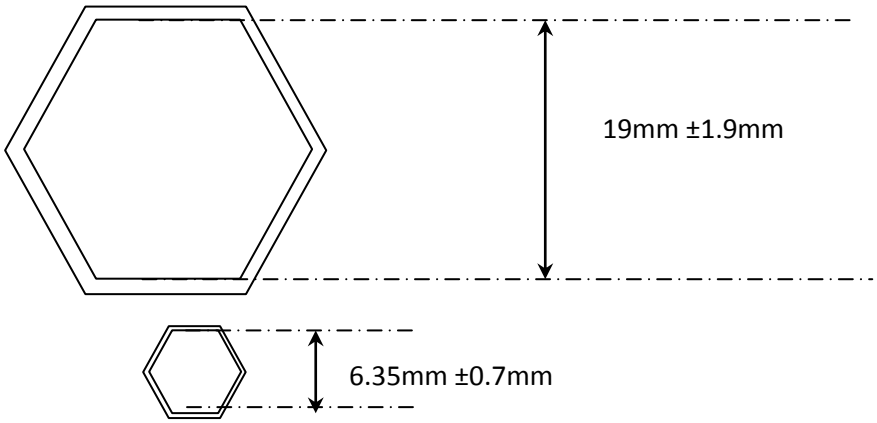

Figure 7: Dimension of Aluminium Honeycomb Cells

7.2 Back plate

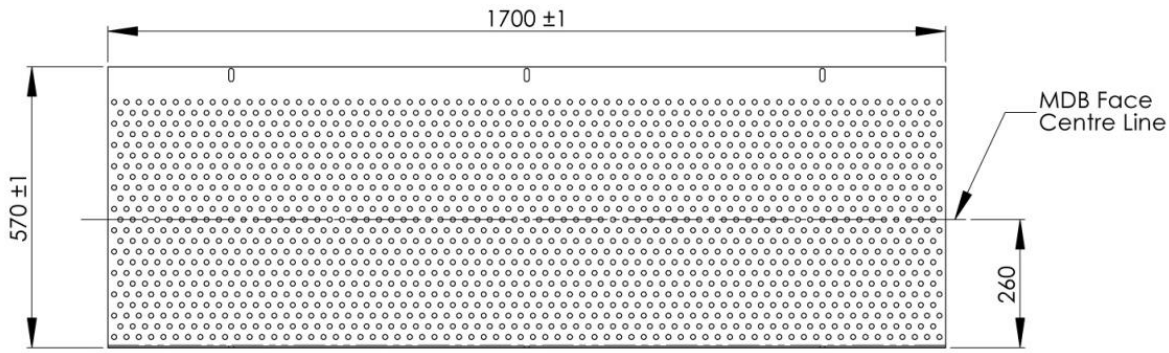

Figure 8: Rear view of the back of the barrier face

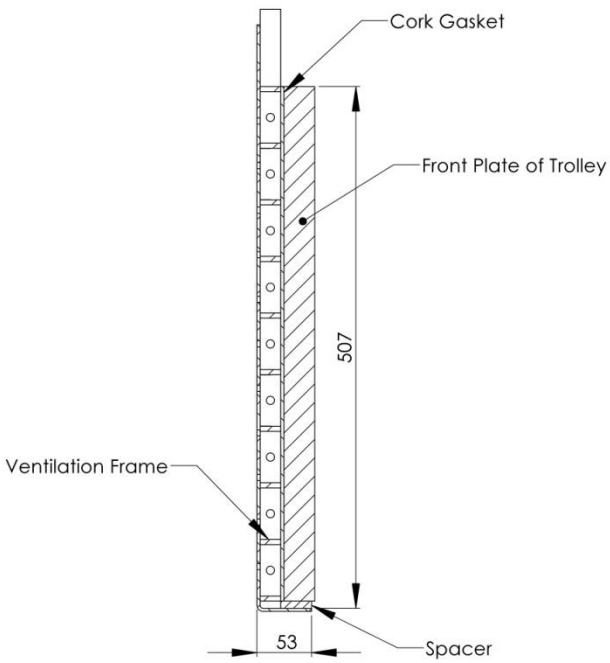

Figure 9: Attachment of backplate to ventilation device and trolley face plate

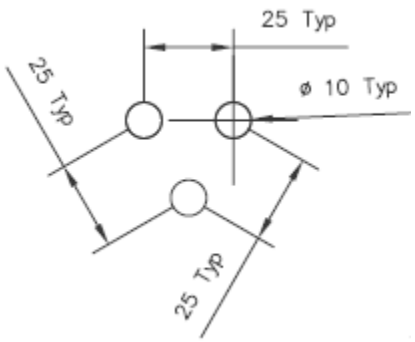

Figure 10: Staggered pitch for the backplate ventilation holes

7.2.1 Top and bottom back plate flanges

7.2.2 The attachment holes in the bottom flange may be opened to slots, as shown below, for ease of attachment provided sufficient grip can be developed to avoid detachment during the whole impact test.

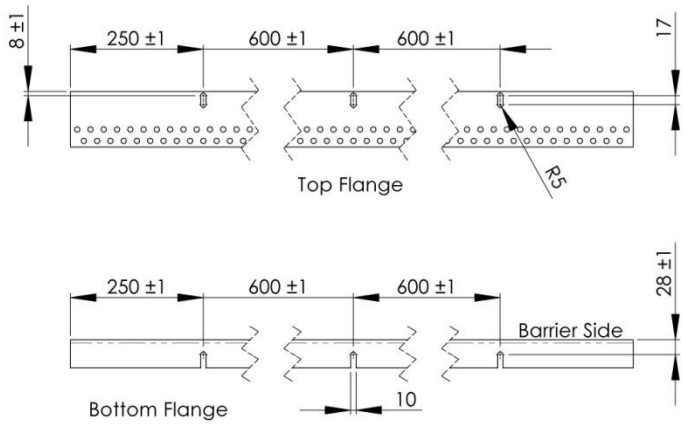

Figure 11: Top and bottom AE-MDB mounting flanges

7.3 Ventilation frame

7.3.1 The ventilation device is a structure made of a plate that is 5mm thick and 20mm wide. Only the vertical plates are perforated with nine 8mm holes in order to let air circulate horizontally.

7.3.2 It is acceptable for ventilation frames that are 1500mm in with to be extended up to 1700mm in width provided that the correct pattern of venting and fixation is used.

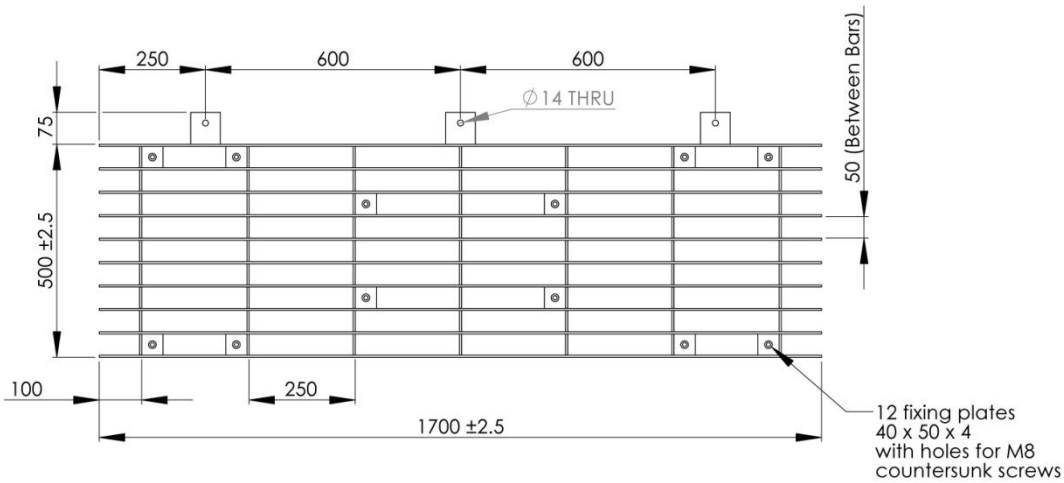

Figure 12: AE-MDB trolley ventilation frame

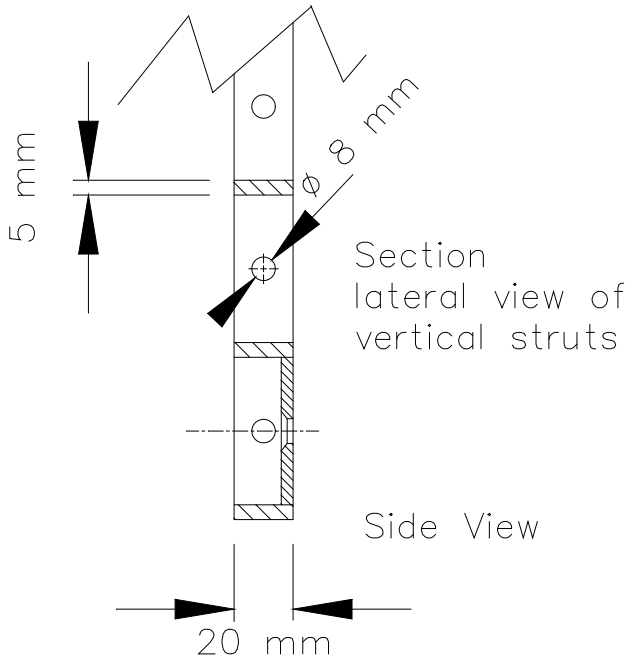

Figure 13: AE-MDB trolley ventilation frame – side view

8. STATIC FORCE DEFLECTION CORRIDORS

Force deflection corridors for quasi-static crush tests to test samples measuring 250 x 500mm for all blocks.

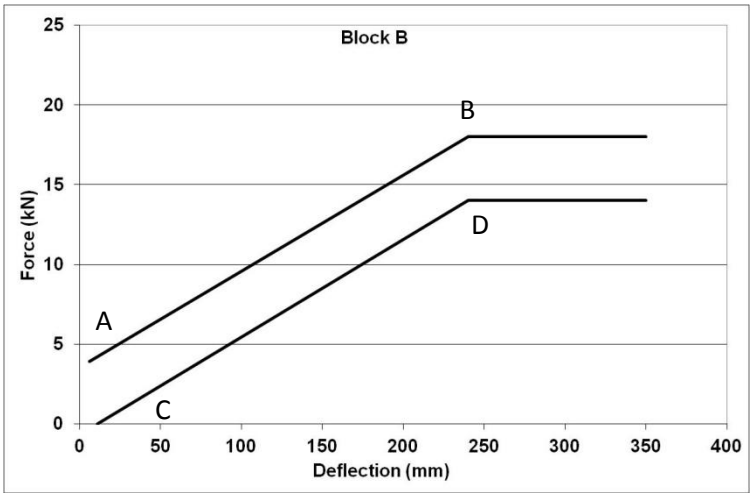

	Force	Deflection
A	3.9kN	6mm
B	18kN	240mm
C	0kN	11mm
D	14kN	240mm

Figure 14: Block B static corridor

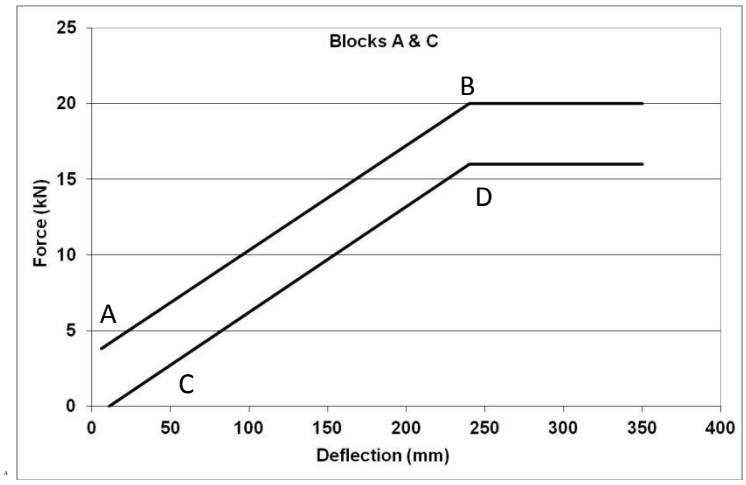

	Force	Deflection
A	3.8kN	6mm
B	20kN	240mm
C	0kN	11mm
D	16kN	240mm

Figure 15: Blocks A & C static corridor

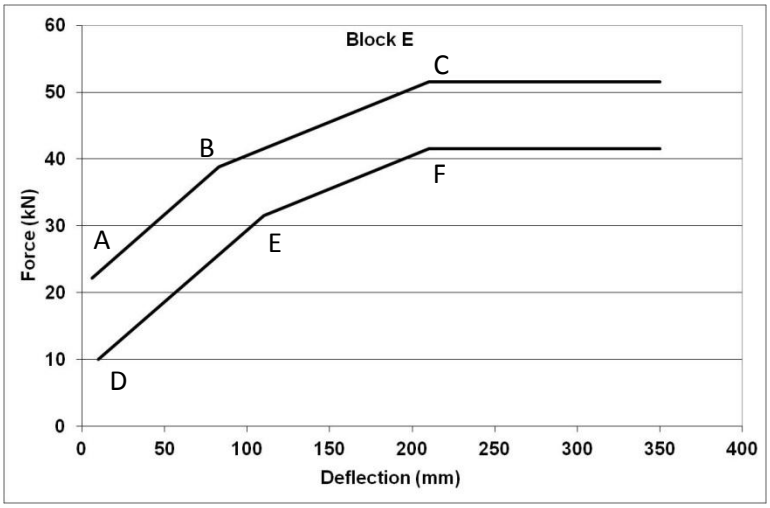

	Force	Deflection
A	22.2kN	6mm
B	38.8kN	83mm
C	51.5kN	210mm
D	10kN	10mm
E	31.5kN	110mm
F	41.5kN	210mm

Figure 16: Block E static corridor

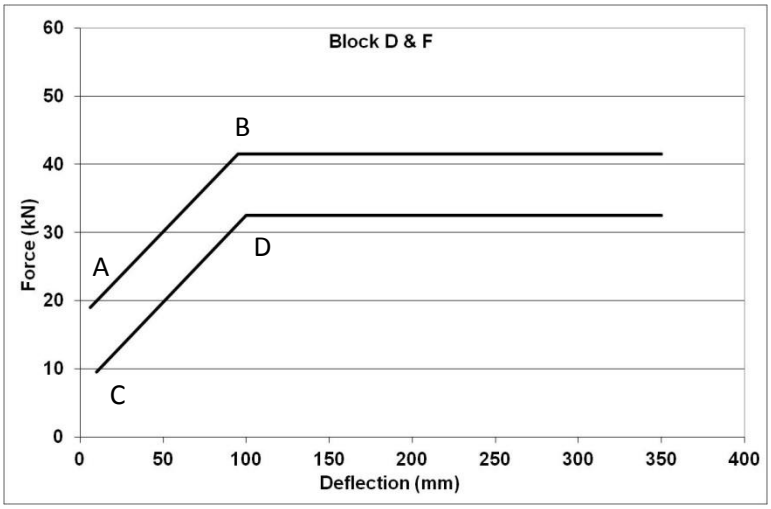

	Force	Deflection
A	19kN	6mm
B	41.5kN	95mm
C	9.5kN	10mm
D	32.5kN	100mm

Figure 17: Blocks D & F static corridor

9. DYNAMIC FORCE DEFLECTION CORRIDORS

Force deflection corridors for dynamic barrier to LCW tests.

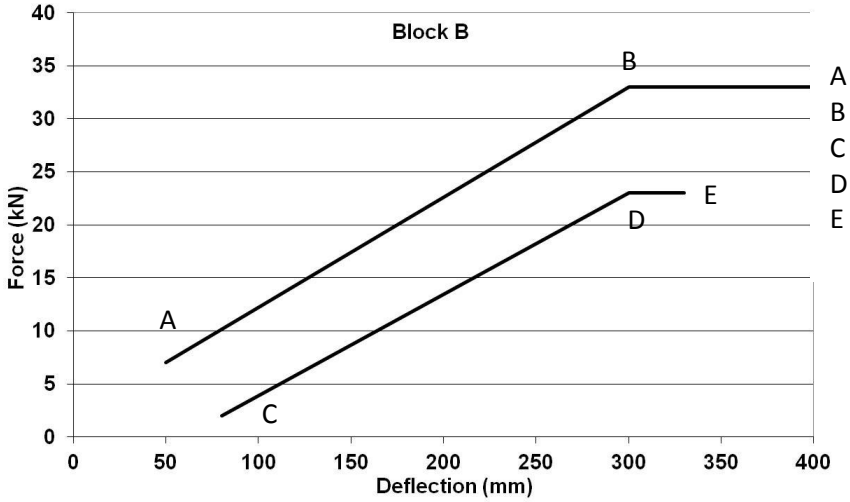

	Force	Deflection
A	7kN	50mm
B	33kN	300mm
C	2kN	80mm
D	23kN	300mm
E	23kN	330mm

Figure 18: Block B dynamic corridor

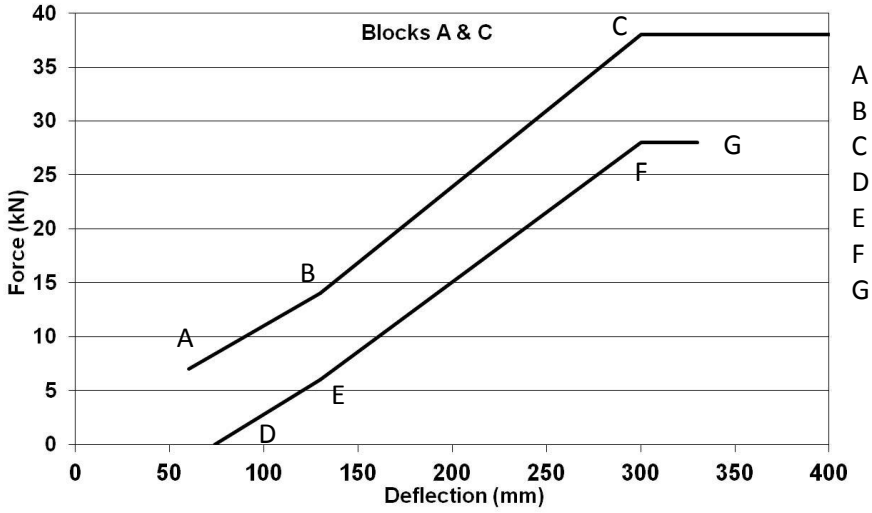

	Force	Deflection
A	7kN	60mm
B	14kN	130mm
C	38kN	300mm
D	0kN	74mm
E	6kN	130mm
F	28kN	300mm
G	28kN	330mm

Figure 19: Blocks A & C dynamic corridor

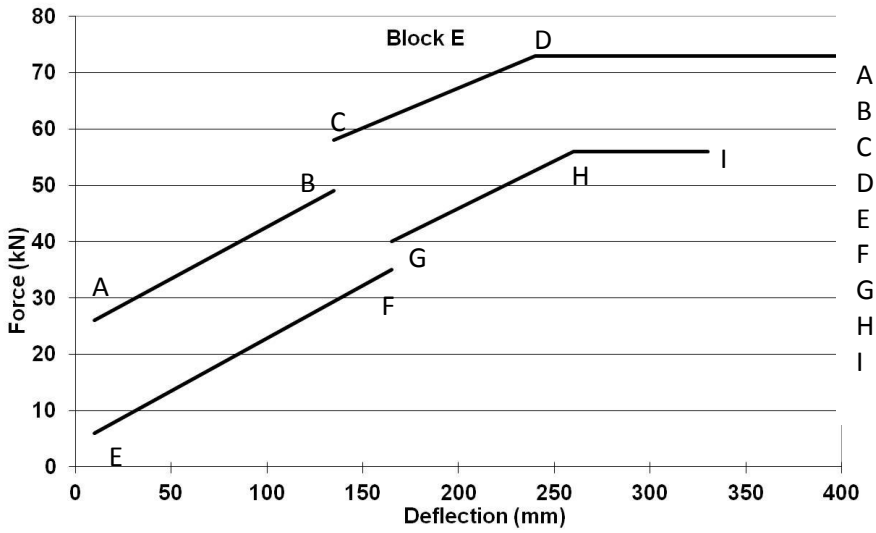

	Force	Deflection
A	26kN	10mm
B	49kN	135mm
C	58kN	135mm
D	73kN	240mm
E	6kN	10mm
F	35kN	165mm
G	40kN	165mm
H	56kN	260mm
I	56kN	330mm

Figure 20: Block E dynamic corridor

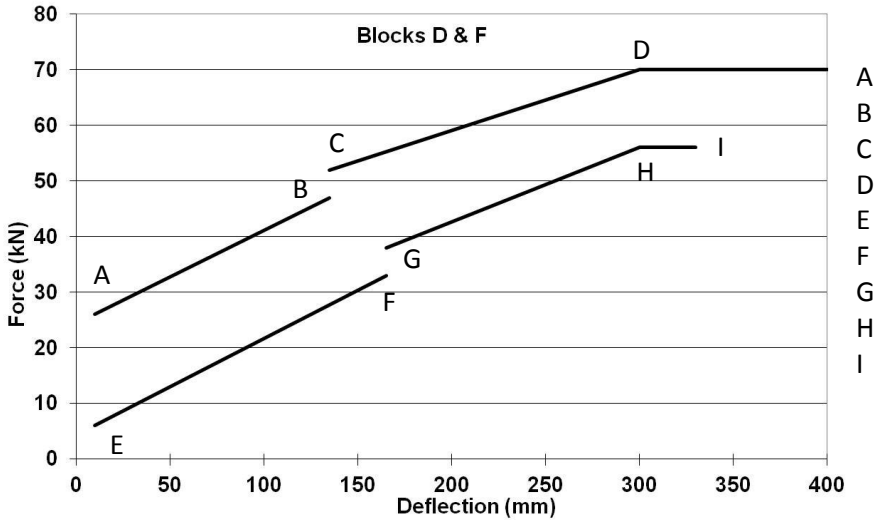

	Force	Deflection
A	26kN	10mm
B	47kN	135mm
C	52kN	135mm
D	70kN	300mm
E	6kN	10mm
F	33kN	165mm
G	38kN	165mm
H	56kN	300mm
I	56kN	330mm

Figure 21: Blocks D & F dynamic corridor

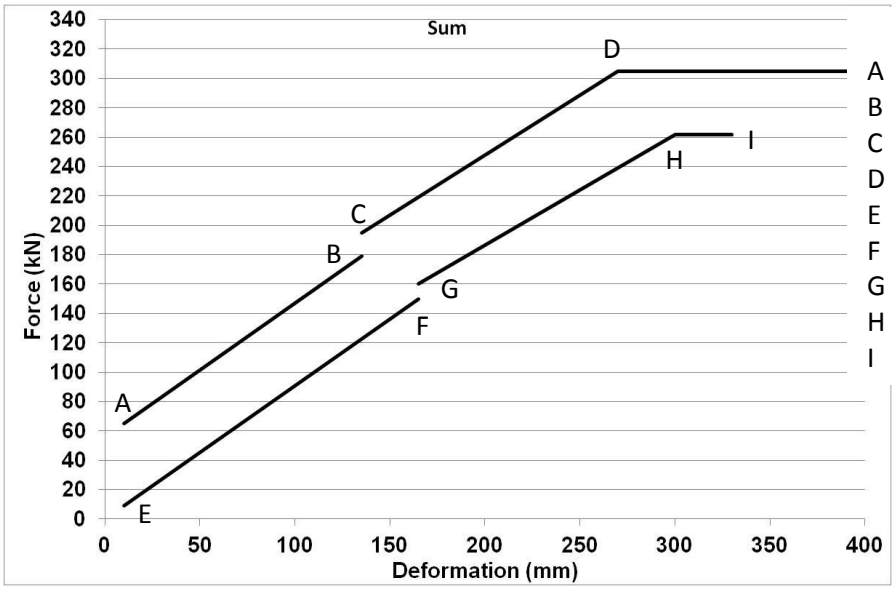

	Force	Deflection
A	65kN	10mm
B	179kN	135mm
C	195kN	135mm
D	305kN	270mm
E	9kN	10mm
F	150kN	165mm
G	160kN	165mm
H	262kN	300mm
I	262kN	330mm

Figure 22: Full barrier dynamic corridor

IMPLEMENTATION OF THE UNSW JORDAN ROLLOVER SYSTEM AT SYDNEY'S CRASHLAB TEST FACILITY

Raphael Grzebieta
Andrew McIntosh
Garrett Mattos
Keith Simmons
George Rechnitzer
Mario Mongiardini
Transport and Road Safety (TARS) Research, University of New South Wales,
Australia
Ross Dal Nevo
Colin Jackson
Crashlab, Roads and Maritime Services, Transport for NSW,
Australia
Paper Number 13-0120

ABSTRACT

This paper describes how the Jordan Rollover System (JRS) dynamic test rig was adapted for research use in the New South Wales State government's Crashlab® crash test facility used for Australian NCAP and regulatory crash testing. Development and installation of the University of New South Wales (UNSW) JRS was funded by the Australian Federal Government's Australian Research Council (ARC) and industry partners. It is one of three rigs now operating in the world: the original Center for Injury Research (CFIR) JRS, the Dynamic Rollover Test System (DRoTS) at the University of Virginia, and the UNSW JRS in Sydney.

Construction of the UNSW JRS was the first phase of the much larger Dynamic Rollover Occupant Protection (DROP) research program which is funded by the ARC and industry partners, to establish which combination of crash severity, roll kinematics, biomechanical injury criteria, crash test dummy, and restraint systems, address the major proportion of fatalities and serious injuries occurring to seat belted and restrained occupants involved in rollover crashes.

The design of the UNSW JRS focused on functionality for research purposes while at the same time ensuring operational flexibility within a regulatory and commercial crash test facility. Data sources used for the design phase included: rollover crash test results on a variety of vehicles carried out using the CFIR JRS; FMVSS 208 dolly rollover crash tests carried out by other researchers; rollover fatality crash data and in-depth crash reconstructions from Australian Coroners Information System (NCIS) and from the NASS-CDS. These data were used to determine what features were essential for using the UNSW JRS as a comprehensive research tool to explore different initial test conditions (roll rate, drop height, roll, pitch and yaw angle) that could possibly replicate real-world rollover crash conditions where serious injuries occurred.

Features of the test rig design adress issues concerning: roadbed decoupling; rig mobility; roadbed towing; lighting; timing synchronisation of the vehicle drop for a given roll rate and roll angle in terms of accuracy and repeatability; and recording data and sensors compatibility. Commissioning rollover crash tests of a small and medium passenger cars and a large four wheel drive vehicle were carried out to establish test rig functionality and identify issues concerning rig operation. Results from the commissioning tests are presented.

It was concluded that the UNSW JRS can be adapted to a commercial or government crash test facility. A critical issue was vehicle impact synchronisation due to the complexity of decoupling roadbed movement from the roll propulsion. Another issue that continues is the ability of the rig to replicate real world crashes which may be significantly more severe than the test rig has to date been used and/or designed for. This is further discussed in the paper.

INTRODUCTION

Rollover crashes are very complex events. Despite over 40 years of international research and expertise devoted to this issue, the solution to the trauma resulting from such crashes continues to be elusive in terms of rating a vehicle's rollover crashworthiness. To date, there is no viable dynamic crash test procedure implemented by either a consumer body or government that protects occupants in rollover crashes. The reasons for this are set out in a sister paper [1] and in a paper which first appeared in the proceedings of the International Crashworthiness Conference ICRASH 2012 held in Milan, Italy, titled "The

Dynamic Rollover Protection (DROP) Research Program" [2]. This paper summarises sections relating to the JRS taken from the ICRASH 2012 paper. Readers are directed to the full ICRASH 2012 paper for a more comprehensive discussion of the issues presented here and in [1].

Presently, two countermeasures have been introduced in Australia to address rollover crashes. The first is a preventative measure, i.e. Electronic Stability Control (ESC). The Australian Government introduced an Australian Design Rule, based on Global Technical Regulation No.8, for the mandatory fitting of ESC to passenger cars and Sports Utility Vehicles (SUVs) from November 2011 (for new models) and November 2013 (for all vehicles) [3, 4].

The second countermeasure is the introduction of a quasi-static roof strength requirement based on the Insurance Institute for Highway Safety (IIHS) rating system [5]. In order to obtain five stars under the Australian New Car Assessment Program (ANCAP) in 2014 and 2015, a vehicle will be required to have at least 'marginal' roof strength where the strength to weight ratio (SWR) for a single sided roof crush will need to be 2.5 or greater. The minimum SWR requirement will rise to 'acceptable' (3.25 or greater) for both 2016 and 2017 [6]. Presumably, the intention is to raise the SWR requirement to 'good' (4.0 or greater) in following years.

The IIHS and ANCAP roof strength requirement is based on a number of studies that to date have found a positive relationship between the amount of roof crush, roof strength and the likelihood of serious injury in rollover crashes [7-16]. However, as argued by Grzebieta *et al*. [1, 2], and identified by Bambach *et al*. and Mattos *et al.* [15-17], analysis of crashes involving contained and restrained occupants involved in single vehicle pure rollover crashes that occurred in the United States (US), serious injuries to the thorax, head and spine can still occur even when there is little or no roof crush. This highlights the need to improve occupant restraint systems in conjunction with strengthening the roof.

It is worth noting that the US introduced two further tests in an attempt to better assess the potential of a vehicle to cause injuries that may occur in a rollover crash, namely Federal Motor Vehicle Safety Standard (FMVSS) 201 for Occupant Protection in Interior Impact which assess interior padding in vehicles [18] and FMVSS 226 Ejection Mitigation standard which is meant to reduce the partial and complete ejection of vehicle occupants through side windows in crashes, particularly rollover crashes [19]. There are no such equivalent standards required in Australia although Australia does have very high seat belt wearing rates, which to some extent helps obviate the need for such requirements.

Australian authorities and consumer groups such as ANCAP are reluctant to implement any dynamic rollover testing procedures until a number of research issues have been resolved. The main issue is a regulatory or consumer test must reliably replicate the dynamic conditions and injury mechanisms associated with a rollover crash so that the efficacy of occupant protection systems can be repeatedly demonstrated. Many researchers (ourselves included) consider the JRS test rig using an appropriate ATD will be able to achieve this, i.e. developing a dynamic crash test rig such as the UNSW JRS and demonstrating it can reproduce rollover crashes and associated injuries with acceptable consistent repeatability. Such a successful outcome could assist designers, regulators and consumer groups in mitigating those injuries using advanced crashworthiness systems.

Currently regulators and ANCAP are open to adopting any suitable test methodology or procedure, as long as it is proven via evidence based real world data driven research and the societal benefits are worthwhile. A review of various rollover crashworthiness tests and dynamic test rigs by Chirwa *et al.* indicated the JRS is the best candidate to date [20]. For this reason the UNSW DROP research team decided to invest in the construction and implementation of the UNSW JRS rig.

UNSW JRS TEST RIG

Funding for the installation of the JRS was obtained as a result of a successful research grant application submitted to the Australian federal government's Australian Research Council's (ARC) Linkage Infrastructure Equipment Facilities (LIEF) Project grants scheme (No: LE0989476). Monash University and Industry Partner Organisations also provided funding, namely, the New South Wales (NSW) state government's Centre for Road Safety at Transport for NSW (formerly the Roads and Traffic Authority – RTA), the NSW state government's 3rd party injury insurer Motor Accident Authority (MAA), the West Australian (WA) state government's Office of Road Safety at Main Roads WA, and the US Center for Injury Research (CFIR).

Research is currently being undertaken to design dynamic tests and test protocols that would provide a more accurate assessment of a vehicle's occupant safety in a rollover crash [21, 19, 24]. Three versions of the Jordan Rollover System (JRS) are

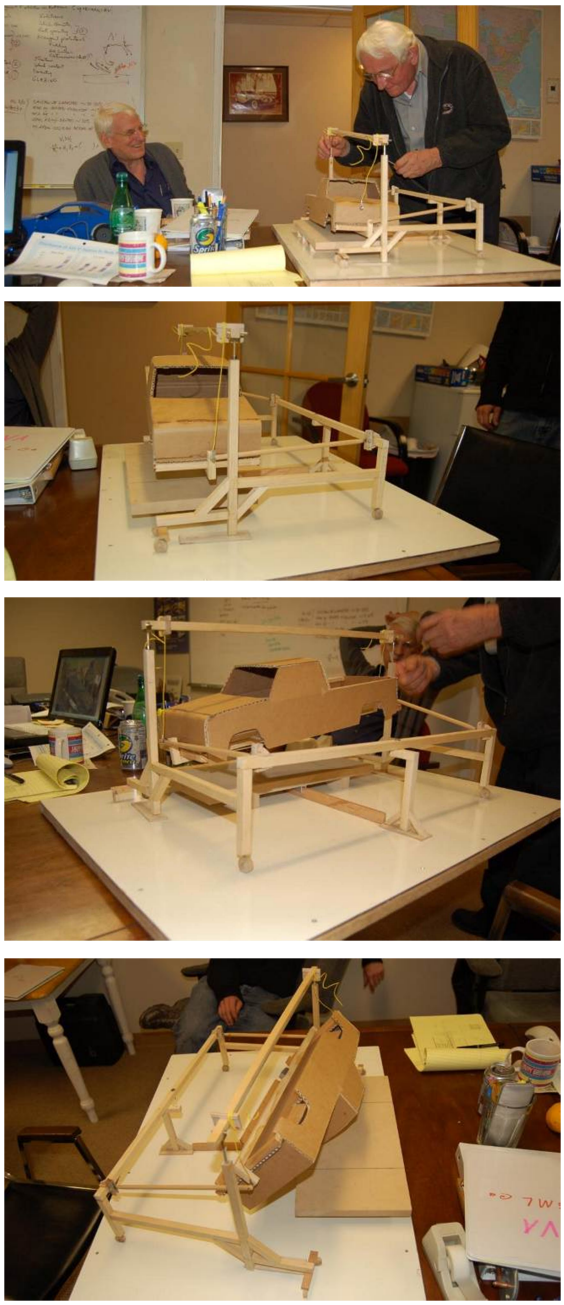

Figure 1. Concept model of UNSW JRS rig. Top frame: Dr. Carl Nash (left) from George Washington University and Acen Jordon (right).

being used at locations around the world (Center for Injury Research (CFIR) in Goleta, CA, USA; University of Virginia in Charlottesville, VA, USA; and the University of New South Wales/Crashlab® in Sydney, NSW, Australia) to study rollover and determine the feasibility of using the JRS to accurately assess a vehicle's ability to protect occupants in the real world.

The first phase of the DROP program was to construct a JRS test rig for use in Australia. Figure 1 shows a scale model and Figure 2 a concept sketch of the UNSW JRS during the design

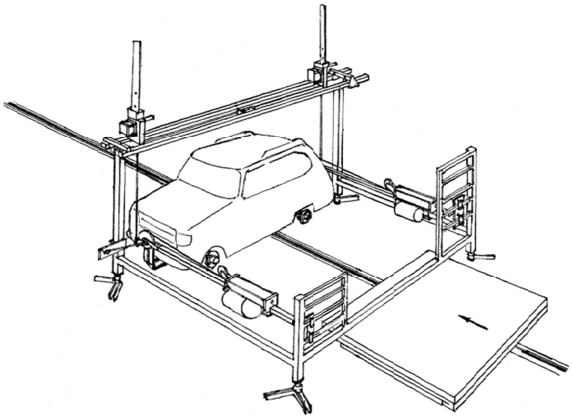

Figure 2. Drawing of Concept model of UNSW JRS rig.

phase. The rig was developed by Acen Jordan and Don Friedman from the USA. The constructed UNSW JRS that was assembled at the Crashlab® facility at Huntingwood near Sydney is shown in Figure 3. The rig was developed collaboratively by the USA designers and JRS rig manufacturers, UNSW researchers and Crashlab® test staff. The rig was then manufactured in the USA, shipped to Australia and eventually integrated into the Sydney Crashlab® facility.

The first author worked closely with the US manufacturer Safety Testing International, who designed and manufactured the rig, to ensure maximum flexibility of the rig for the commercial and regulatory crash testing environment it was going to operate in. The functionality of the UNSW JRS is different to the original CFIR JRS [21] in so far that the roadbed works independently of the roll actuator and the vehicle can be set to as much as 30-degree yaw and 15-degree pitch. The CFIR JRS roll actuator is linked via a cable to the roadbed and the pitch and yaw capacity are more limited. Moreover, the CFIR JRS rig continues to pull the roadbed through the test while the vehicle is impacting the roadbed whereas in the UNSW JRS the independent tow system is released from the roadbed just prior to impact.

Figures 3 and 4 show how the UNSW JRS attaches and suspends the vehicle via the cradle which in turn is suspended by the drop and catch assembly supported by the frame gantry. The vehicle is free to spin about its longitudinal centre of gravity axis above the track independent of the roadbed translational motion which is towed by the Crashlab® drive system. The control arms constrain the vehicle in the direction of the roadbed movement but allow vertical displacement. The roadbed is instrumented with load cells so that the vertical impact load can be measured. The vehicle

Figure 3. UNSW JRS rig assembled at Crashlab®; Top and middle: front view; bottom: side view.

can be positioned with a predetermined pitch, yaw, and drop height.

The terms near and far are used to describe the side of the vehicle that impacts the roadbed first and last, respectively. Figure 4 shows how the vehicle rolls and then drops onto the roadbed and then is caught once the roadbed passes. At the start of the

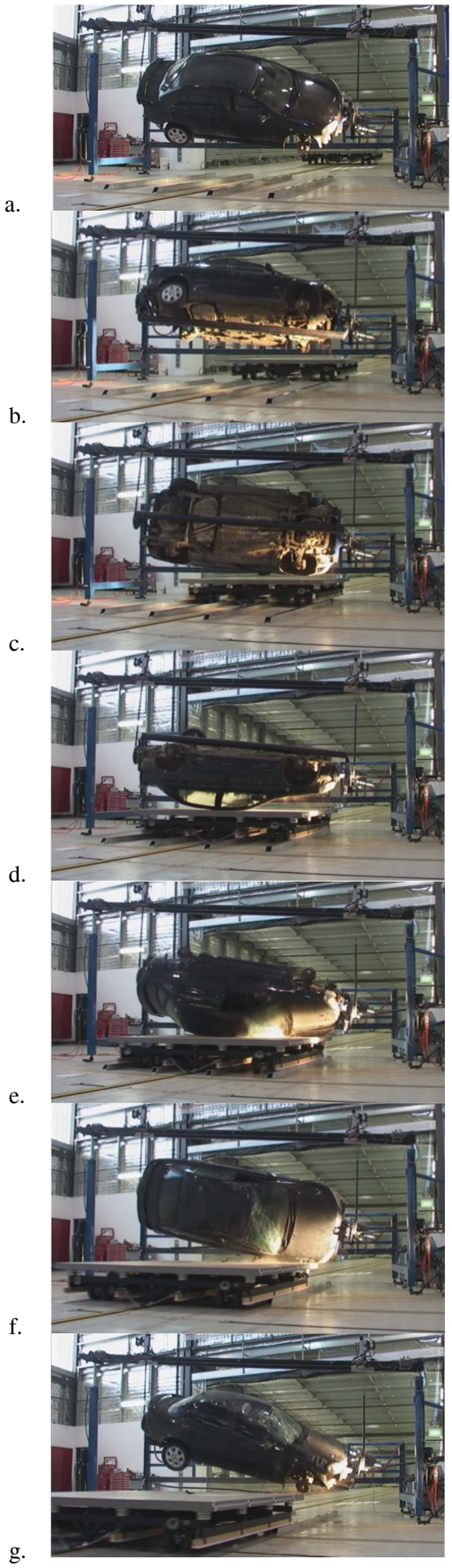

Figure 4. Roll and drop sequence as roadbed moves away under car after roll impact, for the UNSW JRS.

Pre-crash

Post-crash

Figure 5. GM Holden Astra loaded into JRS showing before and after one roll.

Pre-crash

Post-crash

Figure 6. 1998 Toyota Land Cruiser loaded into JRS; before and after one roll shown. Note roadbed under vehicle has stopped under the vehicle. (roadbed has been modified since to correct this)

test (a), when the roadbed is approaching close to the rig, the roadbed is released and the roll propulsion unit is activated such that the vehicle is rotated at a prescribed angular velocity (b & c). The roof then impacts the freely moving roadbed at the designated roll and pitch angle (d) on the near side. The vehicle then rolls on the roadbed over to its far side (e). The roadbed continues down the track and the vehicle is eventually captured so that it does not drop onto the test floor (f & g). It should be noted that the roll sequence for the UNSW JRS is a mirrored rotation process compared to how the US CFIR JRS and DROTS rigs operate. This is due to difference in driver seat position between Australian and US vehicles (left hand drive versus right hand drive vehicles, but in both cases the driver is on the impacting far side).

When the catch assembly releases the vehicle and the roll propulsion reaches the desired roll rate the vehicle can freely rotate and move vertically. Pitch can vary during the roll from the initial setting when it is released. The tow system releases the roadbed just prior to impact. When the vehicle then strikes the roadbed on the near side the roadbed is not being towed. Skate-over rails support the roadbed during the impact albeit the roadbed can skate freely through on the support rails as the vehicle continues to roll on top of it, impacting the far side. Immediately after the roadbed passes, the brakes on the catch assembly activate suspending the vehicle above the test floor. The roadbed is then slowly stopped down the track away from the suspended vehicle.

So far five vehicles have been tested in the UNSW JRS: three commissioning tests and two further training tests for improvements to test procedure and ATD measurements. Figure 5 shows a GM Holden Astra and Figure 6 a 1998 Toyota Land Cruiser both tested at 5-degree pitch, 180deg/sec roll rate, 24km/h roadbed speed, and 10-degree yaw. This is known as the Santos test protocol, named after the US Santos Foundation that sponsored a large portion of the US CFIR JRS tests [21]. The 1998 Toyota Land Cruiser's roof crush performance would be rated poor compared to other vehicles that have undergone a similar crash test.

As shown in Figure 3 the rig can be moved around on wheels and then set down and bolted to the concrete floor as indicated in Figure 7. Similarly Crashlab's tow facility was utilised to tow the roadbed. The CFIR JRS has its own roadbed propulsion system. Building a propulsion system so that the rig is self-contained would have increased costs significantly and reduced its operational flexibility within the Crashlab® facility. The highly sophisticated crash lab towing system allows for a

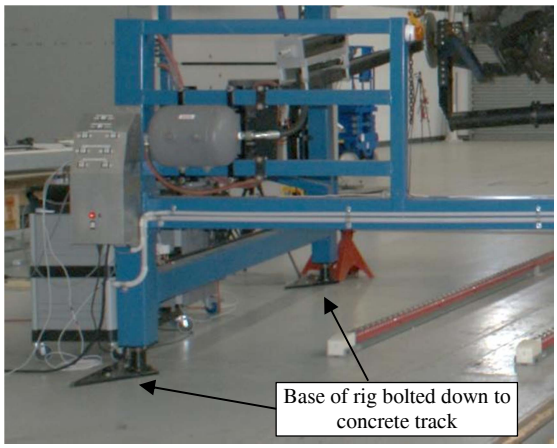

Figure 7. Feet of base of the JRS gantry frame bolted to concrete floor.

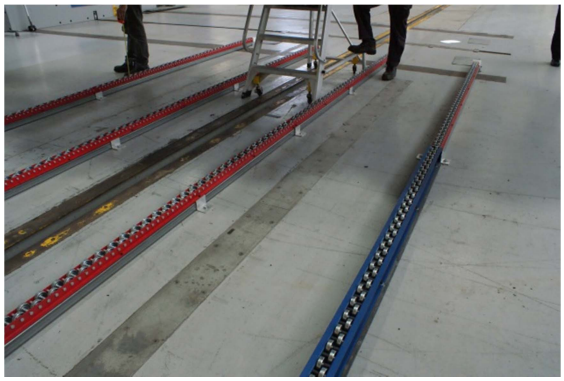

Figure 8. Roller skate tracks help reduce the friction between the roadbed and the tracks.

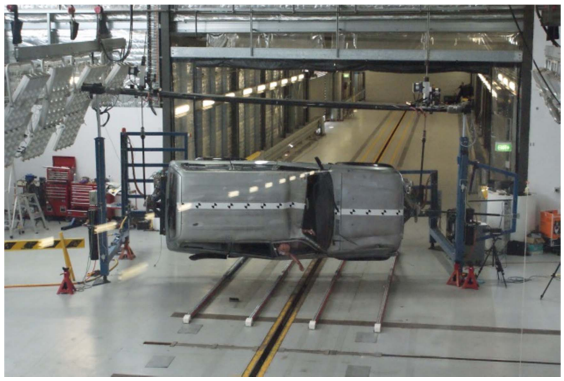

Figure 9. Second Land Cruiser test showing roadbed had passed under the vehicle after the vehicle had impact the roadbed.

better control of the roadbed speed, since it uses a computerised control system that continually checks and appropriately maintains the speed during the run.

An issue that arose was how the roadbed slid on the support rails. The images in Figure 5 show the rectangular aluminium tubing support rails fixed to the concrete test floor. The roadbed is constructed so that it runs on wheels up until the moment it reaches under the vehicle. A matching set of tubing under the roadbed then slides (skates) over the aluminium tubing fixed to the concrete track floor. This tubing also provides load bearing support for the roadbed during impact. Because the sliding coefficient of friction was around 0.19 and the mass of the roadbed was around 1160kg, the combination of a low mass roadbed and relatively high sliding friction caused the roadbed to stop under the vehicle as shown in Figure 6. To address this situation, the mass of the roadbed was increased and the aluminium tube support rails replaced with roller support rails as shown in Figure 8. A subsequent test of another Land Cruiser was run and the roadbed passed readily under the vehicle with the vehicle interacting in a manner similar to that shown in Figure 4.

Finally, it needs to be pointed out that repeated calibration runs are used to achieve synchronisation of the roadbed such that it is located immediately under the vehicle in the correct position at the moment the vehicle drops onto its near side. The roadbed once released freely moves under the vehicle and the vehicle is allowed to drop just short of the roadbed. Timing of the position of the roadbed is thus matched to the moment the near side of the vehicle is intended to impact the roadbed.

CONCLUSIONS

The following conclusions were reached:

- The UNSW JRS provides a much needed rollover test rig, to further research on vehicle rollover crashworthiness, and to help develop improved vehicle design for occupant protection in rollover.

- Observationally the rig appears to function in a manner similar to the USA CFIR JRS and University of Virginia DROTS rigs during the test in regards to the rollover crash mechanism;

- The UNSW JRS can be adapted to a commercial or government crash test facility. The rig can be easily moved from one side of the facility to the other to make way for other testing;

- The critical issue of vehicle roll impact synchronisation (timing) between the decoupled roadbed and vehicle motion (dropping and rotating) was determined via basic physics calculations and then fine-tuned via multiple calibration runs, i.e. matching up the instant the vehicle's near side was directly over the leading front side of the roadbed;

- To ensure the roadbed does not stall under the vehicle, the support rails fixed to the concrete test track over which the roadbed slides were changed to rollers. This in combination with more closely matching the roadbed mass with that of the vehicle eliminated the roadbed stalling problem.

Future work:

- It appears the test rig will be capable of repeatable tests; however this has yet to be assessed. Moreover , detailed comparisons of test results such as deformation, roadbed loads, roll rate, etc. has yet to be carried out to assess repeatability comparisons between the three rigs at Sydney, Goleta and Charlottesville;

- The ability of the UNSW JRS to replicate real world rollover crashes may subject the test rig to significantly more severe loads than it has to date been subjected to and/or designed for. This will be explored through computer simulation using LSDYNA to first to assess what the loads may be and then strengthen the rig to tolerate the higher loads;

- An extended rollover test and research program will be developed, utilising the UNSW JRS, aimed at better replicating real world rollover injury mechanisms, and vehicle design injury mitigation.

ACKNOWLEDGEMENTS

The authors would like to thank the Australian federal government's Australian Research Council for providing funds to carry out this research through the LIEF Project grants scheme (No: LE0989476). The generous funding and in-kind contributions by Monash University and the industry Partner Organisations for provide funding is greatly appreciated, namely, the New South Wales (NSW) state government's Centre for Road Safety at Transport for NSW (formerly the Roads and Traffic Authority – RTA), the NSW state government's 3rd party insurer Motor Accident Authority (MAA), the West Australian (WA) state government's Office of Road Safety at Main Roads WA, and the US Center for Injury Research (CFIR).

The authors would also like to thank Acen Jordan from Jordan & Co, and Josh Jeminez, Susie Bozzini from Safety Testing International and Don Friedman from the US Center for Injury Research, for their valuable contributions and assistance with the conceptual design, manufacture and installation of the UNSW JRS and the staff at Roads and Maritime Services Crashlab® for their generous assistance during installation and ongoing rig development.

REFERENCES

[1] Grzebieta R, Bambach M, McIntosh AS, Mattos G, Simmons K, Rechnitzer G, Digges K., (2013). *Replicating Real World Rollover Crash Injuries*, Proc. 23rd International Technical Conference on the Enhanced Safety of Vehicles, Seoul, Korea.

[2] Grzebieta R., Bambach M., McIntosh A.S., Digges K., Job S., Friedman D., Simmons K., Chirwa C., Zou R., Pintar F. and Mattos G., (2012). *The Dynamic Rollover Protection (DROP) Research Program*, in Proceedings of the International Crashworthiness Conference ICRASH 2012, July, 18-20, Milan, Italy.

[3] United Nations, (2008). *Electronic Stability Control Systems*, Global technical regulation No. 8, ECE/TRANS/180/Add.8, Geneva.

[4] Australian Government, (2010). *Vehicle Standard (Australian Design Rule 31/02 – Brake Systems for Passenger Cars) 2009*, http://www.comlaw.gov.au/Details/F2010C00151

[5] Insurance Institute For Highway Safety, *Procedures for rating roof strength*. http://www.iihs.org/ratings/roof/information.html

[6] ANCAP, (2012). A*NCAP Rating Road Map 2011-2017*. http://www.ancap.com.au/admin/uploadfiles/RoadMap2017.pdf

[7] Brumbelow M.L., Teoh E.R., Zuby D.S., and A.T. McCartt, (2009). *Roof strength and injury risk in rollover crashes*, Traffic Inj. Prev. 10, pp. 252-265.

[8] Brumbelow M.L. and Teoh E.R., (2009). *Roof strength and injury risk in rollover crashes of passenger cars*, Traffic Inj. Prev. 10, pp. 584-592.

[9] Young, D., (2010). PhD Thesis, *Protecting Occupants During Passenger Vehicle Rollover Crashes*, Dept. of Civil Engineering, Monash University.

[10] Grzebieta R.H., Bambach M., McIntosh A.S., (2010). *How Stronger Roofs Prevent Diving Injuries In Rollover Crashes*, Proc. 7th Int. Crashworthiness Conf. ICRASH 2010, ed. Chirwa E.C. and S. Kan, Washington DC.

[11] Grzebieta R.H., Young D., Bambach M., McIntosh A., (2007). *Rollover Crashes: Diving Versus Roof Crush*, Proc. 20th International Technical Conference on the Enhanced Safety of Vehicles, Lyon, France.

[12] Mandell, S.P., Kaufman R., Mack C.D., and Bulger E.M., (2010). *Mortality and injury patterns associated with roof crush in rollover crashes*, Accident Analysis & Prevention, 42 (4): pp. 1326-1331.

[13] Strashny, A., (2007). *The Role of Vertical Roof Intrusion and Post-Crash Headroom in Predicting Roof Contact Injuries to the Head, Neck, or Face During FMVSS No.216 Rollovers; An Updated Analysis*, DOT, Editor 2007, National Highway Traffic Safety Administration: Washington DC.

[14] Young D.P. and Grzebieta R.H., (2010). *Vehicle roof strength as it relates to contained occupant injury prevention during rollover crashes*, Proc. Australasian Road Safety Research, Policing and Education Conference, Canberra, Australia.

[15] Mattos G.A., Grzebieta R.H., Bambach M.R. and McIntosh A.S., (2012). *Head Injuries to Restrained Occupants in Single-Vehicle Rollover Only Crashes*, Traffic Injury Prevention, in press, DOI:10.1080/15389588.2012.722735.

[16] Bambach M.R., Grzebieta R.H., McIntosh A.S., Mattos G.A., (2012). *Cervical and thoracic spine injury from interactions with vehicle roofs in pure rollover crashes*, Accident Analysis and Prevention, vol. 50, pp.34– 43.

[17] Bambach M.R., Grzebieta R.H., McIntosh A.S., (2012). *Thoracic injuries to contained and restrained occupants in single-vehicle pure rollover crashes*, Accident Analysis and Prevention, Volume 50, January 2013, pp. 115-121.

[18] US Department of Transportaion, National Highway Traffic Safety Administration, (1989). *Laboratory Test Procedure for FMVSS 201, Occupant Protection in Interior Impact*, Office of Vehicle Safety Compliance, Washington DC.

[19] National Highway Traffic Safety Administration, (2012). *Standard No. 226; Ejection Mitigation*, Code of Federal Regulations, Section 571.226, Washington DC.

[20] Chirwa EC, Stephenson RR, Batzer SA, & Grzebieta R H, (2010). *Review of the Jordan Rollover System (JRS) vis-a-vis other dynamic crash test devices*, International Journal of Crashworthiness, 15(5), 553-569.

[21] Friedman D and Grzebieta RH, (2009). *A Proposed Rollover and Comprehensive Rating System*, Proc. 21st International Technical Conference on the Enhanced Safety of Vehicles, Stuttgart, Germany, Paper Number 09-0515.

[22] Grzebieta R, McIntosh A, Bambach M, and Young D, (2010). *Dynamic Test Protocol to Assess Rollover Crashworthiness*, Proc. Australasian Road Safety Research, Policing and Education Conference, Canberra, Australia.

[24] Kerrigan J, Jordan A, Parent D, Zhang Q, Funk J, Dennis NJ, Overby B, Bolton J, Crandall J, (2011). *Design of a Dynamic Rollover Test System*, SAE Int. J. Passeng. Cars – Mech. Syst. 4(1):870-903, 2011, doi:10.4271/2011-01-1116.